Chapter 4 Mechanically-Induced Deformations of Composite Plates

4.1 Chapter Outline

Chapter four discusses what will be referred to as the prebuckling, buckling, and postbuckling response of unsymmetrically laminated composite plates in uniaxial compression under various boundary conditions. Several symmetrically laminated plates, and an aluminum one, are studied to serve as comparisons. For symmetric laminates the terms prebuckling, buckling, and postbuckling can be used with no ambiguity. For unsymmetric laminates, which, due to bending-stretching coupling, begin to deform out-of-plane as soon as they are compressed inplane, it is not clear if the concepts of prebuckling, buckling, and postbuckling are valid. However, for lack of better terminology at the moment, these terms will be used. Section 4.2 details the problem description, leading the reader through the nomenclature and analysis. Section 4.3-4.9 presents results for each of the seven types of plates being considered. Conclusions are presented in Section 4.10.

4.2 Problem Description

Nine-noded, two-dimensional, geometrically-nonlinear, shear-deformable shell elements are used to model the plates. The geometry and nomenclature are shown in Fig. 4.2.1. As it makes sense to begin any experimental investigation of the deformation response of unsymmetric laminates by considering small-scale laboratory size specimens, the plate considered is 20 in. long by 16 in. wide. The long dimensions of the plate will be referred to as the sides and the short dimensions the ends. The x-coordinate originates at one end of the plate, and the y-coordinate is cen-

tered between the two sides. All plates considered are 0.04 in. thick. Table 4.1 shows the properties of the composite layers being used. Note that they are the same material properties as those used earlier in Chapter 2 and 3. The principal material coordinate system is located within this geometric coordinate system with the fibers oriented along the *1*-direction, where the layer orientation angle θ is measured from the *x*-axis, as shown. The displacements in the *x*-, *y*-, and *z*-coordinate directions are denoted by *u, v,* and *w,* respectively. The rotations about the coordinate axes are denoted as ϕ_x, ϕ_y, and ϕ_z. These deformations are shown in Fig. 4.2.1. Displacement results will be presented at the three locations labeled I, II, and III on Fig. 4.2.1. Locations I and III are quarter locations, each 5 in. away from the ends, while location II is the center located 10 in. from each end. The uniaxial compressive loading is applied by uniformly displacing the end at *x*=20 in. a known amount U to shorten the plate. Load results will be presented as computed at the positive *x*-normal end. Three combinations of boundary conditions will be prescribed along the ends and sides. Table 4.2 shows the constrained degrees of freedom for each case. The results will be labeled SS-SS, CL-SS, and CL-CL to designate the particular boundary condition combination being considered. The terminology SS is contracted notation for simply-supported conditions and CL is a contraction for clamped conditions. The contraction to the left of the hyphen designates the prescribed boundary condition along the ends, while the contraction to the right of the hyphen designates the prescribed boundary condition along the sides. What is important to realize from the onset of the discussion is that the sides of the plates are assumed to be constrained so that *v*=0 there. This might be considered a somewhat arbitrary and unrealistic condition, but it is also unrealistic to consider plates that might be joined with other elements to form a complete structure to have no restrictions on the *v*-displacements along the sides. Rather than look at a range of elastic restraints, adding another variable to the problem, the case of full restraint is considered. This issue is important because, through Poisson effects, inplane compression in the *x*-direction can cause the plate to expand in the *y*-direction. With *v*=0 along the sides, Poisson expansion is restricted by an inplane compression force in the *y*-direction. With the bending-stretching coupling present in an unsymmetric laminate, this inplane force, along with the applied inplane force, are factors.

Although the goal of this chapter is to investigate the response of highly asymmetric composite plates, results will be presented in order of increasing asymmetry, beginning with the response of an isotropic aluminum plate in Section 4.3. As the response of an aluminum plate to

inplane loading is a classic problem, the nomenclature and the format of presenting results can be introduced without having to concentrate on the response of unsymmetric laminates. The discussion of aluminum plates will be followed by the discussion of the response of selected symmetric and unsymmetric cross-ply and angle-ply laminates in Sections 4.4-4.7. Namely, $[0_2/90_2]_S$ and balanced $[0_4/90_4]_T$ cross-ply laminates, and $[\pm 30_2]_S$ and $[+30_4/-30_4]_T$ angle-ply laminates. Finally, Sections 4.8 and 4.9 present results for general unsymmetric laminates exhibiting full elastic couplings, namely a $[\pm 30/90/0]_{2T}$ laminate and an unbalanced $[30_2/90/0]_{2T}$ laminate. The equivalent inplane properties of the symmetric laminates are listed in Table 4.3. The terms of the *ABD* matrix for all laminates are listed in Table 4.4. It is important to note that the results presented here do not consider plastic deformations or material failure as a result of excessive stresses within the laminate. Therefore, it may be possible that some of the postbuckling response may not be physically conceivable, especially at large magnitudes of normalized endshortening (U/Ucr). However, strain analyses have shown that the strain levels are below typical failure magnitudes. The normalizing factor, Ucr, is computed by assuming a linear, non-shear-deformable eigenvalue solution to a ‘classic SS-SS’ uniaxial buckling problem. The term ‘classic SS-SS’ implies that the boundaries are free to move inplane ($v \neq 0$) and are only constrained from out-of-plane deformation, ($w=0$). These boundary conditions and assumptions significantly reduce the critical endshortening, Ucr, with respect to the three boundary condition combinations being considered in this chapter. Therefore, a normalized endshortening value of 10 does not imply that the plate being discussed is compressed uniaxially to 10 times its own critical value, rather it is compressed to 10 times the critical value of a laminate predicted by the linear eigenvalue solution to the ‘classic SS-SS’ boundary condition, not generally an excessive amount.

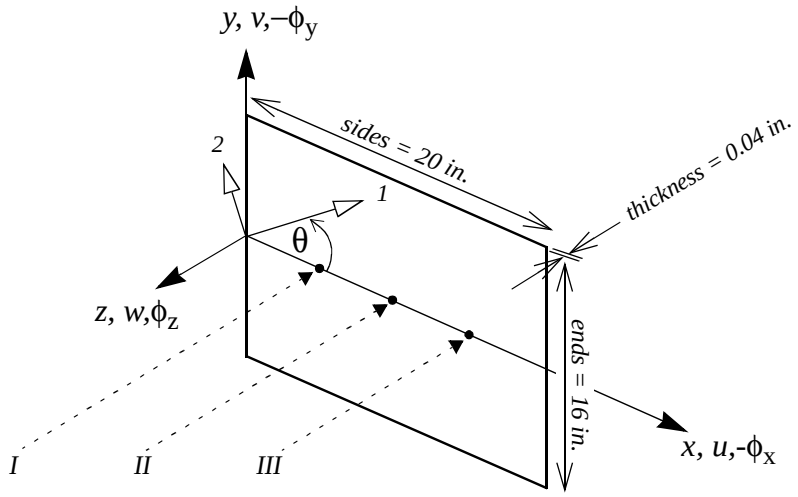

Fig. 4.2.1 Plate geometry and coordinate system

Table 4.1 Composite layer material properties

E_1	22.5 Msi
E_2	1.755 Msi
E_3	1.755 Msi
G_{23}	0.464 Msi
G_{13}	0.638 Msi
G_{12}	0.638 Msi
ν_{23}	0.458
ν_{13}	0.248
ν_{12}	0.248
α_1	-0.01 e-6/ºF
α_2	13.5 e-6/ºF
α_3	13.5 e-6/ºF
h	0.005 in.

Table 4.2 Boundary conditions

	ends	**sides**
SS-SS	u=0 or U, v=0, w=0, ϕ_x=0, ϕ_z=0	v=0, w=0
CL-SS	u=0 or U, v=0, w=0, ϕ_x=0, ϕ_y=0, ϕ_z=0	v=0, w=0
CL-CL	u=0 or U, v=0, w=0, ϕ_x=0, ϕ_y=0, ϕ_z=0	v=0, w=0, ϕ_x=0

Table 4.3 Equivalent inplane properties

	Aluminum	**$[0_2/90_2]_S$**	**$[\pm 30]_{2S}$**
E_x (psi)	1.00 E7	1.018 E7	6.78 E6
E_y (psi)	1.00 E7	1.018 E7	1.59 E6
G_{xy} (psi)	3.85 E7	725,000	3.85 E6
ν_{xy}	0.30	0.0416745	1.32
ν_{yx}	0.30	0.0416745	0.31

Table 4.4 Laminate stiffness properties

	Aluminum	**$[0_2/90_2]_S$**	**$[0_4/90_4]_T$**	**$[\pm30]_{2S}$**	**$[30_4/-30_4]_T$**	**$[\pm30/90/0]_{2T}$**	**$[30_2/90/0]_{2T}$**
A_{11} (lb/in)	879,000	407,000	407,000	458,000	458,000	433,000	433,000
A_{12} (lb/in)	263,000	17,000	16,900	141,800	141,800	79,400	79,400
A_{16} (lb/in)	0	0	0	0	0	0	112,100
A_{22} (lb/in)	879,000	407,000	407,000	107,400	107,400	257,000	257,000
A_{26} (lb/in)	0	0	0	0	0	0	40,000
A_{66} (lb/in)	307,000	29,000	29,000	15,380	15,380	91,000	91,000
B_{11} (lb)	0	0	-3,510	0	0	312	312
B_{12} (lb)	0	0	0	0	0	-312	-312
B_{16} (lb)	0	0	0	0	-2,240	-280	-560
B_{22} (lb)	0	0	3,510	0	0	312	312
B_{26} (lb)	0	0	0	0	-800	-100.0	-200
B_{66} (lb)	0	0	0	0	0	-312	-312
D_{11} (lb·in)	468	89.5	54.4	61.1	61.1	62.1	62.1
D_{12} (lb·in)	140.6	2.27	2.27	18.91	18.91	10.59	10.59
D_{16} (lb·in)	0	0	0	11.21	0	2.80	14.94
D_{22} (lb·in)	468	19.26	54.4	14.33	14.33	29.9	29.9
D_{26} (lb·in)	0	0	0	4.00	0	1.000	5.33
D_{66} (lb·in)	164.1	3.87	3.87	20.5	20.5	12.19	12.19

4.3 Aluminum

As the first step in the investigation of the buckling response of unsymmetric composite panels, this section presents the response of an isotropic aluminum plate under uniaxial compression for the three boundary condition combinations described in Section 4.2. For all three cases, the endshortening has been normalized by the critical value predicted by the 'classic SS-SS' eigenvalue problem, 0.000475 in. The associated load, P_{cr}, is 151.9 lbs. For all three cases, the aluminum plate exhibits classic bifurcation, or buckling, behavior, here referred to as primary instability. While it is well known that at the bifurcation point the plate becomes unstable, here stability is checked using a dynamic approach. This approach is described below and was used for all seven plates studied here. The dynamic approach was used with the aluminum plate since the stability characteristics are known and it was the dynamic procedure that was being studied. Having done this, applying the dynamic procedure to study the stability of unsymmetric composite plates could be done with some experience and confidence.

4.3.1 Aluminum, Clamped Ends and Clamped Sides

Figure 4.3.1 shows the load vs. endshortening and Figs. 4.3.2-4.3.4 illustrate out-of-plane displacements at locations I, II and III vs. endshortening for a uniaxially compressed aluminum plate with clamped ends and clamped sides. As can be seen from Figs. 4.3.2-4.3.4, the plate remains perfectly flat for endshortening values up to the bifurcation point B. Beyond point B the perfectly flat plate continues to remain flat, but the solutions are not statically stable, as indicated by the eigenvalues of the tangent stiffness matrix. Though it is well known that at point B the solution branches into three solutions, here the plate was allowed to remain in the flat configuration for values of endshortening just beyond point B. A transient dynamic analysis was then used to determine what stable configuration the plate would change to. It was possible to simply begin a transient dynamic analysis for an endshortening value beyond point B and have the plate begin to change its configuration with time. However, to accelerate the movement of the plate, a small pressure pulse, perpendicular to the surface of the plate, was used. Figure 4.3.5 shows the pressure pulse profile, where the duration of the pulse is half the natural period of the plate under consideration. Pressures in the +*z*- and -*z*-directions were used. The pressure pulse, P_o, ranged from -0.1 to +0.1 psi. including 0 psi. The transient dynamic analyses resulted in the plate moving to point C

or C', depending on the direction of the pressure pulse. All transient dynamic analyses were computed using geometrically nonlinear kinematic relationships. For the ABAQUS input, a suggested initial time increment of 1.0 E-8 seconds, with a total time period ranging from 1.0 to 3.0 seconds was used. Automatic time incrementation was used with a half-step residual tolerance range, HAFTOL, of 0.1 to 10.0. The maximum number of increments was set to 2500, with typical computations requiring between 300 to 1000 increments. The mass proportional damping factor, α_R, was set to 16.36. The stiffness proportional damping factor, β_R, was set to 2.45 E-5. Figures A.1-A.4 in Appendix A illustrate the transient response of the aluminum plate. After initiation of the dynamic analysis, the plate settles quickly to a stable equilibrium configuration (either C or C'). For endshortening values beyond point C, the plate deforms out-of-plane with increasing magnitude as the endshortening increases. At point D the plate again becomes unstable. The transient analysis is utilized and the plate changes to the configuration given by point E. For point D, even when no pressure pulse is used, the plate moves to point E more rapidly than just beyond point B if no pressure pulse is used. A similar situation occurs for point D' and its associated point E'. It should be noted that there are statically unstable equilibrium solutions on a continuation of paths CD and C'D', but these solutions are not shown. With the transition from point D to E, the load vs. endshortening relation decreases in magnitude and the displacement of the geometric center of the plate, location II, decreases to zero. This transition from point D to E is often referred to as secondary buckling. The detailed results of the transient analysis from point D to E are shown in Appendix A in Figs. A.5-A.8. As the plate is compressed further beyond point E, the load vs. endshortening relations continue to increase monotonically until the analysis is terminated at point F. Figure 4.3.6 shows the deformed shapes of the plate at various points on Figs. 4.3.1-4.3.4. It can be seen that the plate has multiple stable equilibrium shapes, and the transition from point D to E, and point D' to E', represents a change in configuration from one half-wave in the loading direction to two half-waves in the loading direction. Furthermore, the equilibrium paths are not unique, since the panel is just as likely to buckle from shape B into shape C or into shape C' and postbuckle from shape D into shape E or into shape E'.

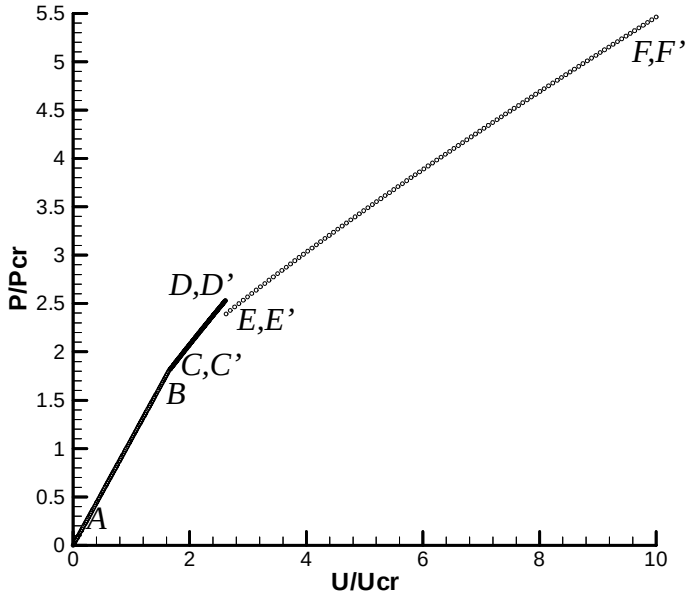

Fig. 4.3.1 Load response of an aluminum plate (CL-CL)

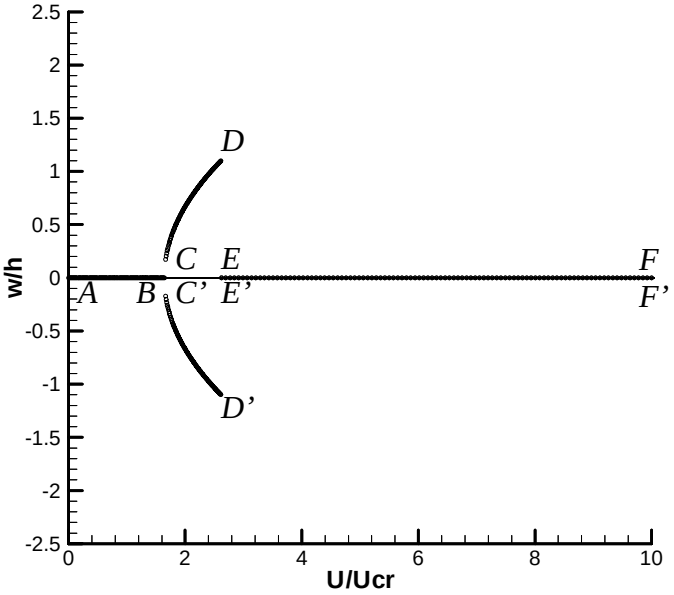

Fig. 4.3.2 Displacement response at II of an aluminum plate (CL-CL)

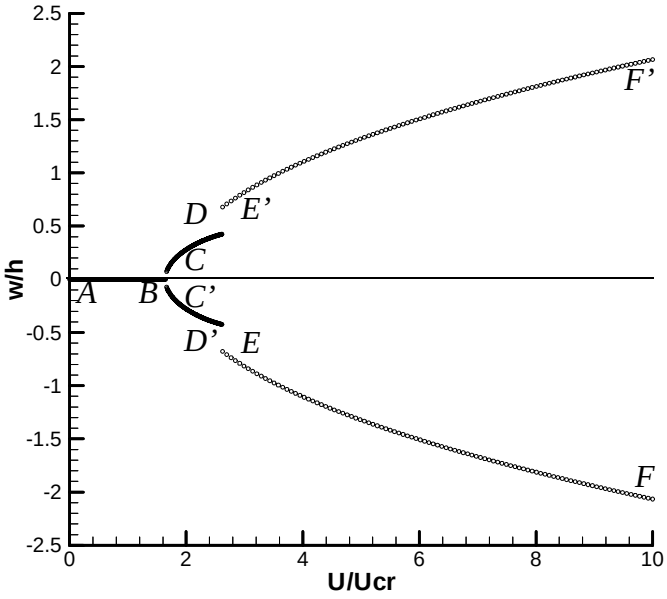

Fig. 4.3.3 Displacement response at III of an aluminum plate (CL-CL)

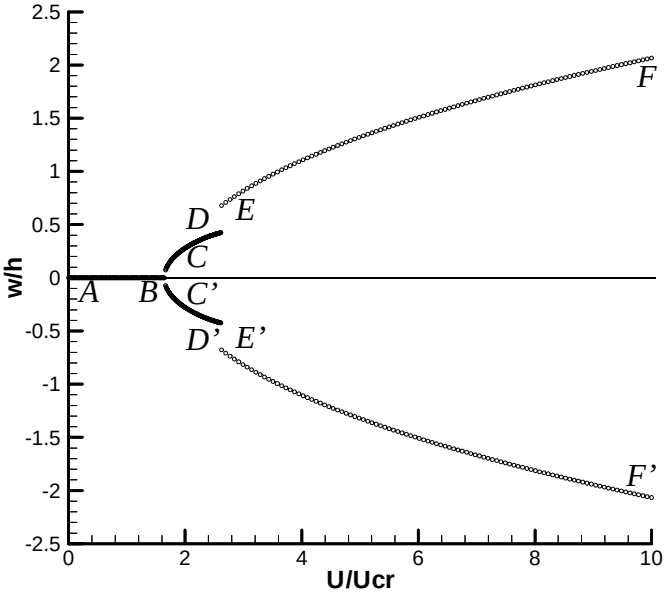

Fig. 4.3.4 Displacement response at I of an aluminum plate (CL-CL)

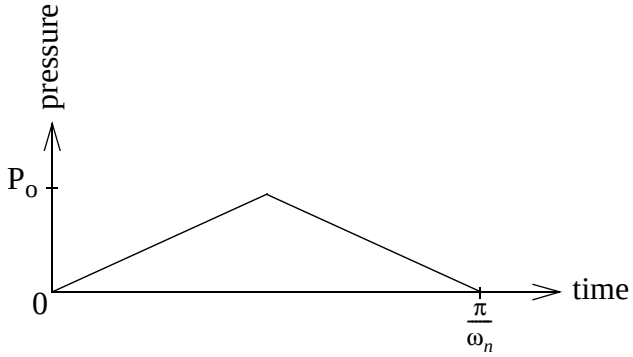

Fig. 4.3.5 Pressure pulse profile

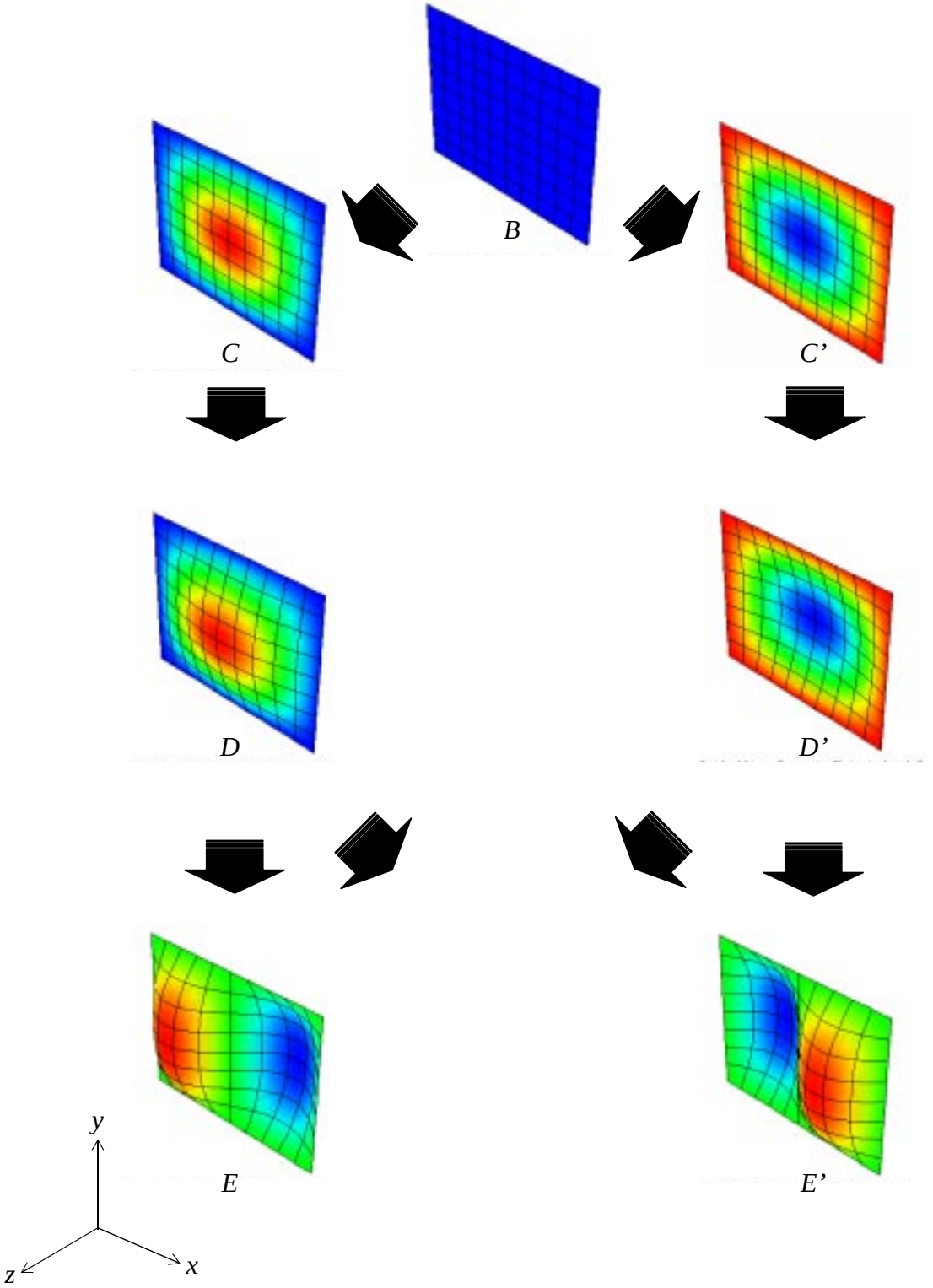

Fig. 4.3.6 Deformed shape flow chart for an aluminum plate (CL-CL)

4.3.2 Aluminum, Clamped Ends and Simply-Supported Sides

Figure 4.3.7 shows the load vs. endshortening and Figs. 4.3.8-4.3.10 illustrate endshortening vs. out-of-plane displacements at locations I, II and III for a uniaxially compressed aluminum plate with clamped ends and simply-supported sides. The responses of the aluminum plate under these boundary conditions are similar to those observed earlier for the CL-CL case. The plate remains perfectly flat for endshortening values up to the bifurcation point B. The load carrying capability of the plate continues to increase smoothly as the plate buckles at point B. Compared with the CL-CL case, the CL-SS case buckles at a slightly lower value of U/Ucr. Again, the transition from a condition just beyond point B to point C was accomplished via transient analysis. The results of the dynamic transient analysis are outlined in Appendix A in Figs. A.9-A.12. For endshortening values beyond point C, the plate deforms out-of-plane with increasing magnitude as the endshortening increases. At point D the plate configuration becomes unstable and, through a dynamic transient analysis, the load vs. endshortening relation decreases in magnitude and the displacement of the geometric center of the plate, location II, decreases to zero. Compared to the CL-CL case, the midplate deflection (location II) at point D is larger. Also, note that for the CL-SS case, as point D is approached on path CD, points I and III do not increase their amplitude much, i.e., paths CD for locations I and III are flatter than the same path for the CL-CL case. Compared with the CL-CL case, the drop in load carrying capacity from point D to E is larger for the CL-SS condition. The detailed results of the transient analysis from point D to E are shown in Appendix A, Figs. A.13-A.16. As the plate is compressed further beyond point E, the load vs. endshortening relations continue to increase smoothly until the analysis is terminated at point F. It can be seen that the ultimate load carried at point F is less than that carried at point F for the CL-CL condition. Figure 4.3.11 shows the deformed shapes of the plate at various points on Figs. 4.3.7-4.3.10. Again, the plate has multiple statically stable equilibrium shapes. The equilibrium paths are not unique since the panel is just as likely to buckle from shape B into shape C or into shape C’, and postbuckle from shape D into shape E or into shape E’.

To investigate the effect of mesh density on the response, an important question when using a finite-element analysis, the results for this case are recomputed using a model with four times the number of elements compared to the nominal model. In Appendix B, Fig. B.1 shows the load vs. endshortening and Figs. C.2-C.4 shows endshortening vs. out-of-plane displacements for a uniax-

ially compressed aluminum plate with clamped ends and simply-supported sides using the refined mesh model. Compared to Figs. 4.3.7-4.3.10, it can be seen that the difference in results is indiscernible. As a brief side bar, the response of the same plate due to a CL-SS boundary condition that does not restrain the *v*-displacements along the sides has been investigated. These boundary conditions are the ones most often simulated in the laboratory. Figures C.1-C.3 in Appendix C show that the plate exhibits classic bifurcation (buckling), with the plate remaining perfectly flat from initial loading, point A, until bifurcation, point B. Following that, the out-of-plane displacements increase in magnitude with increasing endshortening. The plate deforms out-of-plane with one half-wave in the loading direction and one half-wave perpendicular to the loading direction. Compared to the case for v=0, Figs. 4.3.7, the load vs. endshortening relation exhibits a noticeable decrease in slope after bifurcation as the plate deforms out-of-plane. The plate can deform either in the +*z*- or -*z*-direction after the bifurcation point B, and both deformation directions are shown. At point D the plate configuration becomes statically unstable. A dynamic analysis shows that the plate makes a transition to the configuration given by point E. This transition is accompanied by a drop in load to point E. At point E the plate has two half-waves in the loading direction and these half-waves deepen as point F is approached. Figure D.3 illustrates the various plate configurations. Analysis indicates there are equilibrium configurations beyond point D on path CD, but they are statically unstable.

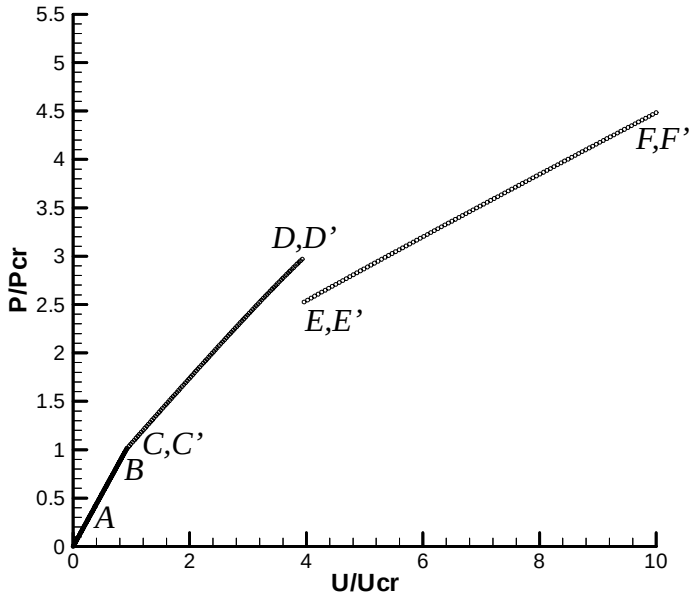

Fig. 4.3.7 Load response of an aluminum plate (CL-SS)

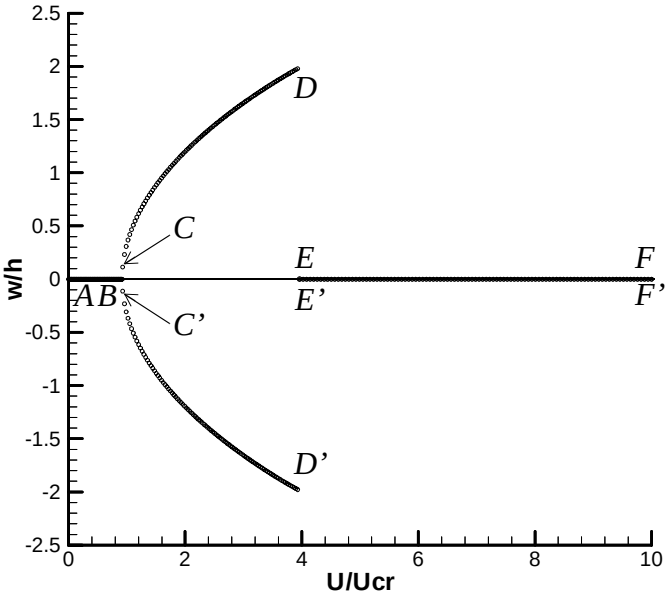

Fig. 4.3.8 Displacement response at II of an aluminum plate (CL-SS)

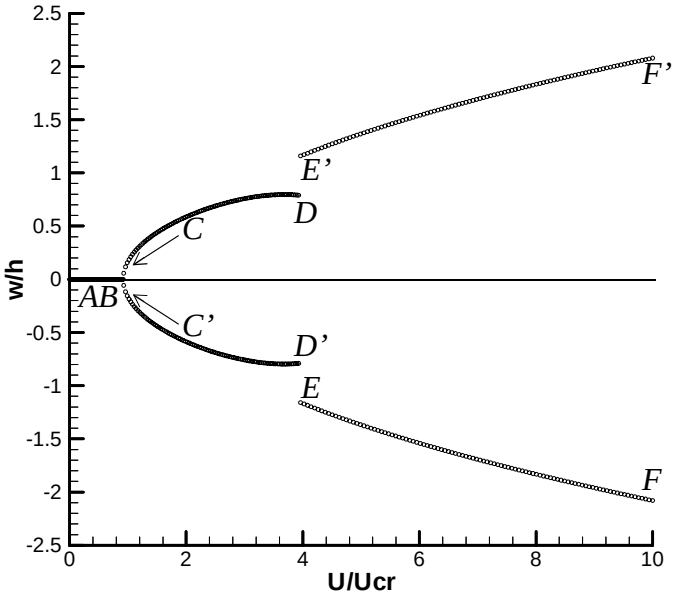

Fig. 4.3.9 Displacement response at III of an aluminum plate (CL-SS)

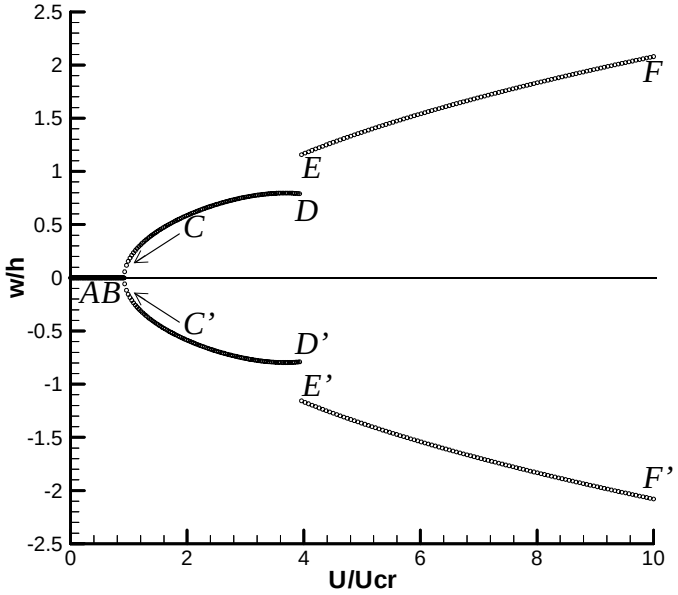

Fig. 4.3.10 Displacement response at I of an aluminum plate (CL-SS)

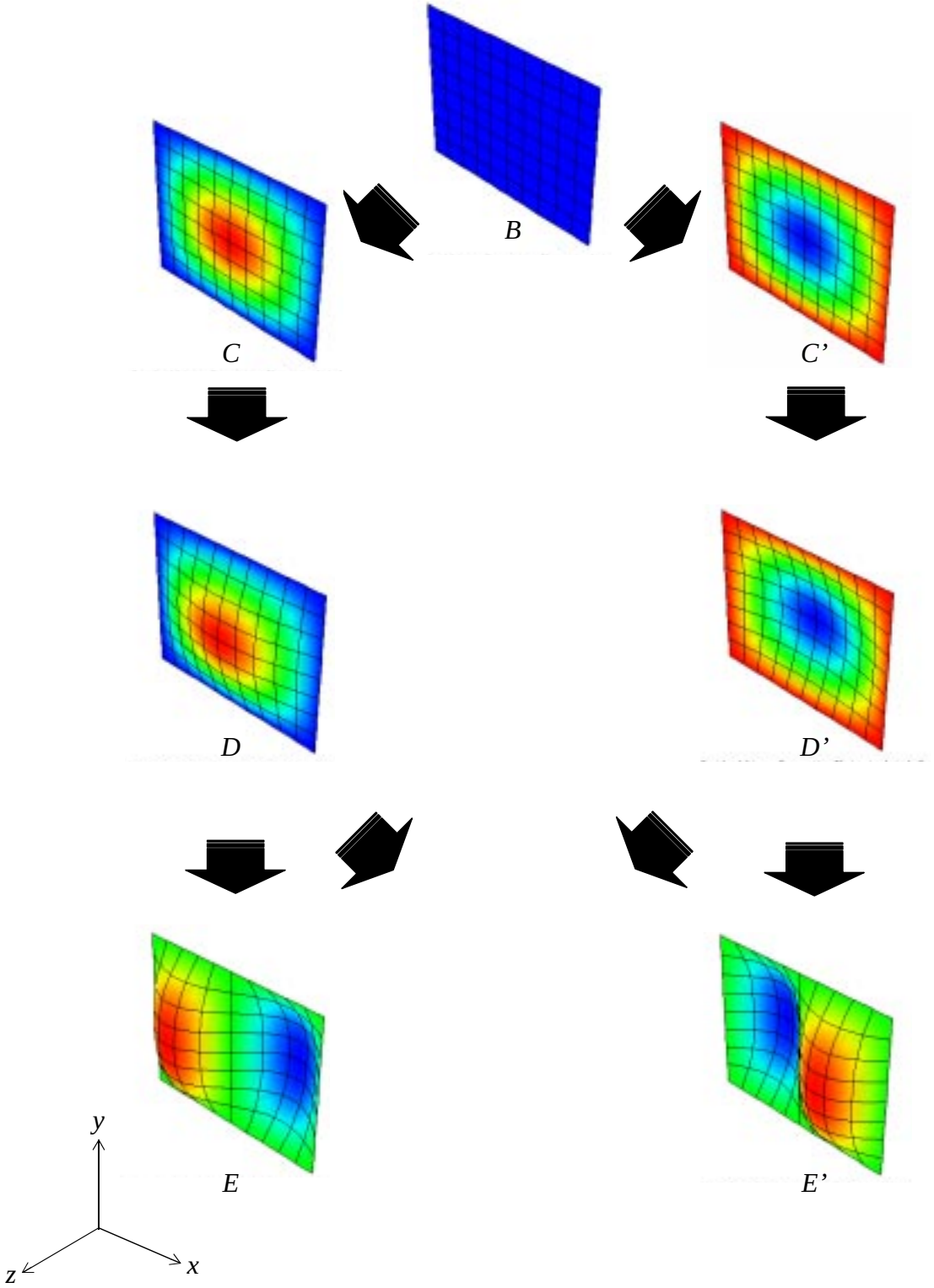

Fig. 4.3.11 Deformed shape flow chart for an aluminum plate (CL-SS)

4.3.3 Aluminum, Simply-Supported Ends and Simply-Supported Sides

Figure 4.3.12 shows the load vs. endshortening and Figs. 4.3.13-4.3.15 show the endshortening vs. out-of-plane displacements at locations I, II and III for a uniaxially compressed aluminum plate with simply-supported ends and simply-supported sides. Except for the constraint of v=0 along the sides, the support conditions are identical to the 'classic SS-SS' case. Though, overall, the SS-SS is similar to the previous two cases, there are some important difference. Like the previous two cases, the plate remains perfectly flat for endshortening values up to the bifurcation point B. The load carrying ability of the plate continues to increase as the plate buckles at point B, accompanied by a change in slope. Compared with the CL-CL and CL-SS conditions, the SS-SS case buckles at a much lower value of U/Ucr. The transition from point B to point C is accomplished via transient analysis, the results of which are shown in Appendix A in Figs. A.17-A.20. In contrast with the other two cases, for endshortening values beyond point B, the plate deforms out-of-plane with increasing magnitude until U/Ucr approximately equal to three, at which point the displacement at the center, location II, begins to decrease monotonically until point D. The displacement of each quarter location continues to increase past U/Ucr=3. Unlike the other two cases, the load vs. endshortening response of the SS-SS case becomes nonlinear and begins to 'soften' as point D is approached. At point D the plate becomes unstable. A transient dynamic analysis is initiated and the plate configuration makes a transition to point E. (A similar situation occurs for locations D' and E'.) In the transition from point D to point E the load vs. endshortening relation decreases in magnitude and the displacement of the geometric center of the plate, location II, decreases to zero. The detailed results of the transient analysis from point D to E are shown in Appendix A in Figs. A.21-A.24. As the plate is compressed further beyond point E, the load vs. endshortening relations continue to increase smoothly until another instability occurs at point F. At point F, a transient dynamic analysis is employed and the plate changes to a configuration given by point G. The transient response from point F to point G is detailed in Appendix A in Figs. A.25-A.28. In the transition from point F to G (or F' to G') the load carrying capacity of the plate is reduced again as the geometric center of the plate suddenly moves from zero to 1.5 times the plate thickness. After point G, the plate deforms continuously until point H, where the analysis is terminated. It can be seen that the ultimate load carried at point H is less than that carried at point F for the CL-CL or CL-SS conditions. Figure 4.3.16 shows the deformed shapes of the plate

at various points on Figs. 4.3.12-4.3.15. Again, the plate has multiple statically stable equilibrium shapes, where the paths are not unique since the panel is just as likely to buckle from shape B into shape C or into shape C', postbuckle from shape D into shape E or into shape E', and postbuckle from shape F into shape G or into shape G'. Similar to the other two cases, there are statically unstable equilibrium solutions that extend beyond point B on path AB, beyond point D on path CD, and beyond point F on path EF. These statically unstable equilibrium solutions are shown in Appendix D in Figs. D.1-D.4, in addition to the stable solutions from Figs. 4.3.12-4.3.15.

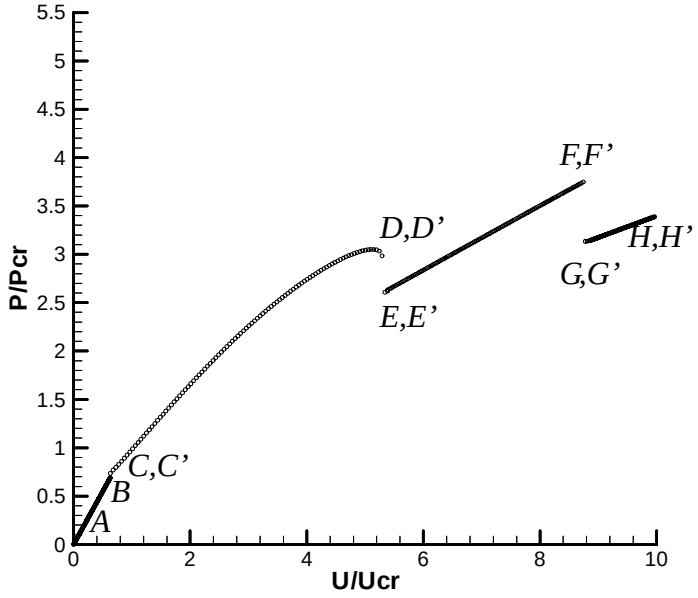

Fig. 4.3.12 Load response of an aluminum plate (SS-SS)

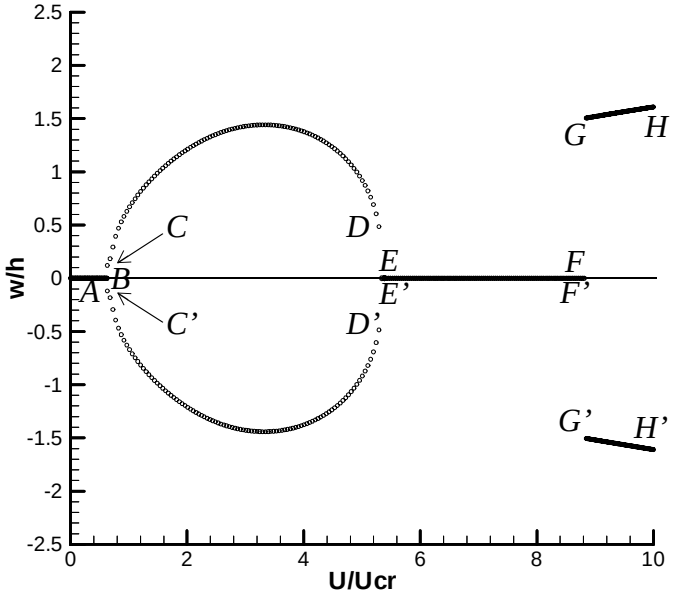

Fig. 4.3.13 Displacement response at II of an aluminum plate (SS-SS)

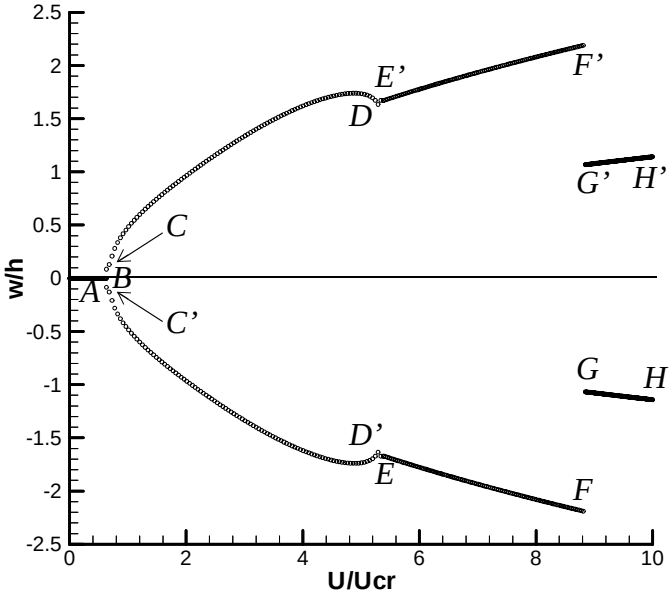

Fig. 4.3.14 Displacement response at III of an aluminum plate (SS-SS)

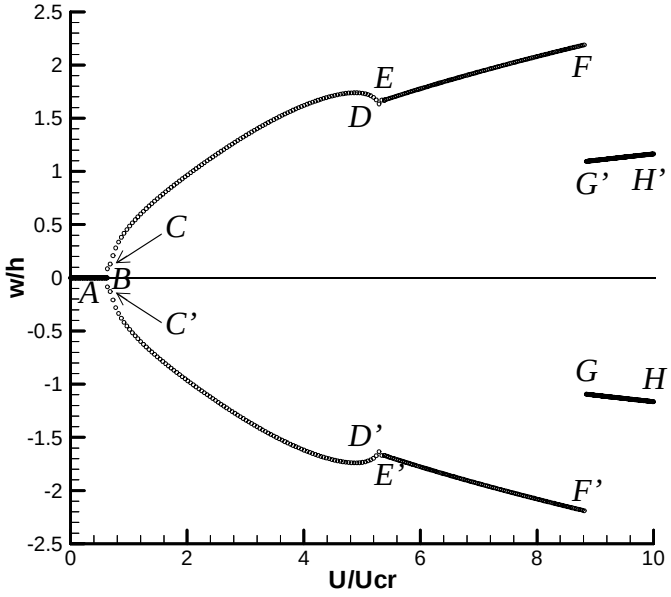

Fig. 4.3.15 Displacement response at I of an aluminum plate (SS-SS)

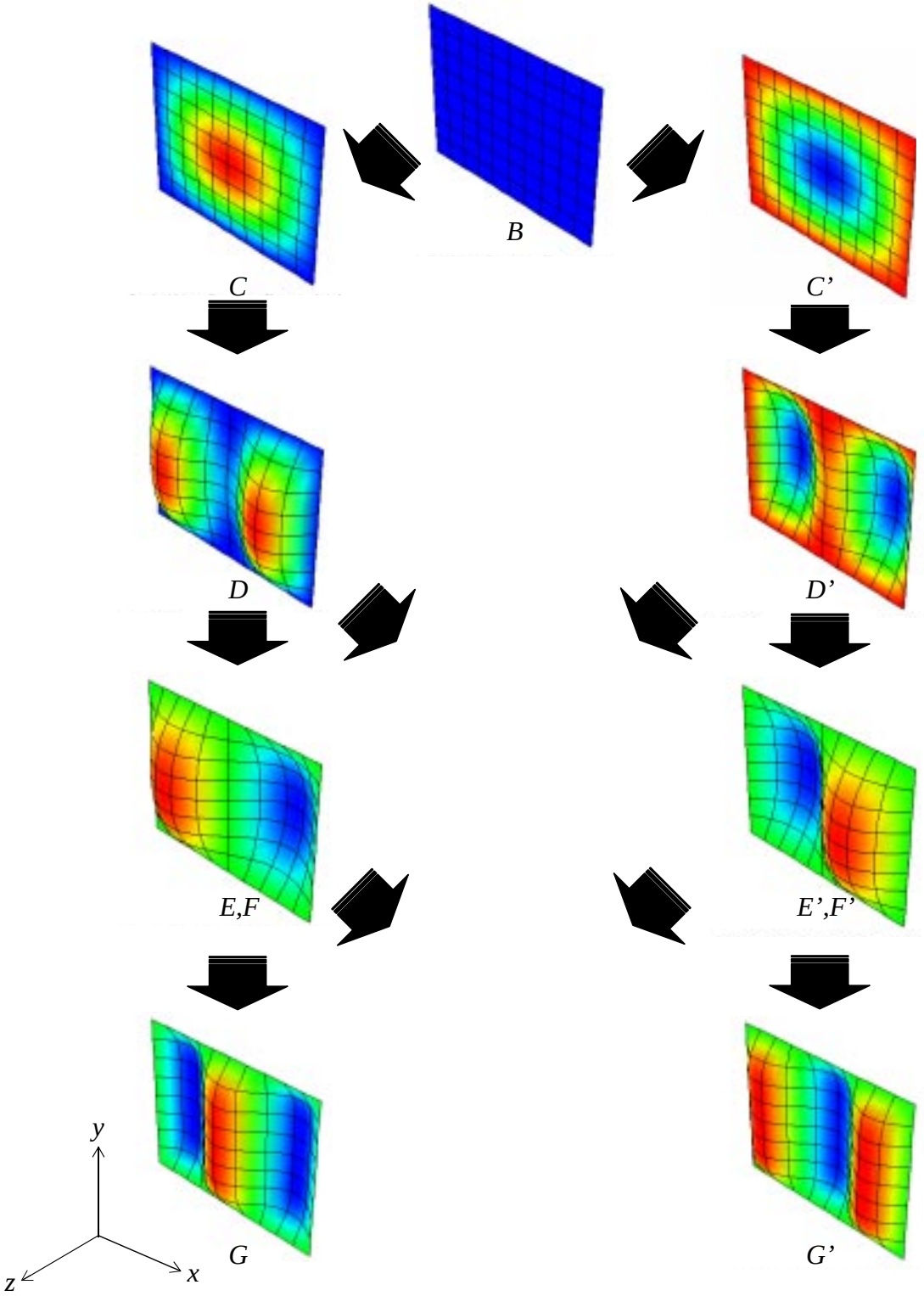

Fig. 4.3.16 Deformed shape flow chart for an aluminum plate (SS-SS)

4.4 $[0_2/90_2]_S$ Symmetric Cross-Ply

Section 4.4 discusses the investigation of the buckling and postbuckling response of symmetrically laminated cross-ply plates. As the name implies, symmetric cross-ply laminates are characterized by the symmetry of the lamination sequence with respect to the geometric midplane of the plate. Furthermore, the laminate is comprised solely of 0° and 90° layers. Again, three boundary condition combinations will be considered, CL-CL, CL-SS, and SS-SS. The response of this symmetric cross-ply laminate under uniaxial compression will serve as a comparison for the response of the unsymmetric cross-ply laminate to follow. As will be seen, the responses of a symmetric cross-ply plate with various boundary conditions are similar to the responses of the aluminum plate. Except for the low inplane shear modulus of the cross-ply plate, the two plate materials are similar. For all of the following cross-ply cases discussed in Sections 4.4 and 4.5, the endshortening has been normalized by the critical value predicted by the 'classic SS-SS' eigenvalue problem for the $[0_2/90_2]_S$ laminate, 0.000203 in. The associated load, P_{cr}, is 66.2 lbs.

4.4.1 $[0_2/90_2]_S$ Clamped Ends and Clamped Sides

Figures 4.4.1-4.4.4 shows the static load response and the corresponding deformations of the plate at locations I, II, and III. The figures show that the plate remains perfectly flat as it is shortened to point B. A statically unstable equilibrium solution continues on path AB, but it is not shown here. At the point just beyond B, a transient dynamic analysis using small pressure pulses, $\pm P_o$, is used to find the two stable solutions C and C'. In Appendix E, Figs. E.1-E.4 show the response of this dynamic transient analysis. The load transition from point B to point C occurs smoothly without a large change in slope. Figure 4.4.5 shows the deformed shape of the plate at this point to have one half-wave in the loading direction. Further compression of the plate causes this shape to deepen until it passes point D, after which the plate become statically unstable. Again, there are unstable equilibrium solutions beyond point D on path CD, but they are not shown here. Compared to the CL-CL aluminum plate, path CD (and C'D') is longer and is flatter at locations I and III as point D is approached. At the point just beyond point D, the dynamic transient analysis is used to find the stable equilibrium shapes E and E'. The details of the the transient analysis are shown in Appendix E, Figs. E.5-E.8. The stable equilibrium shapes at points E

and E’ are shown in Fig. 4.4.5 to have two half-waves in the loading direction. Further compression of the plate beyond point E leads to a deepening of this shape until the analysis is terminated at point F. As has been noted, for the cases discussed so far, the solutions for point C’, D’, etc. are simply mirror images, with respect to the horizontal axis, of the solutions for points C, D, etc. Henceforth, discussions will focus only on points C, D, etc., it being implied that a similar discussion can take place for points C’, D’, etc. If this mirror image symmetry does not occur for a particular case, or there is some other unusual behavior, points C’, D’, etc. will be discussed.

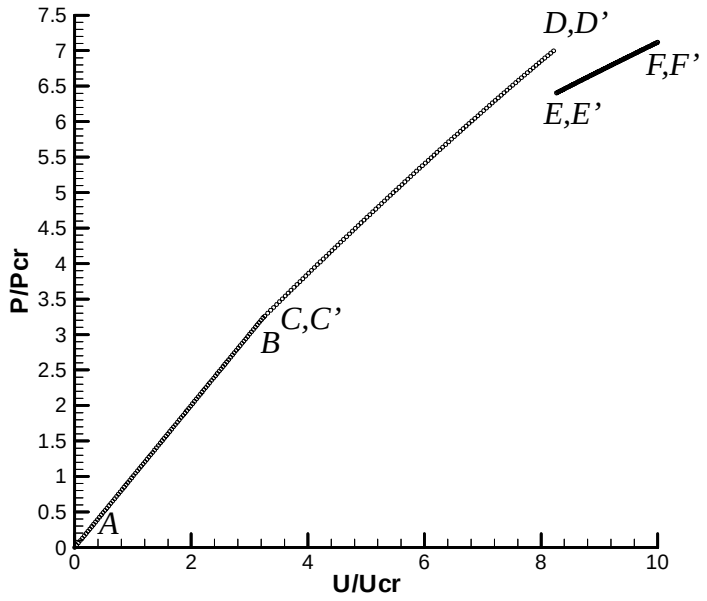

Fig. 4.4.1 Load response of a $[0_2/90_2]_S$ laminate (CL-CL)

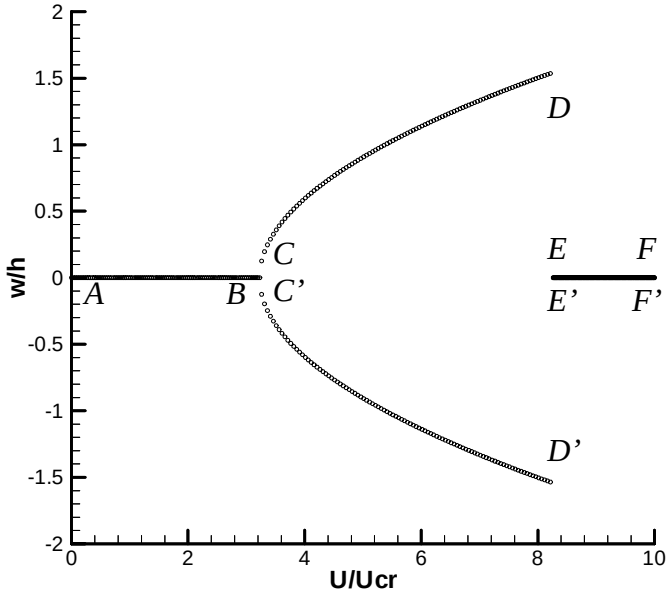

Fig. 4.4.2 Displacement response at II of a $[0_2/90_2]_S$ laminate (CL-CL)

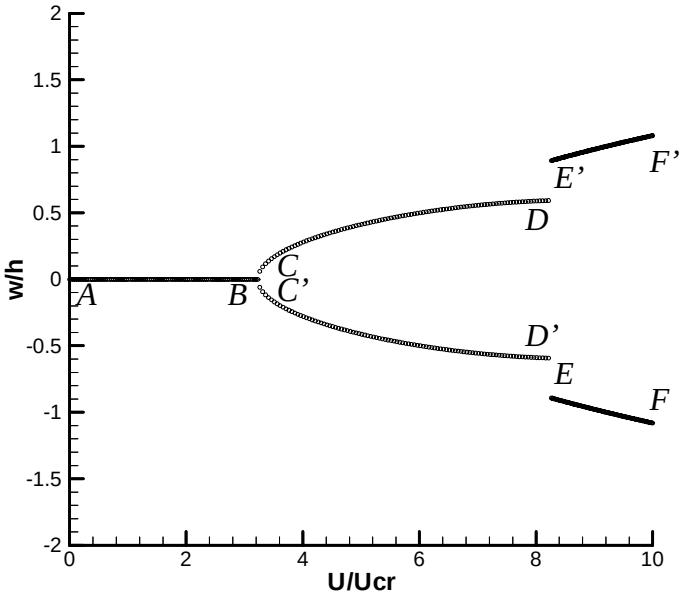

Fig. 4.4.3 Displacement response at III of a $[0_2/90_2]_S$ laminate (CL-CL)

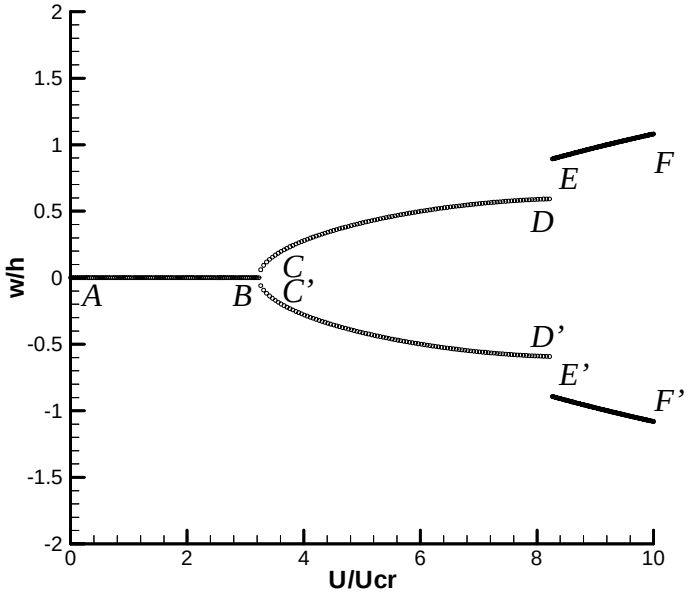

Fig. 4.4.4 Displacement response at I of a $[0_2/90_2]_S$ laminate (CL-CL)

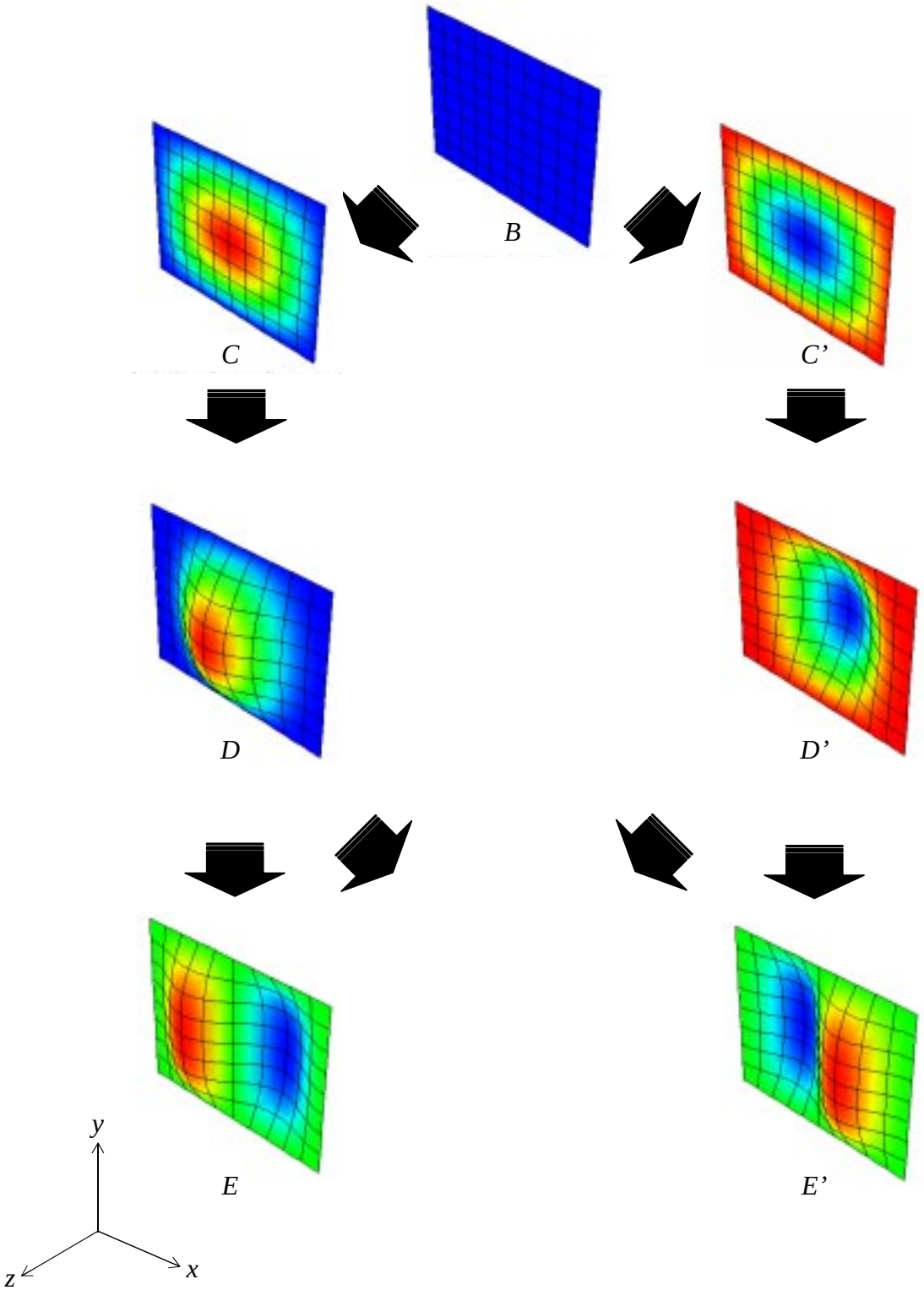

Fig. 4.4.5 Deformed shape flow chart for a $[0_2/90_2]_S$ laminate (CL-CL)

4.4.2 $[0_2/90_2]_S$ Clamped Ends and Simply-Supported Sides

This section reports on the results of uniaxially compressing the same symmetric cross-ply plate as in the previous section, but with clamped ends and simply-supported sides. The results of this problem are very similar to those of the CL-CL case. In brief, the CL-SS plate buckles at a lower value of endshortening and carries slightly less ultimate load at point F. As seen earlier, the plate remains flat from the onset until it passes point B, the point at which the plate becomes unstable. Here the solution transitions into the stable configuration C, and the unstable configuration which extends beyond point B on path AB, which is not shown. Like the earlier cases, the transition from a point just beyond B to point C is accomplished by using a dynamic transient analysis with pressure pulses in the +*z*- and -*z*-directions. The results of the transition can be seen in Appendix E in Figs. E.9-E.12. It should be noted that this transition could have been accomplished without using a pressure pulse, however, the relatively low strain energy stored in the plate at point B leads to a substantial number of time increments before the plate begins to move. Therefore the pressure pulse was used to accelerate the onset of plate motion. Figure 4.4.10 shows that the stable shape at points C has one half-wave in the loading direction. Continued axial compression of the plate past point C leads to a monotonic deepening of this shape and an almost linear increase in load carrying capabilities with a slight change in slope until the plate become unstable again at a point just past D. Paths CD for locations I and III are again quite flat as point D is approached. After point D the solution is again unstable. Then there is the stable configuration E, and the unstable configuration extending beyond point D on path CD, not shown. The transition from point D to E was done using a transient dynamic analysis, the results of which are shown in Appendix E in Figs. E.13-E.16. Figure 4.4.10 shows that the statically stable equilibrium shape at point E has two half-waves in the loading direction. As the plate is compressed beyond point E, this shape deepens until the analysis is terminated at point F. The lower ultimate load carried at point F compared to the CL-CL case can be attributed to the reduced structural stiffness induced by the added degree of freedom present along the sides of this plate.

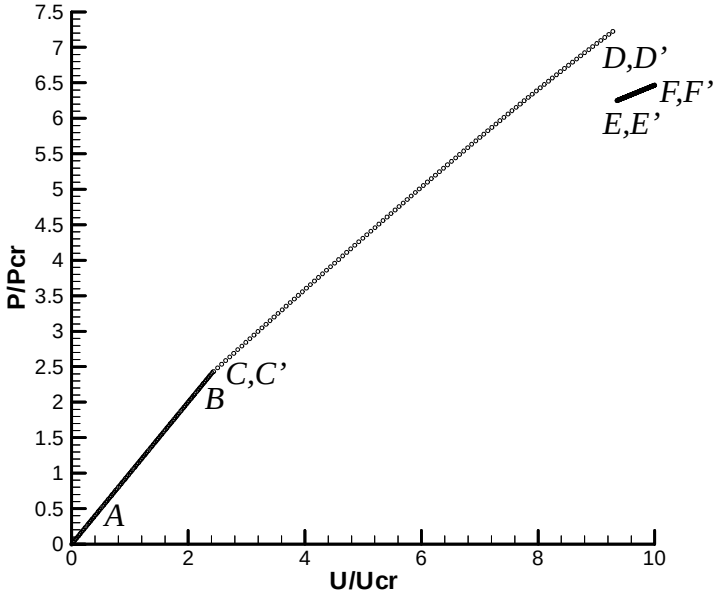

Fig. 4.4.6 Load response of a $[0_2/90_2]_S$ laminate (CL-SS)

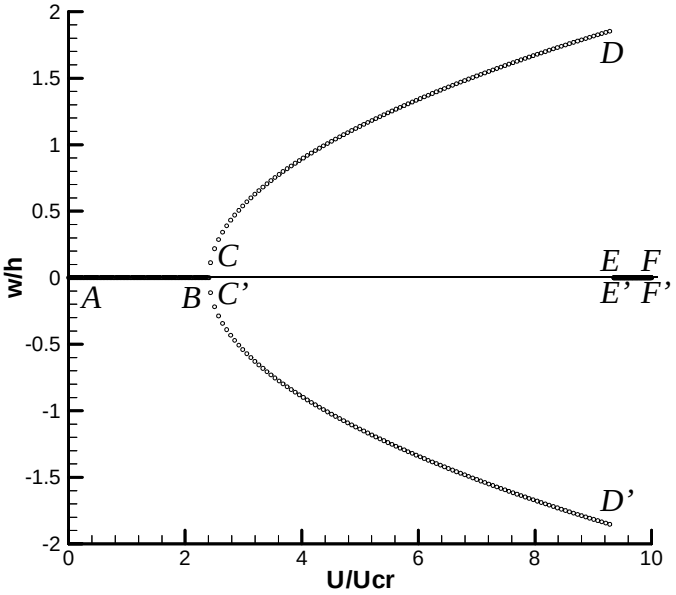

Fig. 4.4.7 Displacement response at II of a $[0_2/90_2]_S$ laminate (CL-SS)

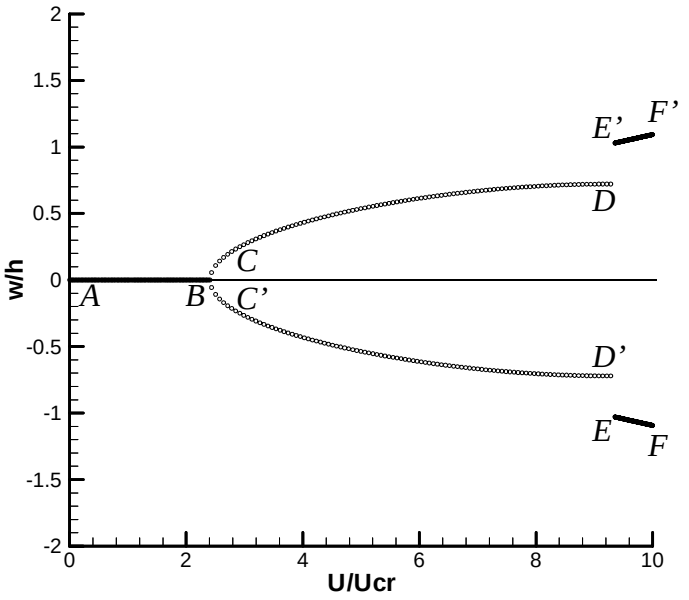

Fig. 4.4.8 Displacement response at III of a $[0_2/90_2]_S$ laminate (CL-SS)

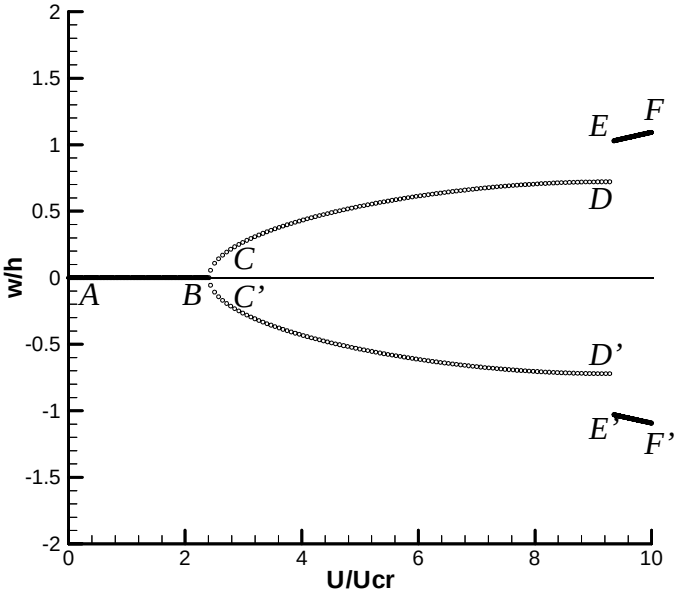

Fig. 4.4.9 Displacement response at I of a $[0_2/90_2]_S$ laminate (CL-SS)

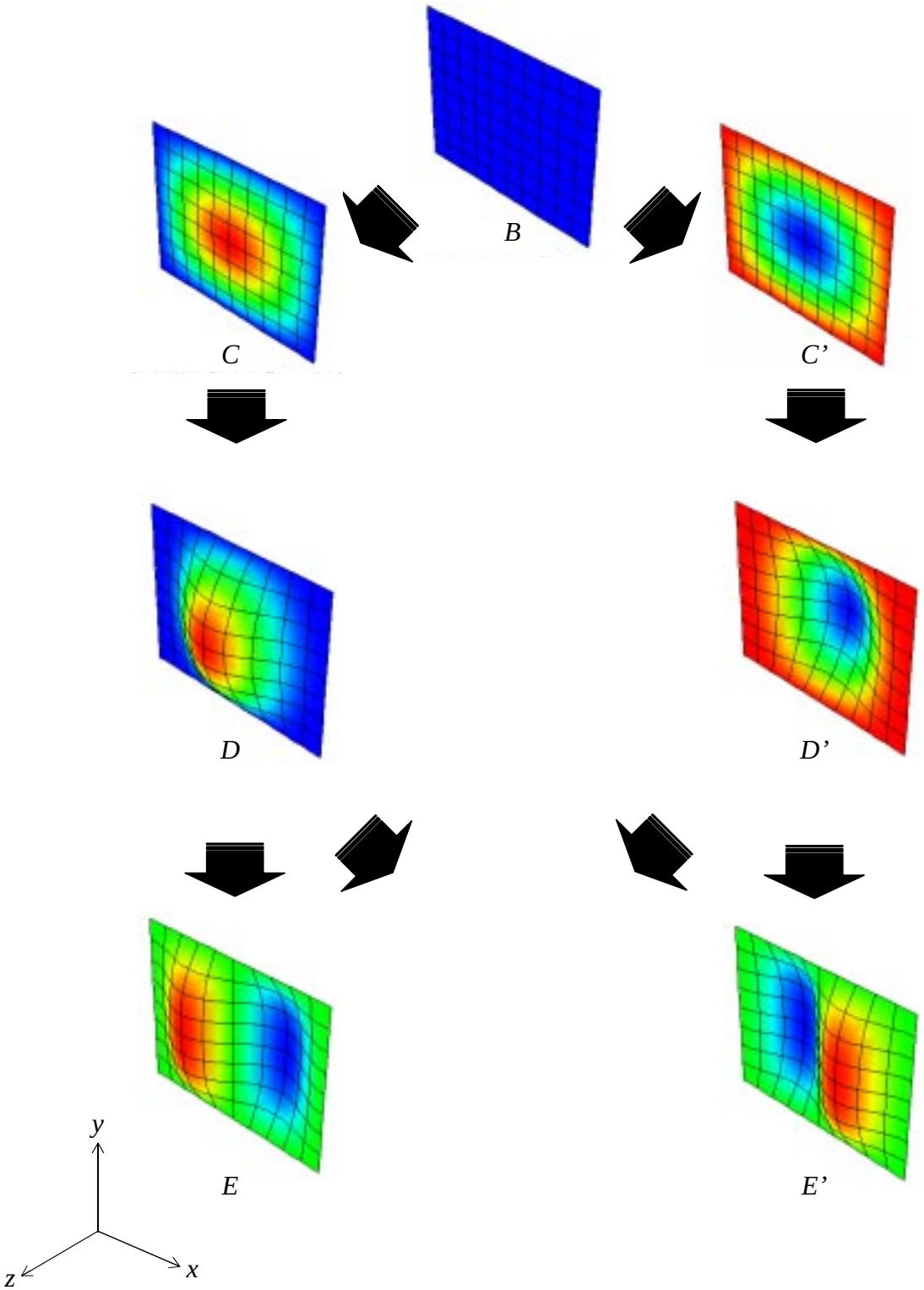

Fig. 4.4.10 Deformed shape flow chart for a $[0_2/90_2]_S$ laminate (CL-SS)

4.4.3 $[0_2/90_2]_S$ Simply-Supported Ends and Simply-Supported Sides

The final boundary condition combination considered for the symmetric cross-ply laminate is the SS-SS case. Figures 4.4.11-4.4.14 show the load and deformation response for this problem. As seen earlier with the other two cases, the plate remains initially flat from point A until point B. At a point just beyond B, the plate can have any of three equilibrium configurations, two of which are stable. Compared to the CL-CL and CL-SS cases, buckling occurs at a significantly lower value of endshortening. Similar to the other two cases, a dynamic transient analysis is initiated at the point just beyond B to find the statically stable equilibrium shapes at that value of endshortening. Figures E.17-E.20 in Appendix E show the result of this analysis. The equilibrium solutions at this value of endshortening are the stable point C and the unstable point beyond point B on path AB, not shown. Figure 4.4.15 shows that the statically stable equilibrium solution at point C to have one half-wave in the loading direction. As the plate is shortened beyond point C, the response of this problem differs from the response of the CL-CL and CL-SS cases discussed earlier. The load response shows that path CD becomes somewhat nonlinear as the plate 'softens' as it approaches the secondary buckling point D. This is accompanied by the flattening of the plate geometry at the center, location II. Unlike the other two cases, the plate develops a new intermediate shape at point D, shown in Fig. 4.4.15. This is similar to the situation with the SS-SS aluminum plate, Fig. 4.4.16, but not so extreme. As the plate becomes unstable beyond point D, the solution makes a transition into stable shape E, and an unstable shape along path CD beyond point D, not shown. This transition is accomplished again by using a dynamic transient analysis, the results of which are detailed in Appendix E in Figs. E.21-E.24. It is interesting to note that the two quarter locations, I and III, move to a lower magnitude of deflection compared with point D. This is interesting because for the other two symmetric cross-ply cases and two of the three aluminum cases considered previously, the displacements at locations I and III moved to a higher magnitude of deflection with respect to point D. It is also of interest to note that the center location deflection, location II, at E does not go to zero like the other two cross-ply cases. Figure 4.4.15 shows the statically stable equilibrium shape at point E to have two half-waves in the loading direction. Finally, it can be observed that the ultimate load carried at point F is much less than that carried by the other two cases at the same point.

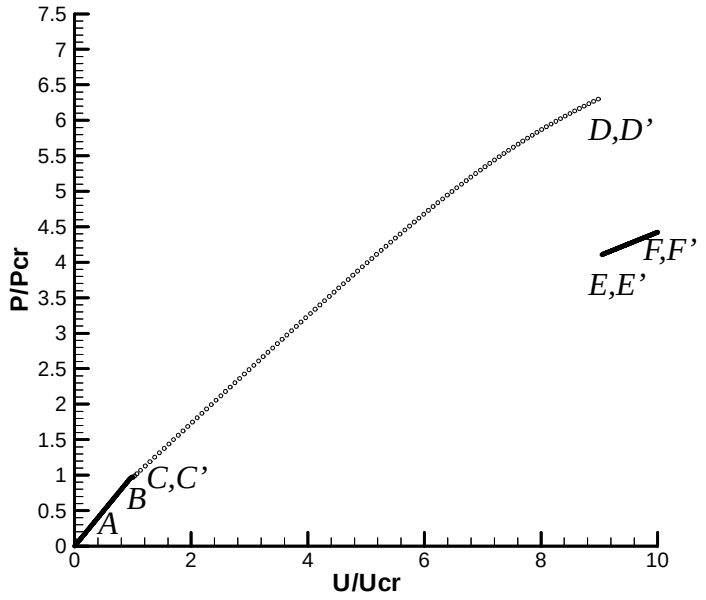

Fig. 4.4.11 Load response of a $[0_2/90_2]_S$ laminate (SS-SS)

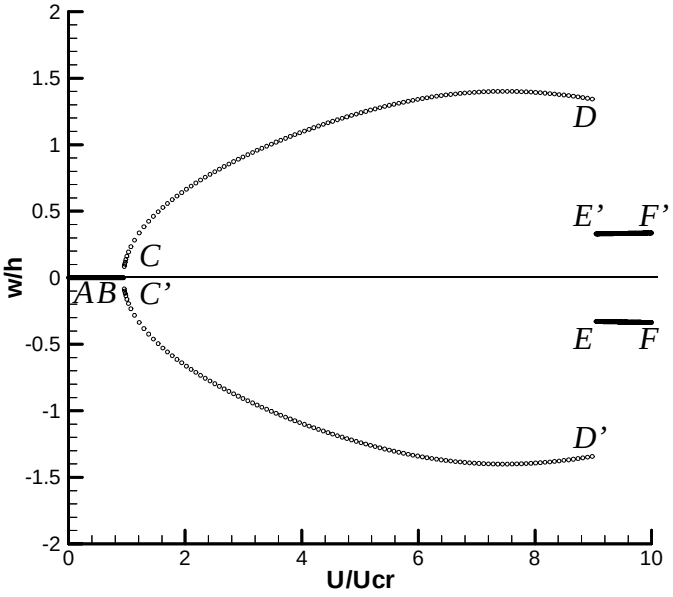

Fig. 4.4.12 Displacement response at II of a $[0_2/90_2]_S$ laminate (SS-SS)

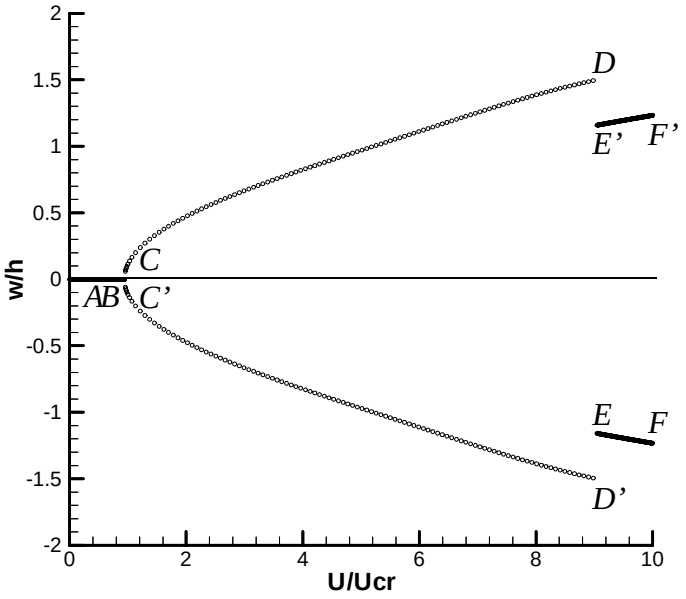

Fig. 4.4.13 Displacement response at III of a $[0_2/90_2]_S$ laminate (SS-SS)

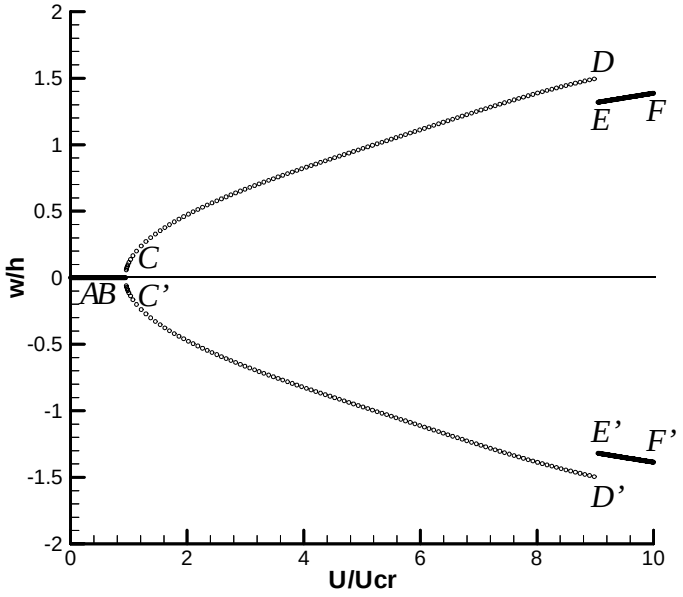

Fig. 4.4.14 Displacement response at I of a $[0_2/90_2]_S$ laminate (SS-SS)

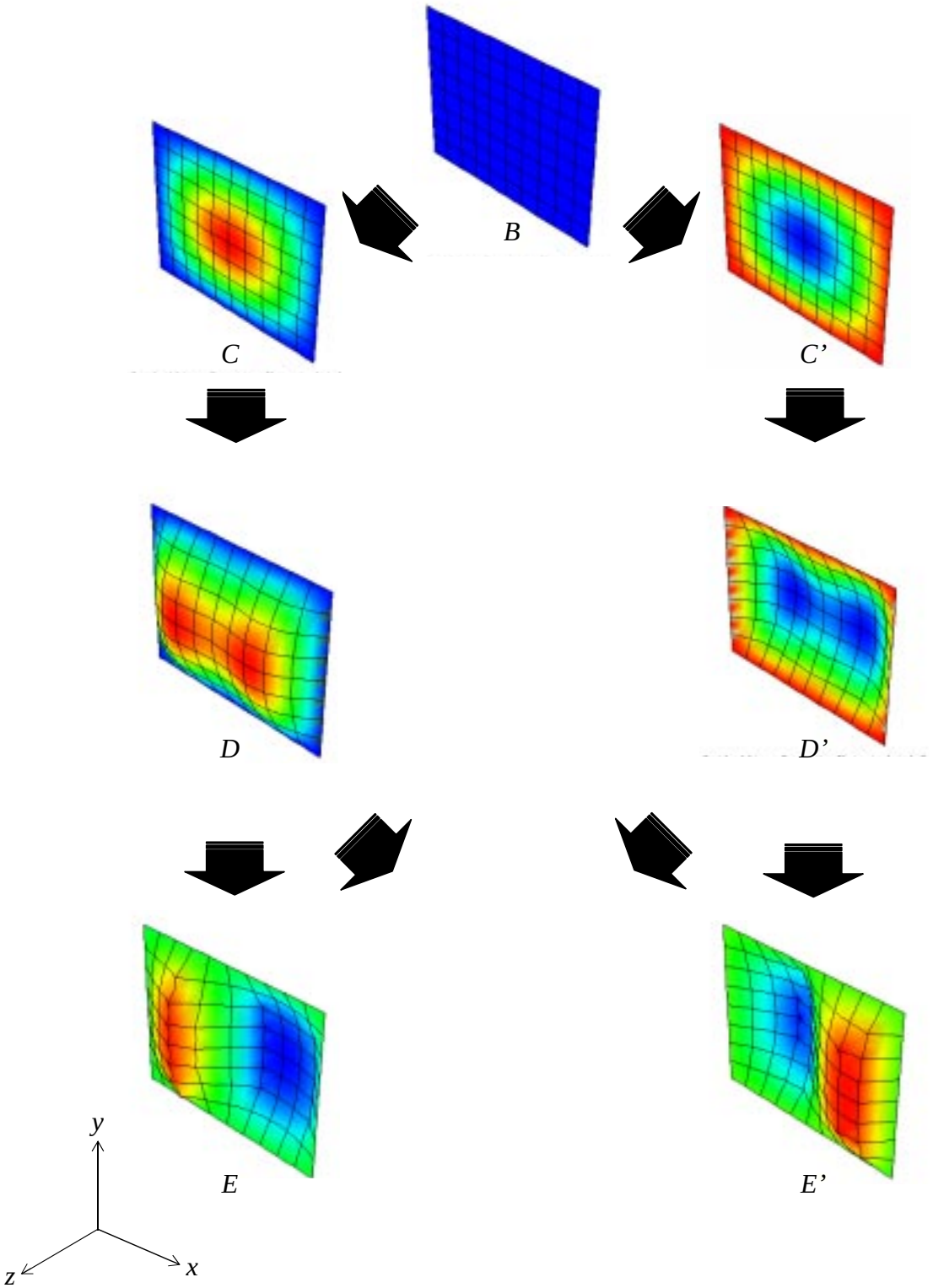

Fig. 4.4.15 Deformed shape flow chart for a $[0_2/90_2]_S$ laminate (SS-SS)

4.5 $[0_4/90_4]_T$ Anti-symmetric Cross-ply

This section discusses the response of anti-symmetric cross-ply laminated plates in uniaxial compression under various boundary conditions. The boundary conditions considered are consistent with those considered for the earlier cases, namely CL-CL, CL-SS, and SS-SS. Unlike the symmetric cross-ply laminates discussed in Section 4.4, anti-symmetric cross-ply laminates are not symmetric with respect to the geometric midplane of the plate. The fiber orientation of the layers on one side of the midplane is orthogonal to the fiber orientation in the layers on the other side of the midplane. Since this laminate is a cross-ply, the ply orientations are comprised solely of 0° and 90° layers. This laminate is the unsymmetric counterpart to the symmetric cross-ply laminate considered in Section 4.4 and is a departure from the previous six cases discussed.

Before discussing the response of the $[0_4/90_4]_T$ unsymmetric laminate under the various boundary conditions, it is important to summarize the conclusions of a very relevant paper by Leissa [8]. The paper shows that perfectly flat unsymmetric laminates under inplane loads, such as the axial compression being discussed here, do not exhibit prebuckling deformations if all four edges are clamped. The clamped conditions are capable of supplying the necessary bending and twisting moments required to keep the laminate in the flat configuration when subjected to inplane compressive loading. Furthermore, it is shown that simply-supported boundary conditions can only supply the necessary twisting moments, but not the bending moments required to constrain the prebuckling deformations. Therefore, it could be concluded that unsymmetric laminates under inplane compressive loads with CL-CL boundary conditions will exhibit classic buckling (bifurcation) behavior, or a primary instability, while the same laminate with simply-supported sides could deform out-of-plane without exhibiting the classic buckling (bifurcation) response. The sections that follow will discuss this issue.

4.5.1 $[0_4/90_4]_T$ Clamped Ends and Clamped Sides

As will be seen shortly, the 16 in. by 20 in. CL-CL $[0_4/90_4]_T$ laminate exhibits what could be considered anomalous behavior when compared to the behavior of the previous cases. For that reason, the response of a 16 in. by 16 in. square CL-CL $[0_4/90_4]_T$ laminate will be discussed first. Figures 4.5.1 shows the load vs. endshortening response of the square $[0_4/90_4]_T$ laminate with

clamped ends and clamped sides. Corresponding displacements at locations I, II, and III are shown in Figs. 4.5.2-4.5.4. The latter three figures show that the laminate appears to remain perfectly flat from the onset of endshortening at point A until point B, as predicted by Leissa. However, the finite-element analysis indicates there is an infinitesimally small out-of-plane deflection at point B, as indicated in Fig. 4.5.5. This small deflection is felt to be due to numerical round-off within the finite-element code.

Just past B, the laminate deforms out-of-plane. The laminate appears to exhibit classic buckling response. A statically unstable solution continues on path AB past point B, not shown, making up the first of the two solutions beyond point B. Just beyond B, a dynamic transient analysis is initiated using small pressure pulses, $\pm P_o$, perpendicular to the plate. The response of the laminate during this transient analysis is shown in Appendix E in Figs. E.25-E.28. Both pressure pulses, the one in the +*z*-direction and the one in the -*z*-direction, led to the same solution, indicating that the laminate has one statically stable equilibrium solution at point C. The configuration is illustrated in Fig. 4.5.5. This configuration has one half-wave in the loading direction and one half-wave perpendicular to the loading direction. Figure 4.5.1 shows that the load vs. endshortening relationship at this point is continuous with a small reduction in slope. Having just one rather than two stable equilibrium shapes past point B is the major difference between this unsymmetric cross-ply laminate and its symmetric counterpart seen in Section 4.4. This was an expected result due to the asymmetry of the laminate. As the laminate is further shortened past point C, the out-of-plane displacements at locations I, II, and III increase monotonically until at a point just past D. The laminate configuration then becomes statically unstable again. Here, a dynamic transient analysis is initiated with and without a pressure pulse. The response of the laminate during this analysis is shown in Appendix E in Figs. E.29-E.32. The results show that the laminate deforms into a new configuration, given by point E, with two half-waves in the loading direction and one half-wave perpendicular to the loading direction, as shown in Fig. 4.5.5. It is important to note that at point E, the center of the laminate, location II, has a nonzero out-of-plane displacement. Also, the out-of-plane displacements at locations I and III are of opposite sign but not equal magnitude. The load vs. endshortening relationship, Fig. 4.5.1, shows a small drop in load from point D to E. As the plate is further shortened from point E, the load increases smoothly while the two half-wave shape deepens even further, until the analysis is terminated at point F. Note also that as the shortening is increased to point F, the out-of-plane displacement of the center of the laminate

approaches zero and the displacements at locations I and III approach being equal in magnitude but opposite in sign.

Returning to the 16 in. by 20 in. dimensions, Figs. 4.5.6-4.5.9 show the load vs. endshortening response and the corresponding displacements at locations I, II, and III for the rectangular $[0_4/90_4]_T$ laminate with clamped ends and clamped sides. The work of Leissa again can be used to show that the plate remains flat up to point B, even though the finite-element analysis indicates there is a very small deflection at point B, as shown in Fig. 4.5.10. This again is felt to be due to numerical round-off in the finite-element calculations. As with the previous cases, the load carrying capacity of the plate increases linearly from point A to point B until the plate becomes statically unstable. The statically unstable solution continues on path AB past point B, not shown, making up the first of the two solutions at the bifurcation point B. A transient dynamic analysis is initiated just past point B using a small pressure pulse, $\pm P_o$. Both pressure pulses, the one in the +*z*-direction and the -*z*-direction, led to the same solution, indicating that there is only one statically stable equilibrium solution past point B. The result of the transient analysis is shown in Appendix E in Figs. E.33-E.36. Figure 4.5.10 shows the deformed shape at point C to have two half-waves in the loading direction. After point C there is a reduction in slope as the plate is continued to be compressed towards point D. As the plate is loaded past point C to point D, the geometric center of the plate does not deflect much, while the quarter locations deform out-of-plane, deepening the two half-waves in the loading direction until the analysis is terminated at point D. The plot on the right portion of Fig. 4.5.7 shows the enlarged view of the deflection of location II. In this plot the range of the vertical axis is reduced considerably so more detail is seen. As can be observed, after point B, there is a very small but nonzero out-of-plane deflection at the center of the laminate. Comparison of this result with its symmetric counterpart in Section 4.4.1 shows that the ultimate load carried at the point where the analysis is terminated is significantly less for this anti-symmetric laminate. Furthermore, the anti-symmetric laminate does not exhibit secondary buckling like its symmetric counterpart does. And most significantly, the anti-symmetric cross-ply laminate has only one statically stable equilibrium solution throughout the whole range of endshortening considered here. The lack of secondary buckling from a configuration with one half-wave in the loading direction to two half-waves in the loading direction is attributed to the

fact that after point B, the configuration already has two half-waves in the loading direction. This is a geometric effect, as the 16 in. by 16 in. plate exhibited secondary buckling.

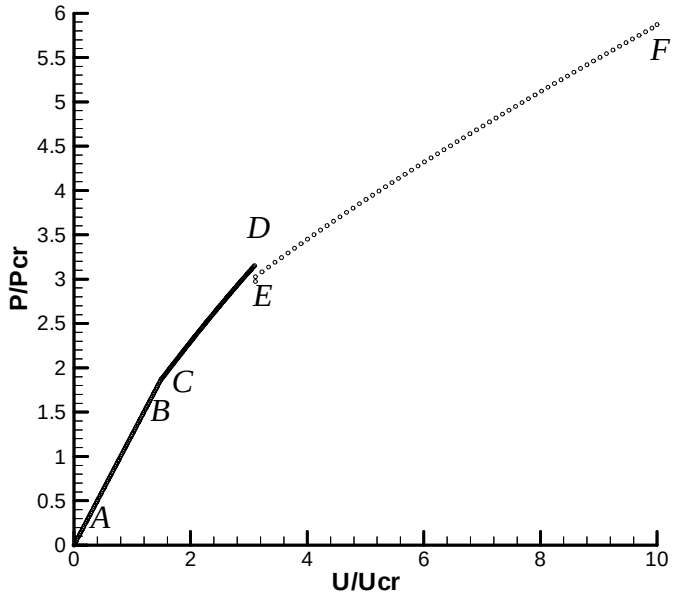

Fig. 4.5.1 Load response of a 16 in. by 16 in. $[0_4/90_4]_T$ laminate (CL-CL)

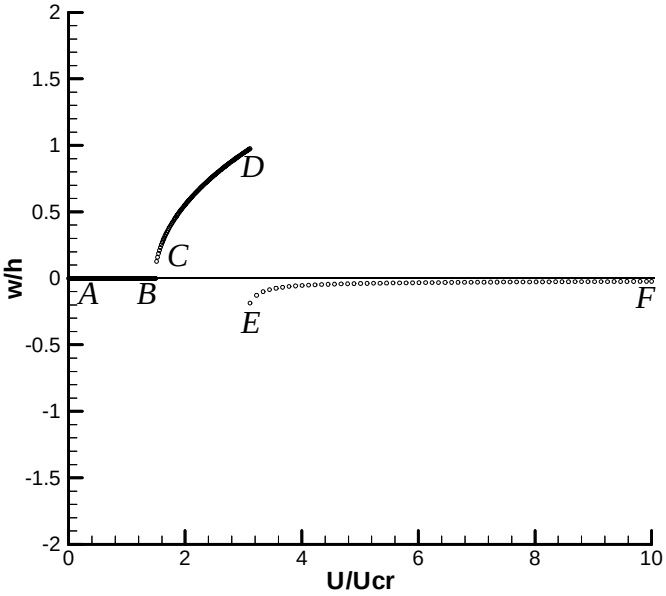

Fig. 4.5.2 Displacement response at II of a 16 in. by 16 in. $[0_4/90_4]_T$ laminate (CL-CL)

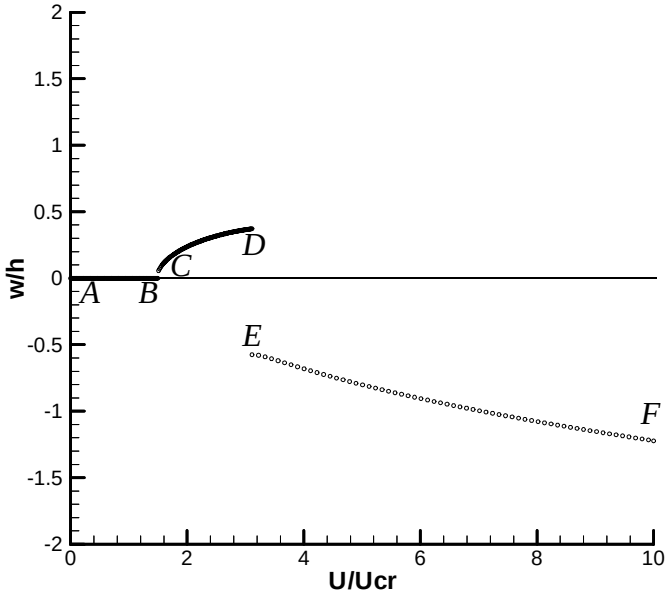

Fig. 4.5.3 Displacement response at III of a 16 in. by 16 in. $[0_4/90_4]_T$ laminate (CL-CL)

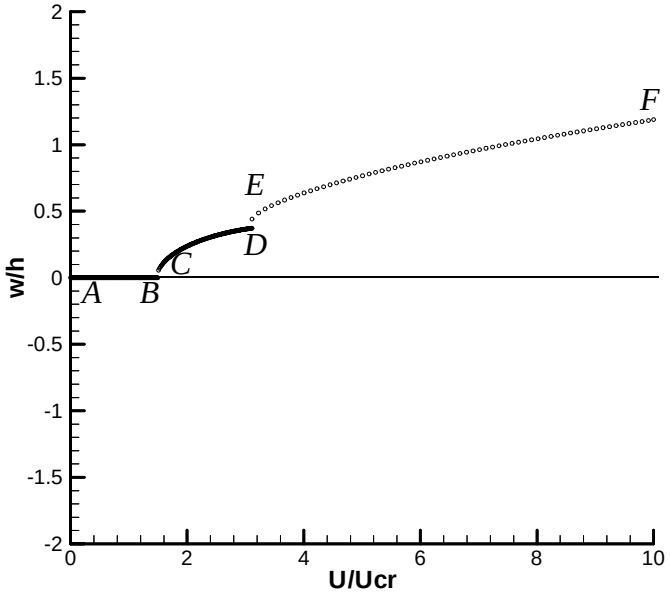

Fig. 4.5.4 Displacement response at I of a 16 in. by 16 in. $[0_4/90_4]_T$ laminate (CL-CL)

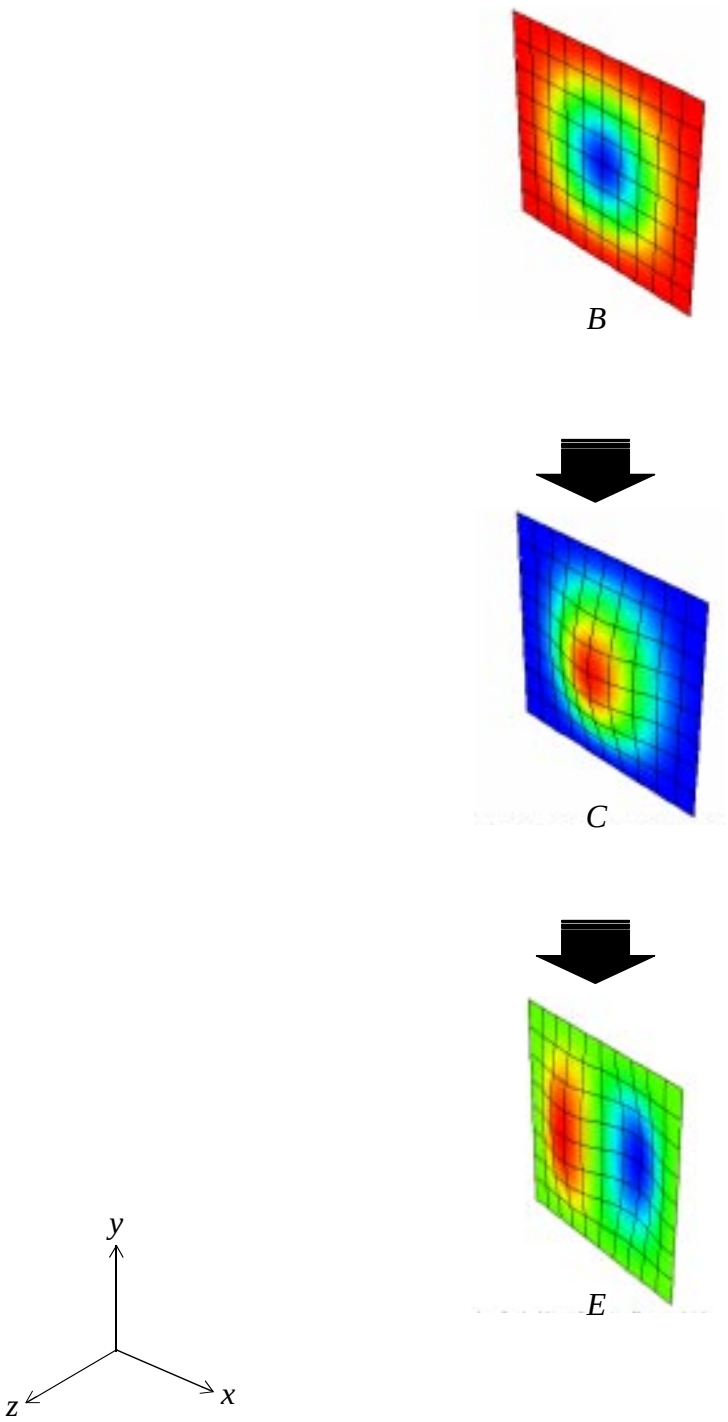

Fig. 4.5.5 Deformed shape flow chart for a 16 in. by 16 in. $[0_4/90_4]_T$ laminate (CL-CL)

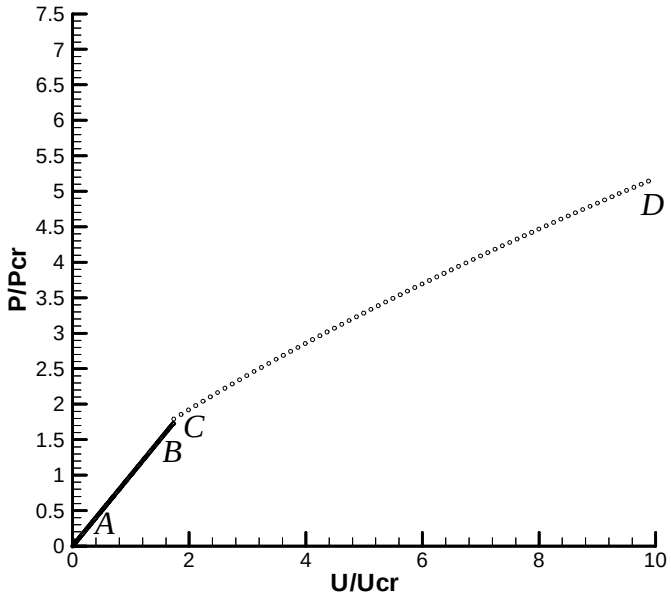

Fig. 4.5.6 Load response of a $[0_4/90_4]_T$ laminate (CL-CL)

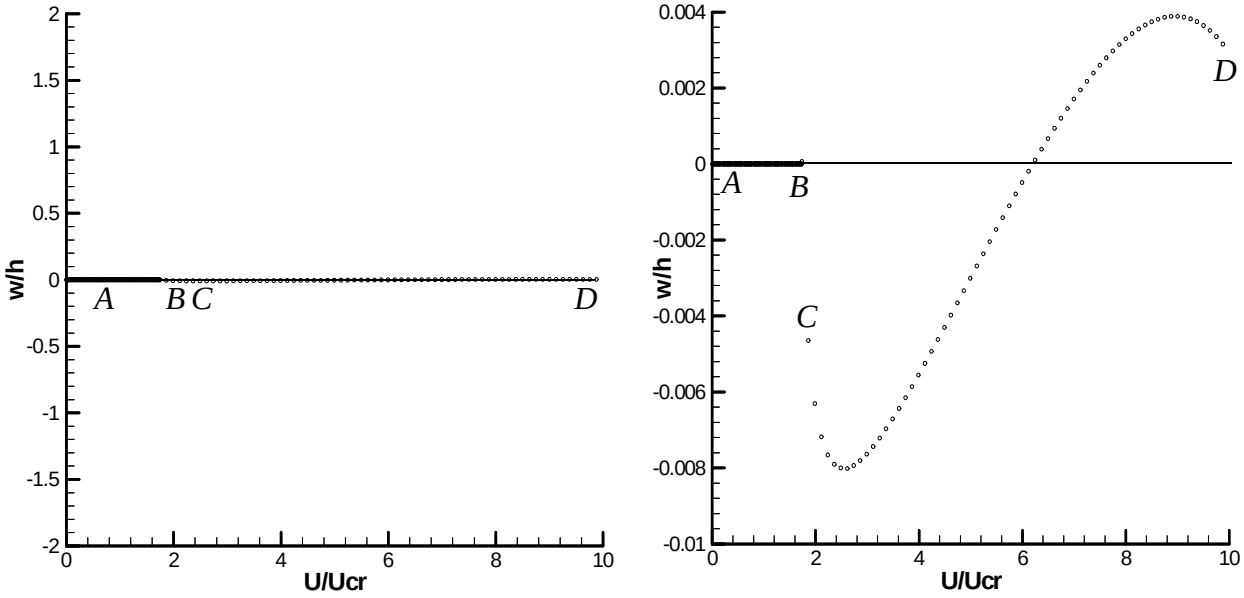

Fig. 4.5.7 Displacement response at II of a $[0_4/90_4]_T$ laminate (CL-CL)

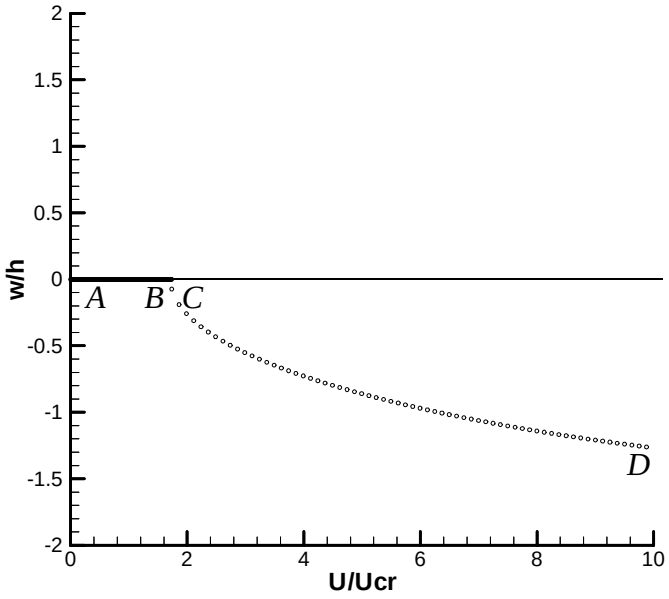

Fig. 4.5.8 Displacement response at III of a $[0_4/90_4]_T$ laminate (CL-CL)

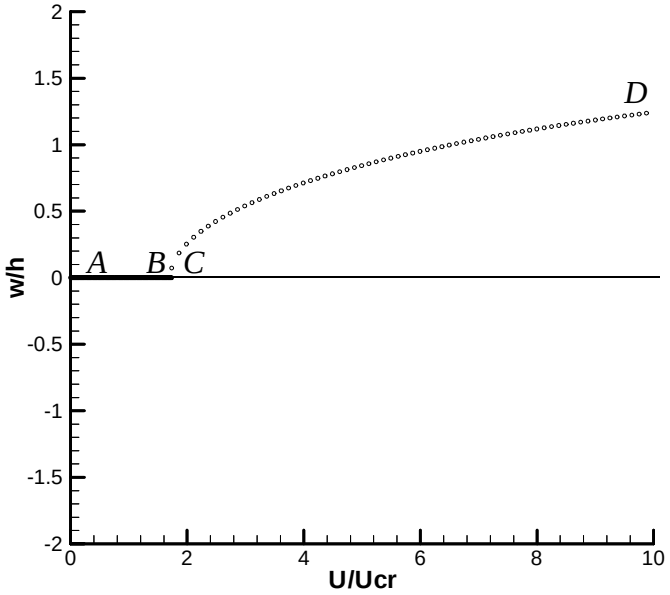

Fig. 4.5.9 Displacement response at I of a $[0_4/90_4]_T$ laminate (CL-CL)

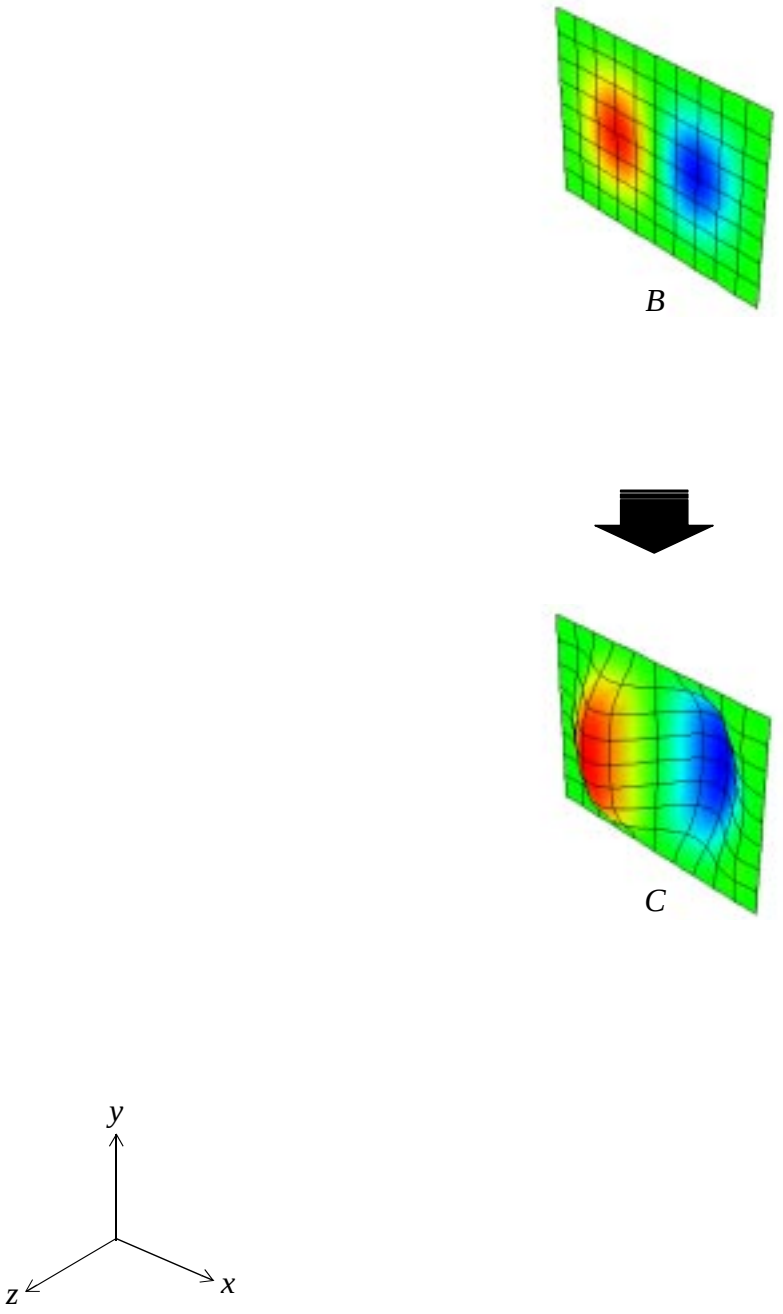

Fig. 4.5.10 Deformed shape flow chart for a $[0_4/90_4]_T$ laminate (CL-CL)

4.5.2 $[0_4/90_4]_T$ Clamped Ends and Simply-Supported Sides

This section discusses the buckling and postbuckling response of the same unsymmetric cross-ply laminate considered in the previous section, Section 4.5.1, but with clamped ends and simply-supported sides. Based on the work by Leissa [8], the laminate might be expected to exhibit out-of-plane displacements from the initial loading condition. Figure 4.5.11 shows the load vs. endshortening response of this laminate, with corresponding deflections at locations I, II and III shown in Figs. 4.5.12-4.5.14. By carefully examining the finite-element results, it can be recognized that there is a big difference between the response of this CL-SS case compared to the CL-CL case just discussed. For the CL-SS case the plate deforms out-of-plane a small amount from point A to past point B. There the plate becomes statically unstable. Figure 4.5.15 shows that the plate develops a shallow half-wave in the loading direction at point B. Compared to the computed prebuckling deformations that were dismissed as being due to numerical error in the finite-element code for the CL-CL case, the magnitude of the prebuckling deformations seen here indicate that these deformations are indeed real, and not numerical anomalies. Figure 4.5.16 shows the out-of-plane displacements for the CL-CL case and the CL-SS case at location II, from point A to a point just before point B. Despite the small magnitudes, it shows that the deflections in the CL-SS case are larger than those of the CL-CL case, particularly at U/Ucr approaching unity, indicating that the deflections in the CL-SS case are real. In comparison to the CL-CL case, the plate becomes unstable at a slightly lower value of endshortening at point B. Again, a dynamic transient analysis is initiated just beyond point B using a small pressure pulse in the +*z*- and -*z*-direction. Some of the results of this dynamic transient analysis from point B to point C are shown in Appendix E in Figs. E.37-E.40. The analyses show that all three locations (i.e., I, II, and III) move in the -*z*-direction, regardless of the direction of the pressure pulse, accompanied by a small drop in the load. This indicates that there is only one statically stable equilibrium solution at this point. Again this was an expected result due to the unsymmetric lamination of this cross-ply plate forcing the laminate to one side of the flat condition. After point B, for a very slight increase in endshortening, the out-of-plane displacement increases rapidly. Many attempts were made to determine if the gap between points B and C was actually closed. This did not seem to be the case. With the finite-element analysis it was not possible to have the endshortening values increase continuously. However, even using fine increments beyond point B, there appeared to be a jump to

point C. This underscores an important point: this particular unsymmetric laminate does not exhibit bifurcation. Further shortening of the plate from point C causes the shape to deepen, as shown in Fig. 4.5.15. Just past point D, the plate configuration becomes statically unstable again. As was the case for points beyond B on path AB, there are statically unstable equilibrium solutions past point D on path CD, making up the first of the two solutions at this point. The fact that this plate postbuckles is a significant difference compared with the the 16 in. by 20 in. CL-CL case seen in the previous section, Section 4.5.1, but it is more like the behavior of the 16 in. by 16 in. CL-CL case. Transient dynamic analyses are used at a point just past D with and without a pressure pulse. In all cases the results show that the only statically stable solution at this point is E. Figure 4.5.15 shows the deformed shape at point E to have one half-wave perpendicular to the loading direction, and something like one half-wave in the loading direction. At point E the out-of-plane deflections at locations I and II have significant amplitudes, while location III has little amplitude. The one half-wave type shape in the loading direction is not symmetric with respect to the center of the laminate. Appendix E in Figs. E.41-E.44 shows the results of the dynamic transient analysis from point D to E. As the plate is further shortened beyond point E to point F, the shape develops smoothly into a shape that looks more like two half-waves in the loading direction, as shown by the displacements of the two quarter locations, locations I and III. Note again that the deflection of the center of the plate, location II, is not zero, and the deflections at locations I and III are not equal in magnitude. The ultimate load carried at the point where the analysis is terminated is less than that carried by the CL-CL case.

The effect of mesh density on the response of this case is investigated by recomputing the problem using a model with four times the number of elements compared to the nominal model. Appendix B, in Figs. B.5-B.8, shows the load vs. endshortening and endshortening vs. out-of-plane displacements for the same problem using the refined mesh model. It is seen that that the difference in results using the two mesh densities is indiscernible. As a brief side bar, the response of the same plate due to a CL-SS boundary condition that does not restrain the *v*-displacements along the sides is investigated. These are the boundary conditions most often used in the laboratory to study the behavior of plates. Appendix C, in Figs. C.4-C.6, shows that the response varies significantly from the case where the *v*-displacements along the sides have been restrained. The difference in response is remarkable. Rather than initially remaining almost flat, the laminate deforms out-of-plane from initial loading, point A, until the analysis is terminated. The plate

deforms out-of-plane with one half-wave in the loading direction and one half-wave perpendicular to the loading direction. There is only one solution throughout the range of endshortening. The load vs. endshortening relation exhibits nonlinear behavior over the range of endshortening. This is attributed to the fact that Poisson-induced deformations are no longer restricted along the sides. The Poisson-induced deformations along the sides reduce the inplane loads in the *y*-direction that would have otherwise developed to cause a state of biaxial compression. The biaxial stress state created by restricting the *v*-displacements along the sides causes the plate to undergo the deformation responses seen in Figs. 4.5.11-4.5.14 and absent in Figs. C.4-C.6.

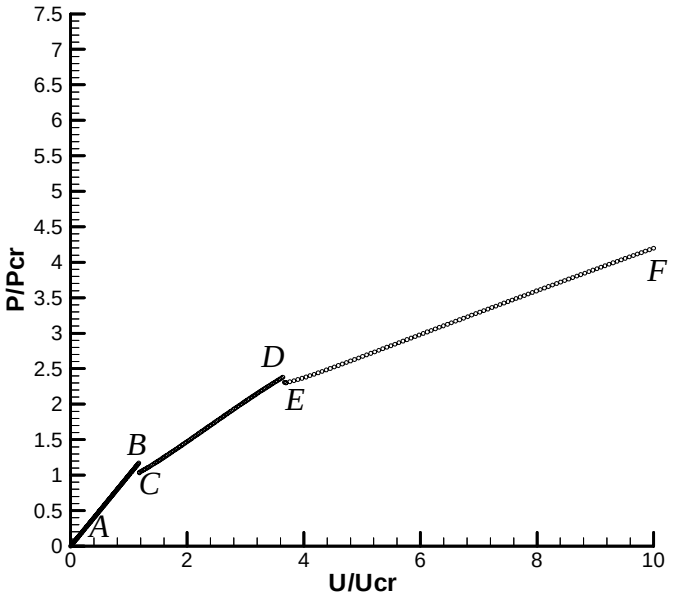

Fig. 4.5.11 Load response of a $[0_4/90_4]_T$ laminate (CL-SS)

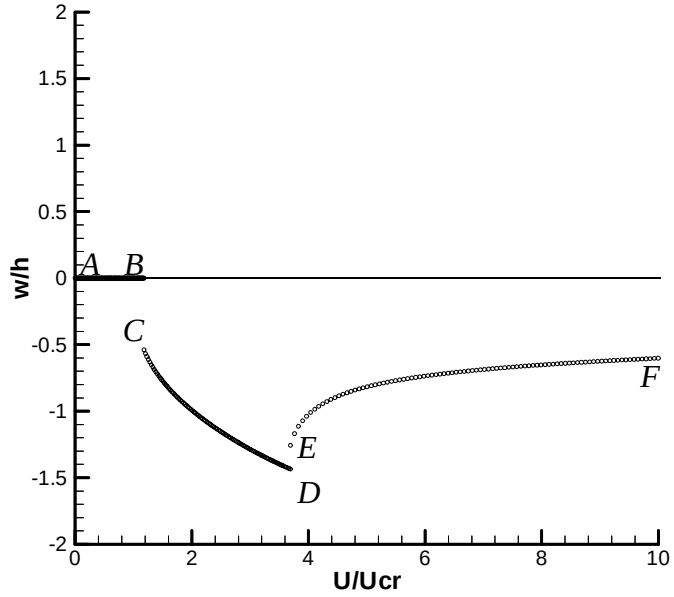

Fig. 4.5.12 Displacement response at II of a $[0_4/90_4]_T$ laminate (CL-SS)

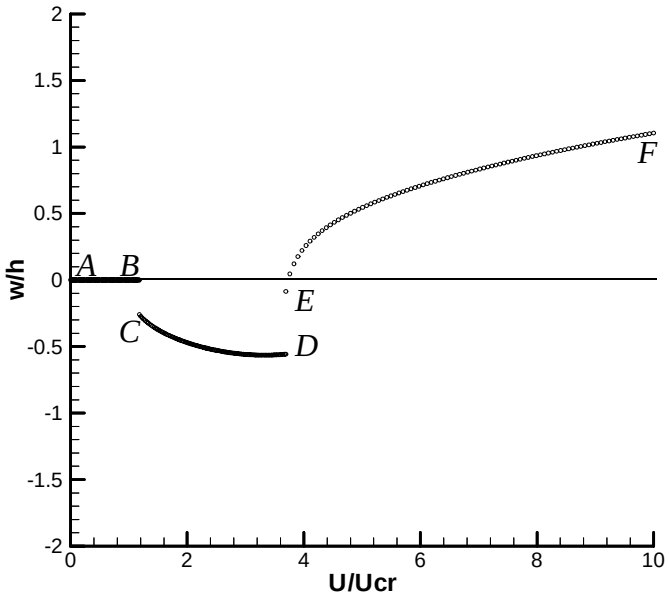

Fig. 4.5.13 Displacement response at III of a $[0_4/90_4]_T$ laminate (CL-SS)

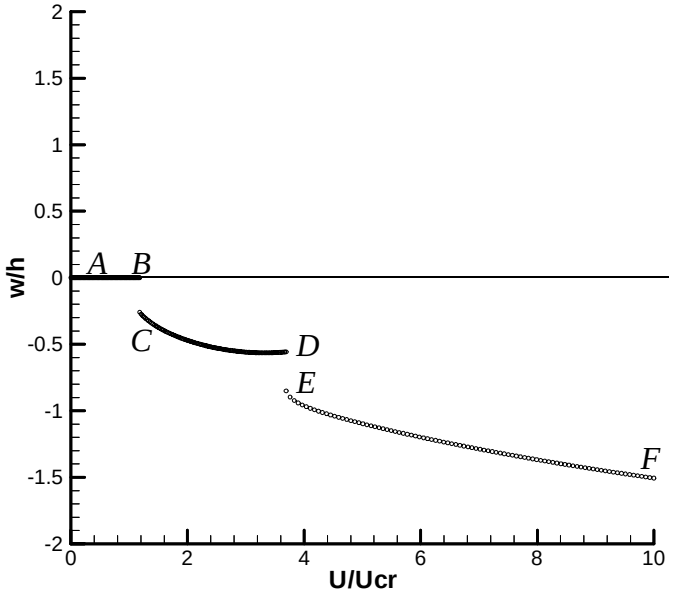

Fig. 4.5.14 Displacement response at I of a $[0_4/90_4]_T$ laminate (CL-SS)

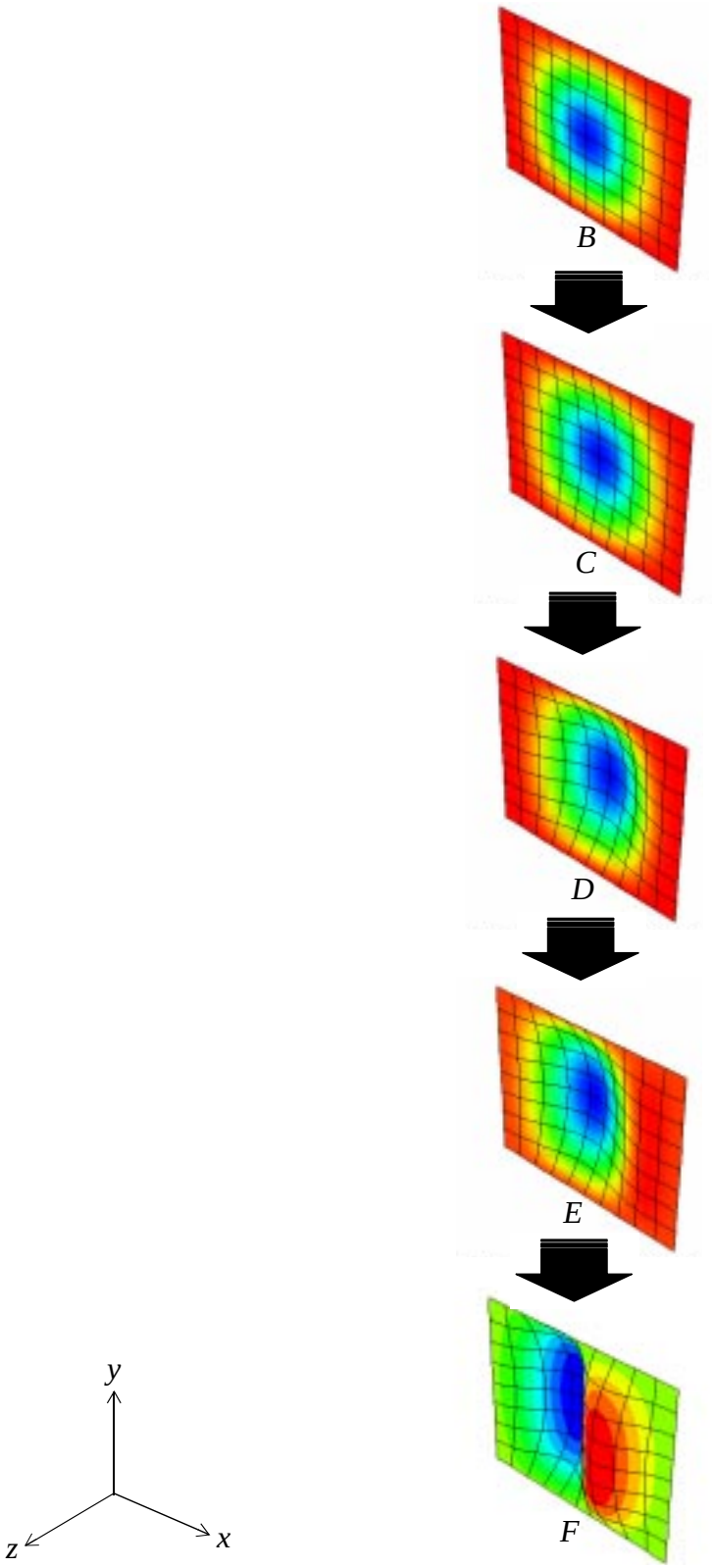

Fig. 4.5.15 Deformed shape flow chart for a $[0_4/90_4]_T$ laminate (CL-SS)

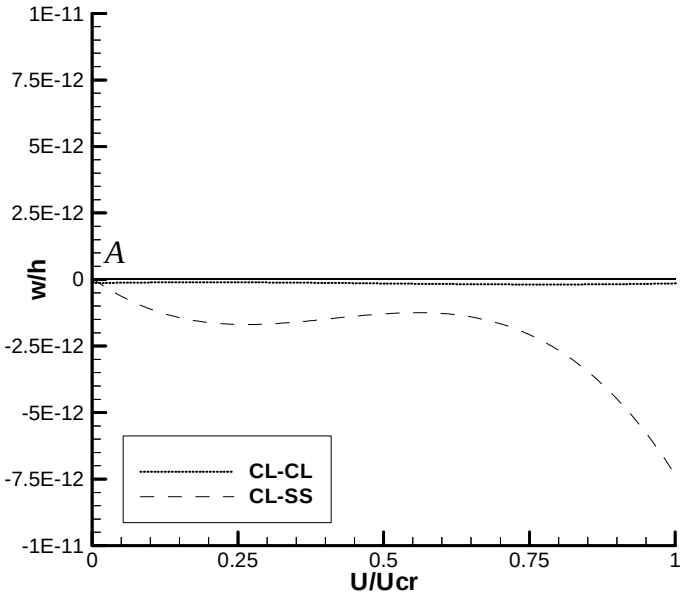

Fig. 4.5.16 Displacement response at II of a $[0_4/90_4]_T$ laminate

4.5.3 $[0_4/90_4]_T$ Simply-Supported Ends and Simply-Supported Sides

This section discusses the deformations of the unsymmetric cross-ply laminate under uniaxial compression with simply-supported sides and ends. Figures 4.5.17-4.5.20 show the load response and the corresponding displacement response of the plate at locations I, II, and III. Immediately, it can be seen that the response of this case varies significantly with respect to the CL-CL and CL-SS cases. The plate deforms immediately out-of-plane and develops one half-wave in the loading direction and one half-wave perpendicular to the loading direction as it is compressed from point A. The load response behaves nonlinearly from the onset, without the relatively linear segments seen in the CL-CL and CL-SS cases. As the plate is continually compressed along path AB and then BC, the deformed shape transitions smoothly, without classic buckling behavior, into shape C shown in Fig. 4.5.21. The plate geometry makes a transition from the one half-wave shape to a three half-waves shape without primary or secondary buckling. At a point past C, the plate becomes statically unstable. Dynamic transient analyses are initiated with and without a pressure pulse. All cases showed that the only statically stable shape at this value of endshortening is point D. Results of the dynamic transient analysis are shown in Appendix E in Figs. E.45-E.48. Figure 4.5.21 shows that the shape jumps from the three half-waves in the loading direction to a shape with three deeper half-waves in the loading direction, characterized by the now positive displacement of the center location, location II. Further compression of the plate beyond point D leads to a further deepening of this shape until the analysis is terminated at point E. The ultimate load carried at the point where the analysis is terminated is significantly lower than for the other two cases considered. Furthermore, compared to its symmetric counterpart with SS-SS boundary conditions, the deformed shape and buckling behaviors differ significantly. The anti-symmetric cross-ply laminate changes configuration only once. Also, over much of the endshortening range there is only one statically stable equilibrium solution path for the anti-symmetric laminate, while there are two statically stable solution paths for its symmetric counterpart.

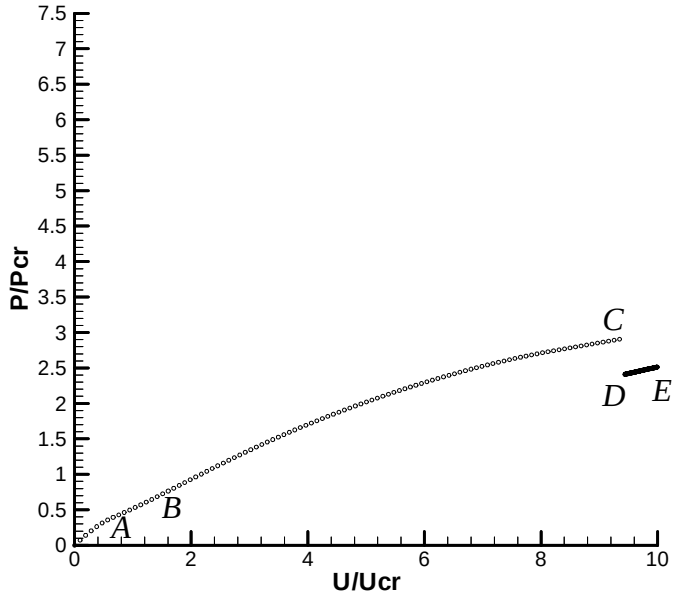

Fig. 4.5.17 Load response of a $[0_4/90_4]_T$ laminate (SS-SS)

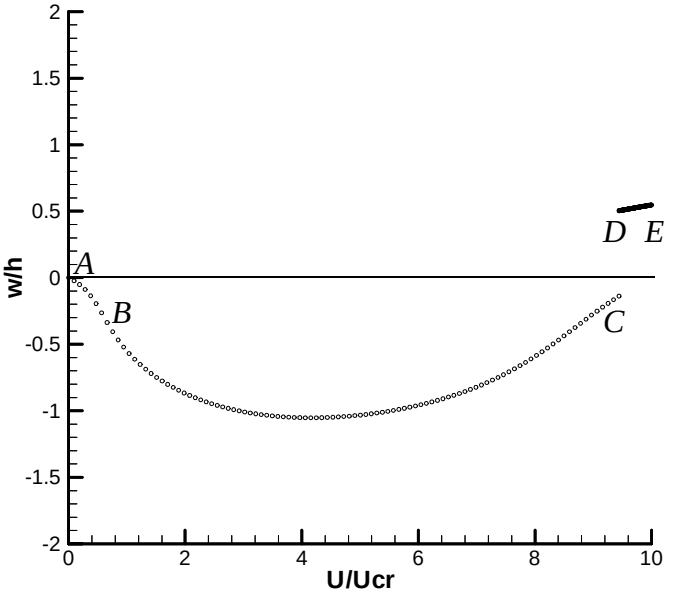

Fig. 4.5.18 Displacement response at II of a $[0_4/90_4]_T$ laminate (SS-SS)

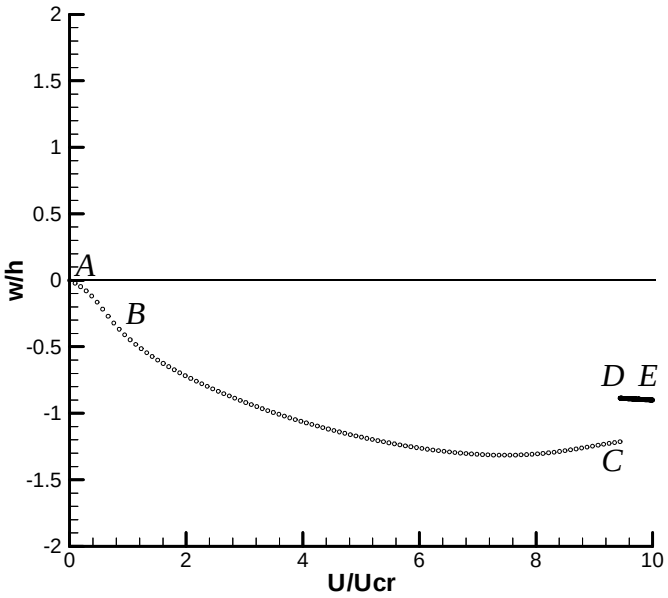

Fig. 4.5.19 Displacement response at III of a $[0_4/90_4]_T$ laminate (SS-SS)

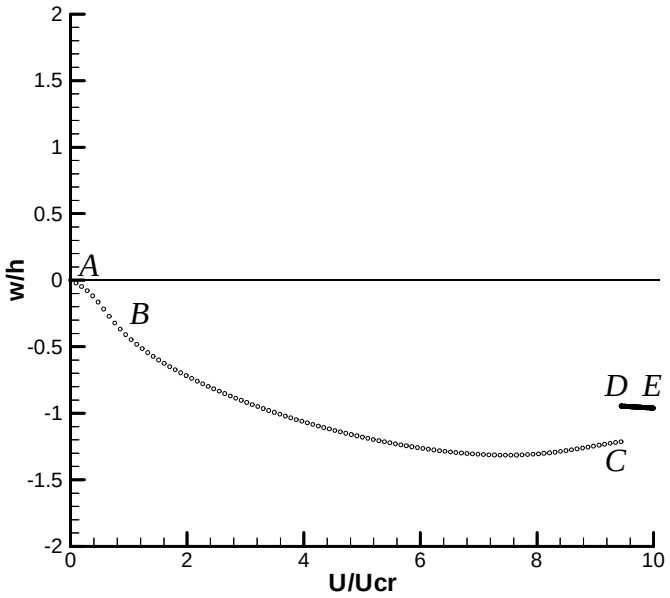

Fig. 4.5.20 Displacement response at I of a $[0_4/90_4]_T$ laminate (SS-SS)

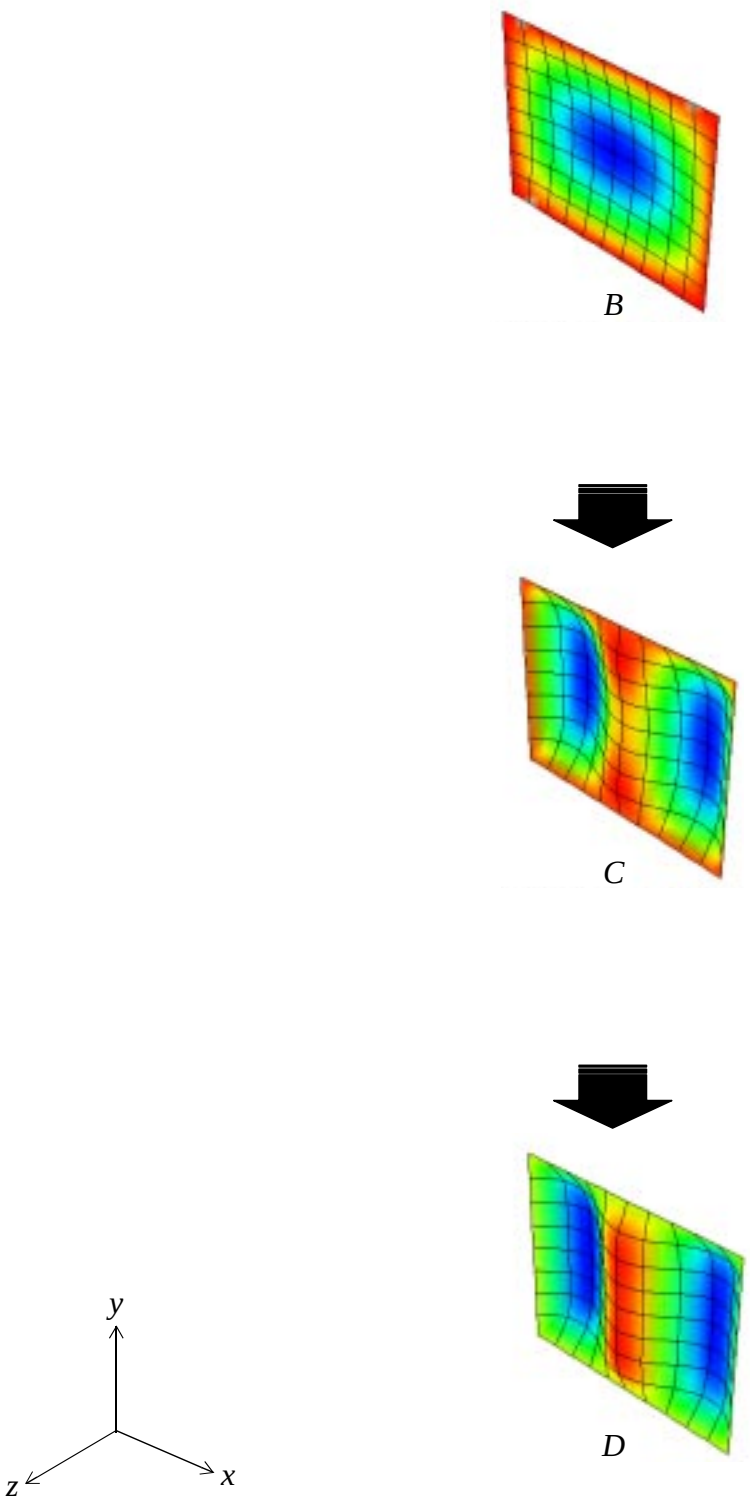

Fig. 4.5.21 Deformed shape flow chart for a $[0_4/90_4]_T$ laminate (SS-SS)

4.6 $[\pm 30_2]_S$ Symmetric Angle-ply

This chapter discusses the deformations of a $[\pm 30_2]_S$ symmetric angle-ply laminate due to axial endshortening. Unlike the cross-ply laminates considered in Sections 4.4 and 4.5, angle-ply laminates are constructed of layers oriented at angles other than 0° or 90°. The particular laminates being considered in this section and the following section are angle-ply laminates constructed with +30° and -30° layers. Like the previous sections, three boundary condition combinations will be evaluated, namely CL-CL, CL-SS, and SS-SS. The $[\pm 30_2]_S$ angle-ply will serve as the symmetric counterpart for comparison with the anti-symmetric angle-ply laminate to be discussed in Section 4.7. For all of the following angle-ply and generally unsymmetric cases discussed in Sections 4.6-4.9, the endshortening has been normalized by the critical value predicted by the 'classic SS-SS' eigenvalue problem for the $[\pm 30_2]_S$ laminate, 0.000493 in. The associated load, P_{cr}, is 99.8 lbs.

4.6.1 $[\pm 30_2]_S$ Clamped Ends and Clamped Sides

The first boundary condition combination applied to the $[\pm 30_2]_S$ symmetric angle-ply laminate is that of clamped ends and clamped sides. Figure 4.6.1 shows the load vs. endshortening response. Out-of-plane displacement vs. endshortening responses at locations I, II, and III are shown in Figs. 4.6.2-4.6.4. Figures 4.6.2-4.6.4 show that the plate remains perfectly flat until it is compressed beyond B, at which point the flat configuration becomes statically unstable. The flat solution continues past point B on path AB. At a point just past B, a dynamic transient analysis is initiated using a small pressure pulse, $\pm P_o$, perpendicular to the plate. The results of this transient analysis are shown in Appendix F in Figs. F.1-F.4. Figure 4.6.5 illustrates the deformed shapes of the plate at selected points from Figs. 4.6.1-4.6.4. The figure shows that the statically stable equilibrium solution at point C has one half-wave in the loading direction and one half-wave perpendicular to the loading direction. It can be seen from Fig. 4.6.1 that the slope of the load response is reduced after the plate buckles at point B. Furthermore, the figure shows that the response is slightly nonlinear as the plate 'softens' as it is further compressed towards point D. Figures 4.6.2-4.6.4 show that all three locations monotonically deform out-of-plane, deepening the one half-wave configuration seen at point C as point D is approached. Interestingly enough, unlike the CL-

CL aluminum plate or the $[0_2/90_2]_S$ laminate, this plate does not exhibit snap-through after classic bifurcation.

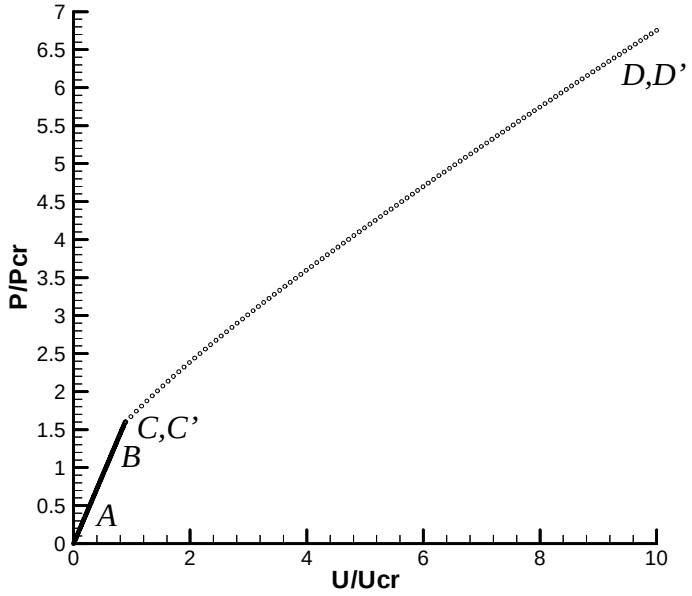

Fig. 4.6.1 Load response of a $[\pm 30_2]_S$ laminate (CL-CL)

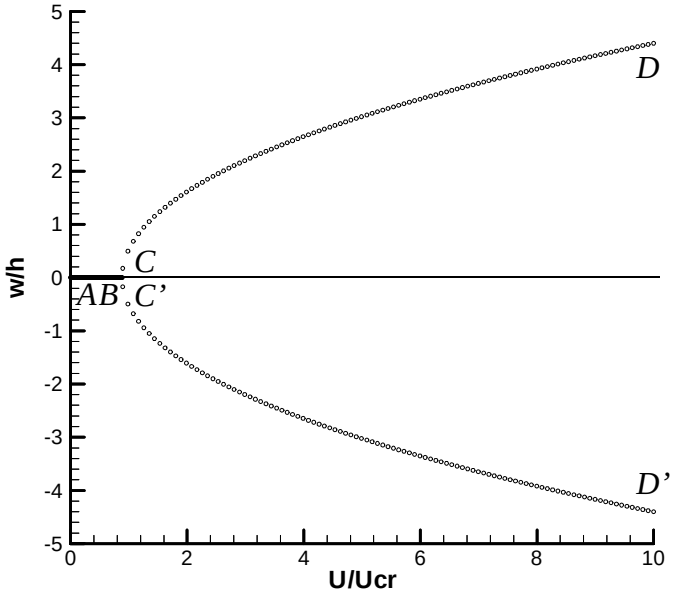

Fig. 4.6.2 Displacement response at II of a $[\pm 30_2]_S$ laminate (CL-CL)

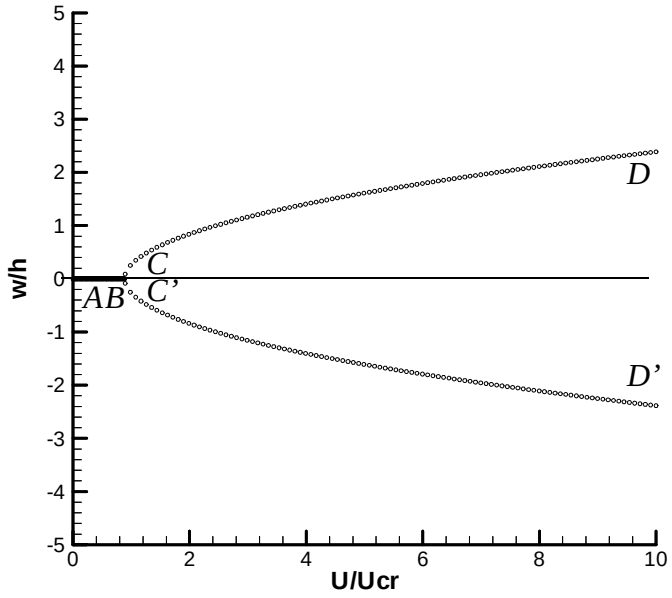

Fig. 4.6.3 Displacement response at III of a $[\pm 30_2]_S$ laminate (CL-CL)

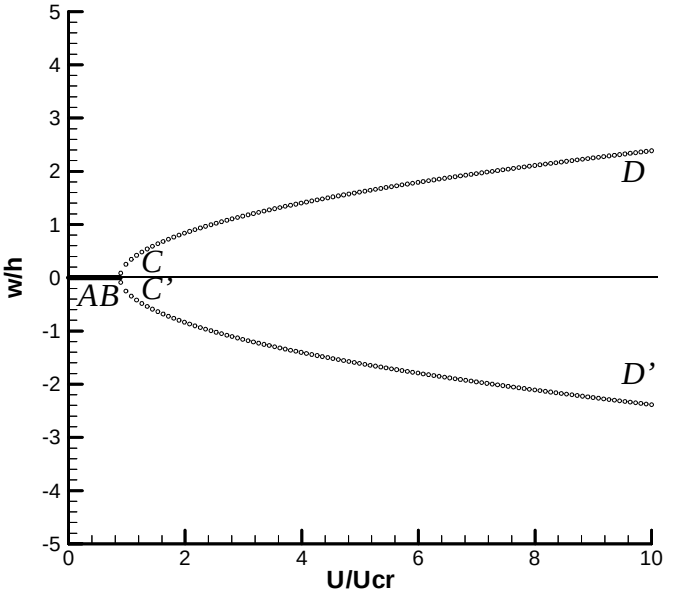

Fig. 4.6.4 Displacement response at I of a $[\pm 30_2]_S$ laminate (CL-CL)

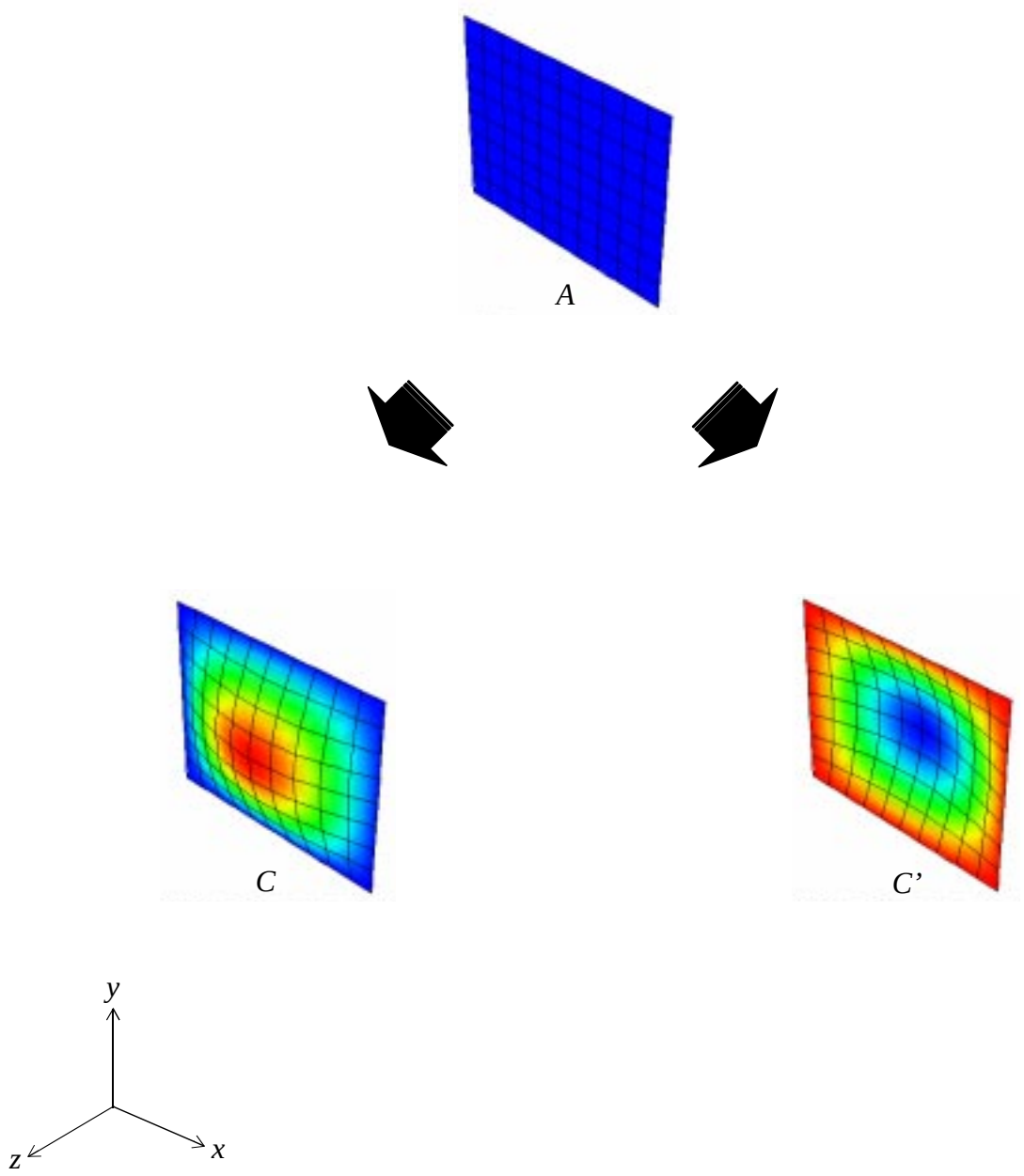

Fig. 4.6.5 Deformed shape flow chart for a $[\pm 30_2]_S$ laminate (CL-CL)

4.6.2 $[\pm 30_2]_S$ Clamped Ends and Simply-Supported Sides

This section discusses the deformations of the $[\pm 30_2]_S$ symmetric angle-ply laminate with clamped ends and simply-supported sides. Figure 4.6.6 illustrates the load vs. endshortening response, while Figs. 4.6.7-4.6.9 show the out-of-plane displacements vs. endshortening response at locations I, II, and III. Like the previous case, the plate remains initially flat as it is compressed from point A to B. There are statically unstable equilibrium solutions on path AB past point B, however they are not shown here. Compared to the CL-CL case discussed in Section 4.6.1, the SS condition along the sides add a degree of freedom to the plate, effectively reducing the overall structural stiffness. This effect is observed by the fact that the plate buckles at a lower value of endshortening when compared to the CL-CL case. Furthermore, Fig. 4.6.6 shows that the buckling load at point B is lower than that at point B for the CL-CL case, Fig. 4.6.1. At the point just past B, a dynamic transient analysis is employed again using small pressure pulses, $\pm P_o$, perpendicular to the plate. The response of the plate during the transient dynamic analysis is shown in Appendix F in Figs. F.5-F.8. Figure 4.6.10 illustrates the deformed shape of the plate at point C. It shows that the statically stable equilibrium solution at point C has one half-wave in the loading direction and one half-wave perpendicular to the loading direction. From this statically stable point at point C the loading is continued until the analysis is terminated at point D. Figures 4.6.7-4.6.9 show that the plate continues to deform out-of-plane, deepening the one half-wave shape seen at point C. Figure 4.6.6 shows that slope of the load vs. endshortening relation is reduced after buckling at point B. It is interesting to note that the load response remains relatively linear without the postbuckling nonlinear ‘softening’ that was observed in the CL-CL case, Fig. 4.6.1. It is also noted that the ultimate load carried at point D is less than that carried at point D for the CL-CL case. Furthermore, the out-of-plane deformation at the center of the plate, location II, is about the same for both cases at point D, but the out-of-plane displacements at locations I and III are slightly less than those at the same point for the CL-CL case.

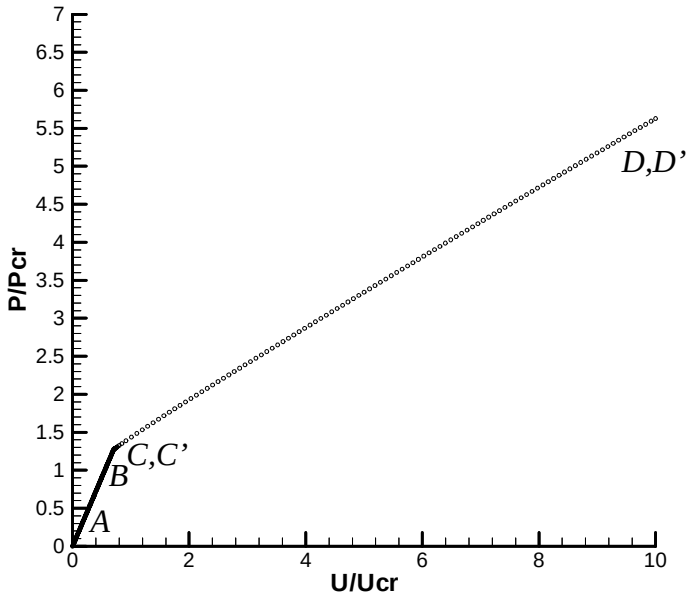

Fig. 4.6.6 Load response of a $[\pm 30_2]_S$ laminate (CL-SS)

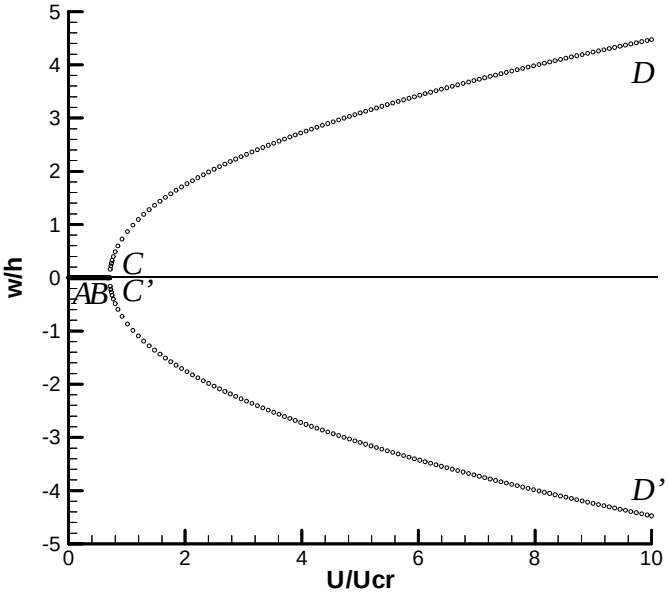

Fig. 4.6.7 Displacement response at II of a $[\pm 30_2]_S$ laminate (CL-SS)

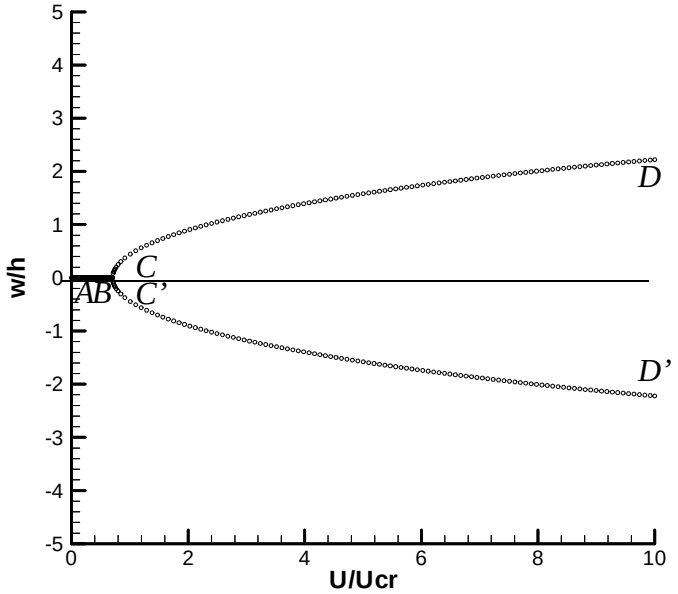

Fig. 4.6.8 Displacement response at III of a $[\pm 30_2]_S$ laminate (CL-SS)

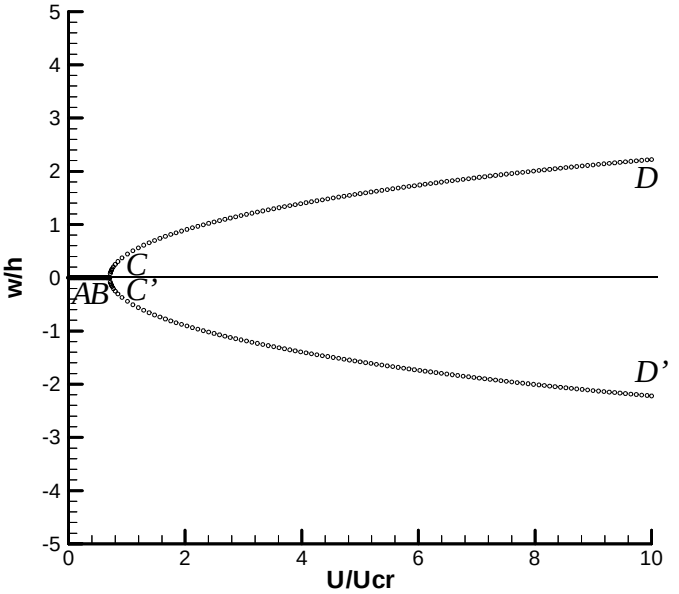

Fig. 4.6.9 Displacement response at I of a $[\pm 30_2]_S$ laminate (CL-SS)

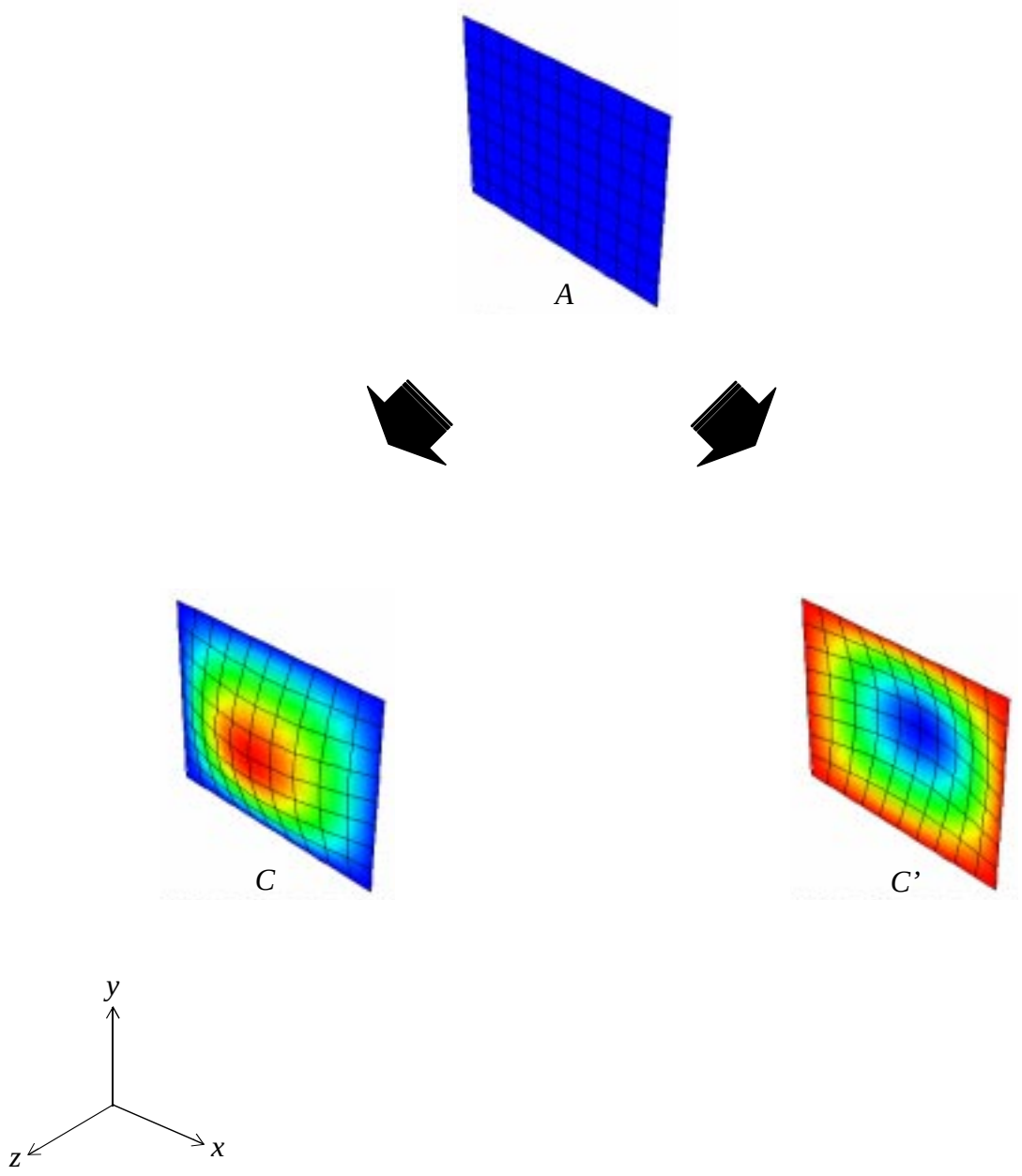

Fig. 4.6.10 Deformed shape flow chart for a $[\pm 30_2]_S$ laminate (CL-SS)

4.6.3 $[\pm 30_2]_S$ Simply-Supported Ends and Simply-Supported Sides

This section discusses the response of a $[\pm 30_2]_S$ symmetric angle-ply laminate with simply-supported ends and simply-supported sides. Figure 4.6.11 shows the load vs. endshortening response, while Figs. 4.6.12-4.6.14 illustrate the out-of-plane displacements vs. endshortening response at locations I, II, and III. Like the previous two boundary condition cases just discussed in Sections 4.6.1 and 4.6.2, the plate remains initially flat as it is compressed from point A to B. At a point just past B, the flat configuration becomes statically unstable. Compared to the CL-CL and CL-SS boundary condition cases, the SS conditions along the ends and sides add even more degrees of freedom to the plate, effectively reducing the overall structural stiffness. This effect can be observed in Figs. 4.6.11-4.6.14 by the fact that the plate buckles at a lower value of endshortening when compared to the other two cases. Figure 4.6.11 shows that the buckling load at point B is lower than that at point B of the CL-SS case, Fig. 4.6.6, and significantly less than that of the CL-CL case, Fig. 4.6.1. It is again noted that there are statically unstable equilibrium solutions past point B on path AB, but they are not shown in this figure. At the point just past B, a dynamic transient analysis is employed using a small pressure pulse, $\pm P_o$. The details of the response of the plate during the transient dynamic analysis are shown in Appendix F, Figs. F.9-F.12. Figure 4.6.15 illustrates the deformed shape of the plate corresponding to selected points on Figures 4.6.11-4.6.14. Again, it shows that the statically stable equilibrium solution at point C has one half-wave in the loading direction and one half-wave perpendicular to the loading direction. The plate is further compressed from this statically stable configuration at point C until the analysis is terminated at point D. It can be seen from Figs. 4.6.12-4.6.14 that the plate continues to deform out-of-plane, deepening the one half-wave shape. Figure 4.6.11 shows that slope of the load vs. endshortening relation is significantly reduced after point B. Like the CL-SS case, the load response remains relatively linear without the nonlinear ‘softening’ that was observed in the CL-CL case, Fig. 4.6.1. The ultimate load carried at point D is less than that carried at point D for the CL-SS, Fig. 4.6.6, and significantly less than the ultimate load carried at the same point for the CL-CL case, Fig. 4.6.1. It should be noted that the out-of-plane deformation at point D at the center of the plate, location II, is very close to being the same for all three cases. Most interestingly, the out-of-plane displacements at locations I and III are largest at point D for the SS-SS case. This response is in line with the fact that the boundary layer length in the *x*-direction created by the

clamped conditions at the ends serve to reduce the out-of-plane deformations at the two quarter locations, I and III, closest to the clamped ends. The removal of the clamped end conditions for the SS-SS case leads to a reduction of the boundary layer length, allowing the two quarter locations to deform further out-of-plane with respect to the CL-CL and CL-SS cases.

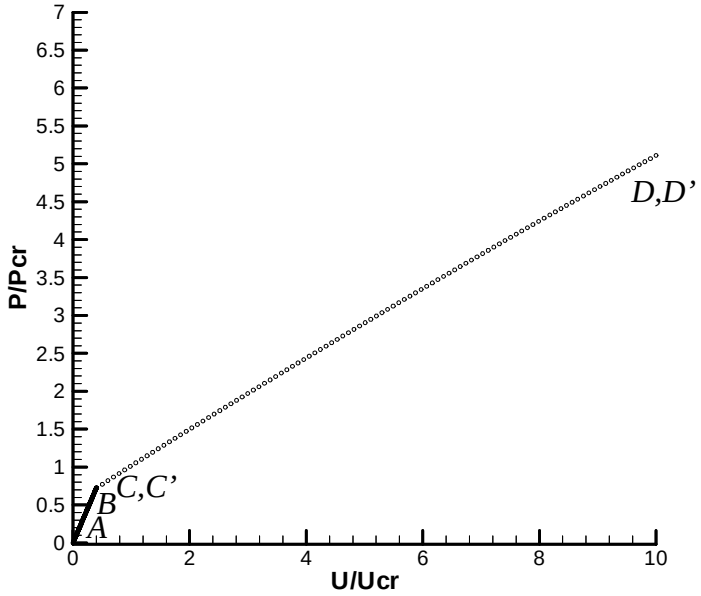

Fig. 4.6.11 Load response of a $[\pm 30_2]_S$ laminate (SS-SS)

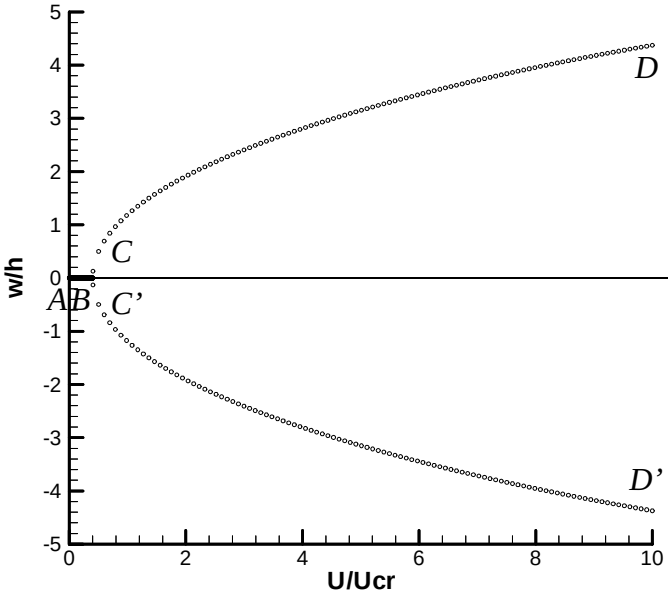

Fig. 4.6.12 Displacement response at II of a $[\pm 30_2]_S$ laminate (SS-SS)

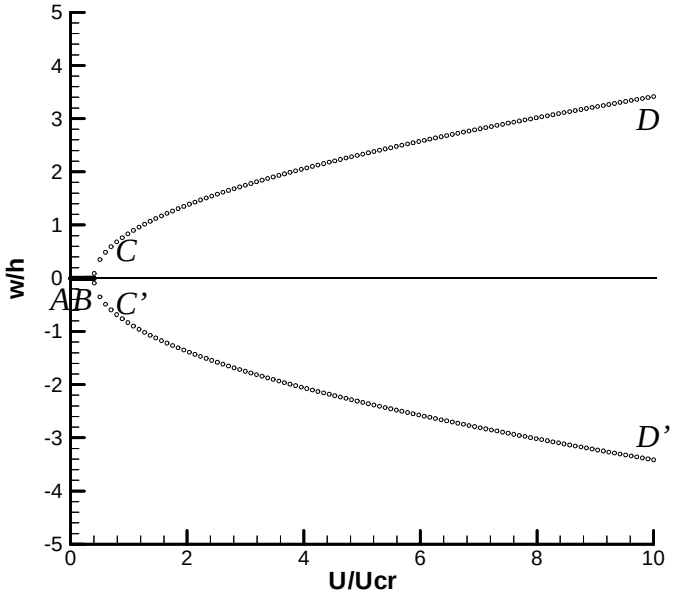

Fig. 4.6.13 Displacement response at III of a $[\pm 30_2]_S$ laminate (SS-SS)

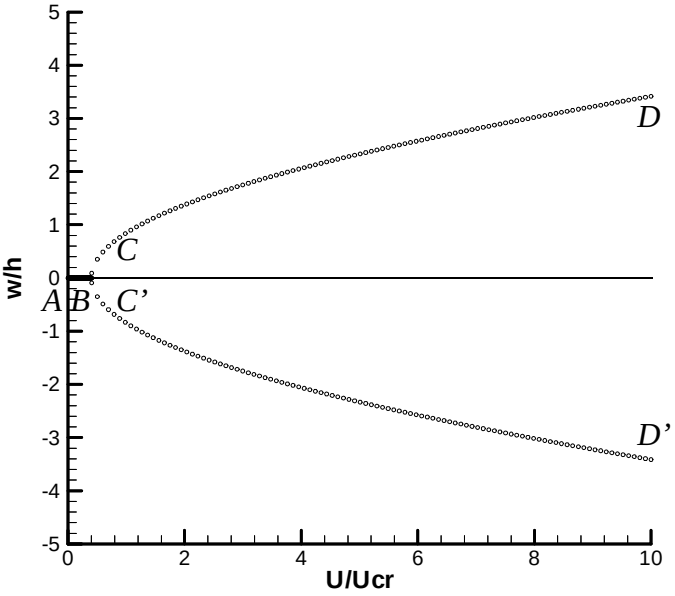

Fig. 4.6.14 Displacement response at I of a $[\pm 30_2]_S$ laminate (SS-SS)

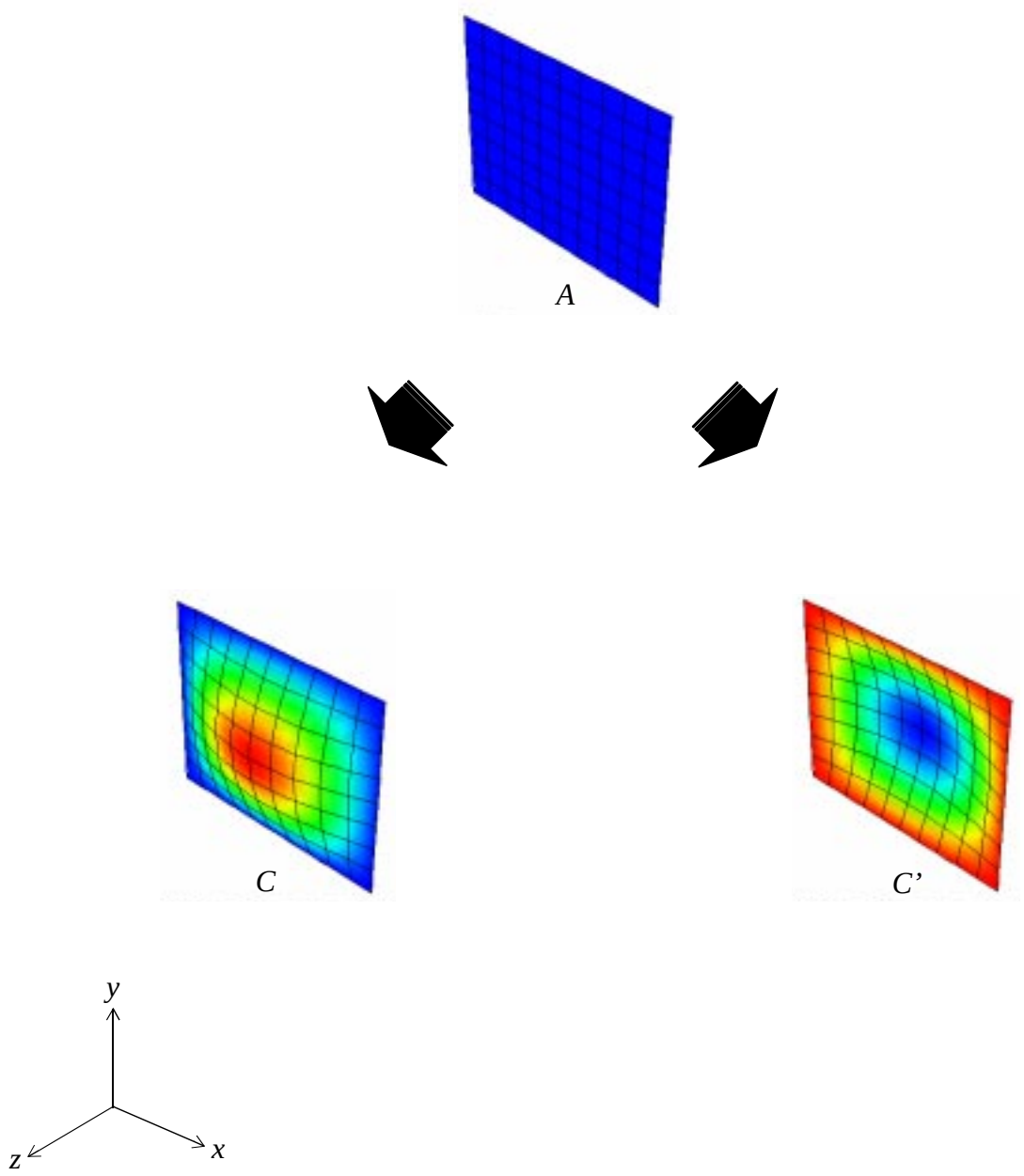

Fig. 4.6.15 Deformed shape flow chart for a $[\pm 30_2]_S$ laminate (SS-SS)

4.7 $[+30_4/-30_4]_T$ Anti-symmetric Angle-ply

Section 4.7 discusses the deformations of an anti-symmetric angle-ply laminate. Unlike the anti-symmetric cross-ply laminate, the layers to one side of the geometric midplane are not orthogonal to the layers on the other side. In this case, the layers on one side are oriented at +30° while the layers on the other side are oriented at -30°, making up the $[+30_4/-30_4]_T$ laminate and resulting in a 60° angle between fiber directions. This laminate is the anti-symmetric counterpart to the $[\pm 30_2]_S$ laminate discussed in Section 4.6. Results in this section will serve as a comparison to those of the previous section. Therefore, the deformation response for the $[+30_4/-30_4]_T$ laminate will be evaluated with the same three boundary condition combinations considered previously in this chapter. Again, these boundary condition combinations are, CL-CL, CL-SS, and SS-SS.

4.7.1 $[+30_4/-30_4]_T$ Clamped Ends and Clamped Sides

This section discusses the deformations of a $[+30_4/-30_4]_T$ laminate in axial endshortening with clamped ends and clamped sides. Figure 4.7.1 shows the load vs. endshortening response of the laminate, with corresponding out-of-plane deformations at locations I, II and III shown in Figs. 4.7.2-4.7.4. Based on the results from Leissa [8], the plate should remain perfectly flat from the onset until past point B, where the flat configuration loses its static stability. There are statically unstable equilibrium solutions, not shown, that continue past point B on path AB. Figure 4.7.5 illustrates the deformed shape of the plate at various points along the statically stable equilibrium solution paths. It shows that there are very small deformations prior to buckling at point B, however, the relatively small magnitudes of this deformation imply that this is not a real deformation, but rather a manifestation of the numerical errors inherent in the finite-element method. At a point just past B, a dynamic transient analysis was initiated using a small pressure pulse, $\pm P_o$, to induce motion of the plate. The results of this transient analysis is shown in Appendix F, Figs. F.13-F.16. The configuration at point C has one half-wave in the loading direction and one half-wave perpendicular to the loading direction. From point C, the plate is again axially compressed until the analysis is terminated at point D. Figure 4.7.1 shows that the postbuckling load response is nonlinear with a noticeable change in slope occurring past U/Ucr of eight. Figures 4.7.2-4.7.4

show that the plate continues to deform out-of-plane as it is loaded past point C towards point D, deepening the one half-wave shapes. However, these figures also show a change of slope past U/Ucr of eight, like the load response of Fig. 4.7.1. Figure 4.7.2 shows that the geometric center, location II, begins to flatten, then the out-of-plane displacement decreases slightly in magnitude. Figures 4.7.3 and 4.7.4 show that the two quarter locations I and III increase in out-of-plane displacements. This may imply that the plate is deforming towards a new configuration with three half-waves in the loading direction.

Comparing the load response of this case with its symmetric counterpart in Section 4.6.1, it can be observed that the anti-symmetric angle-ply buckles at a lower value of endshortening at a lower load. The postbuckling response is similar except for the nonlinear response observed in the unsymmetric case at U/Ucr of eight, Fig. 4.7.1. It is further noted that the ultimate load carried at point D is higher for the symmetric laminate, Fig. 4.6.1, than for the anti-symmetric laminate. Comparing the displacement responses at the geometric center, Figs. 4.7.2 vs. 4.6.2, it can be seen that the symmetric laminate has a larger magnitude of out-of-plane displacement at point D. In contrast, the out-of-plane displacements of the two quarter locations, Figs. 4.7.3-4.7.4 vs. Figs. 4.6.3-4.6.4, show that the maximum out-of plane displacements at point D are smaller for the symmetric laminate compared to the anti-symmetric counterpart.

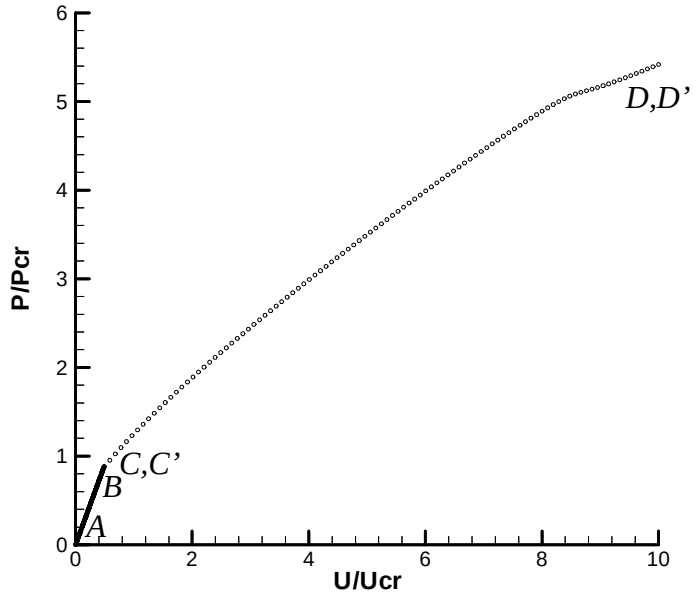

Fig. 4.7.1 Load response of a $[+30_4/-30_4]_T$ laminate (CL-CL)

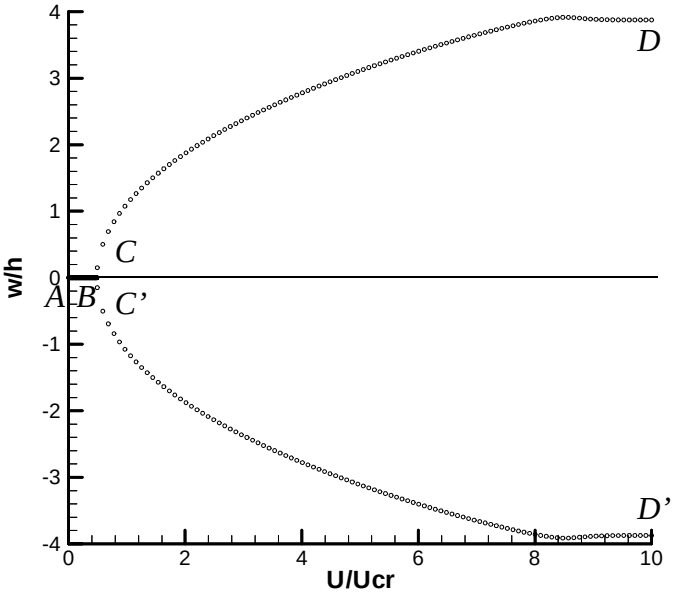

Fig. 4.7.2 Displacement response at II of a $[+30_4/-30_4]_T$ laminate (CL-CL)

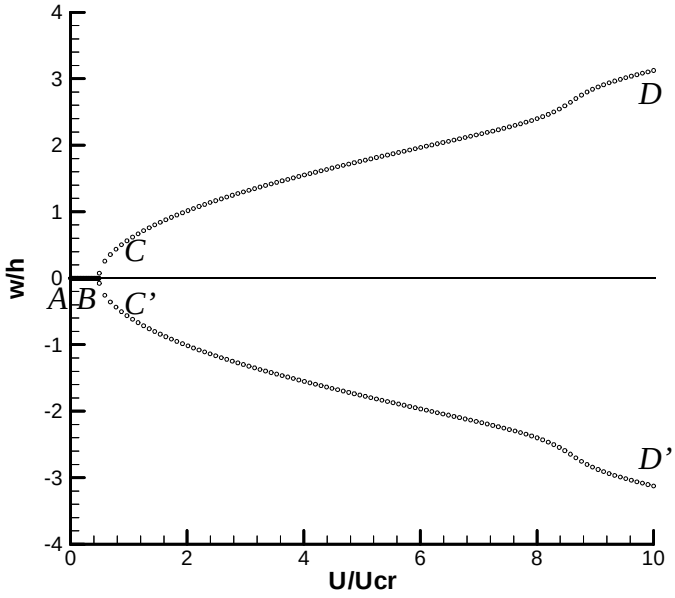

Fig. 4.7.3 Displacement response at III of a $[+30_4/-30_4]_T$ laminate (CL-CL)

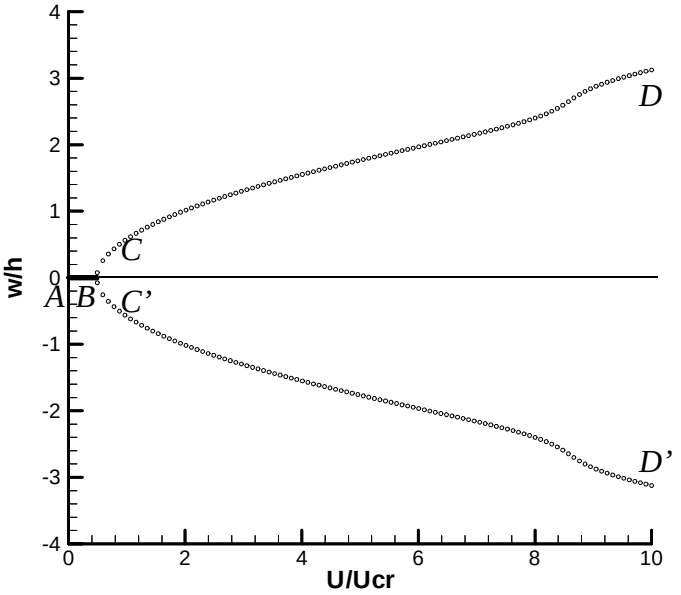

Fig. 4.7.4 Displacement response at I of a $[+30_4/-30_4]_T$ laminate (CL-CL)

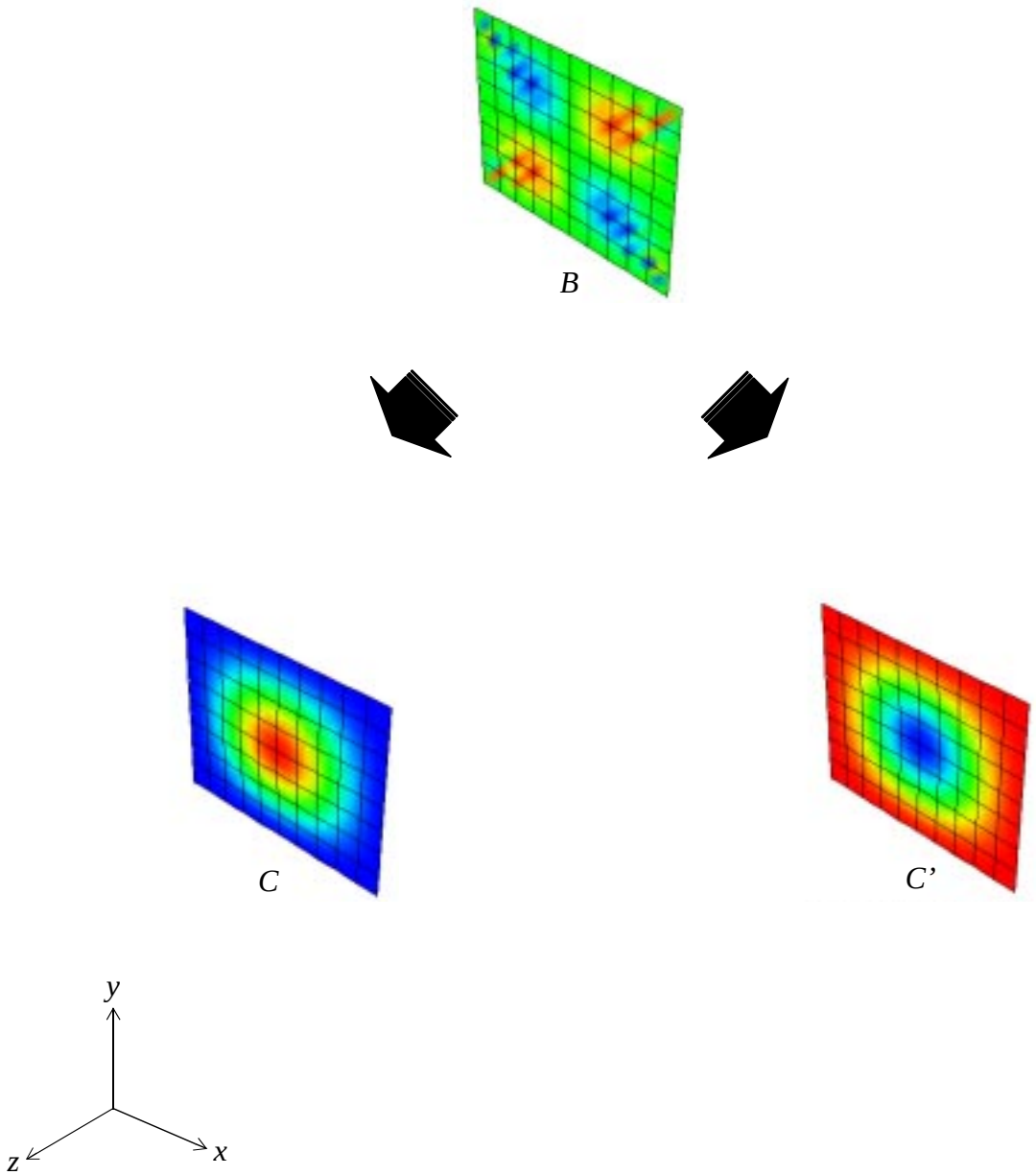

Fig. 4.7.5 Deformed shape flow chart for a $[+30_4/-30_4]_T$ laminate (CL-CL)

4.7.2 $[+30_4/-30_4]_T$ Clamped Ends and Simply-Supported Sides

Section 4.7.2 discusses the deformations of a $[+30_4/-30_4]_T$ anti-symmetric angle-ply laminate due to axial endshortening with clamped ends and simply-supported sides. This case serves as the anti-symmetric counterpart to the $[\pm 30_2]_S$ laminate discussed in Section 4.6.2. The paper by Leissa [8] also shows that anti-symmetric angle-ply plates, such as the one being discussed here, will remain flat when subjected to inplane loading if the four sides are only simply-supported, or as here, if only two sides are simply-supported. Figure 4.7.6 shows the load vs. endshortening response while Figs. 4.7.7-4.7.9 illustrate the corresponding out-of-plane displacements vs. endshortening response for the $[+30_4/-30_4]_T$ anti-symmetric angle-ply laminate. The figures show that the plate remains flat from the onset. The small magnitudes of the out-of-plane displacements indicate that these deformations are numerical anomalies and not real deformations. At a point just past B, the plate configuration becomes unstable. At this point, a dynamic transient analysis is initiated using a small pressure pulse. The statically stable equilibrium configuration at point C has one half-wave in the loading direction and one half-wave perpendicular to the loading direction. The detailed results of the dynamic transient analysis is shown in Appendix F, Figs. F.17-F.20. Compared to the CL-CL case discussed in Section 4.7.1, the plate buckles at a lower magnitude of endshortening and at a lower buckling load. As the plate is compressed beyond point C, Fig. 4.7.6 shows that the load vs. endshortening relation decreases in slope while remaining relatively linear. Figures 4.7.7-4.7.9 show that the geometric center of the plate deforms out-of-plane, monotonically deepening the one half-wave shape seen at point C. This behavior continues to point D. At a point just past D the plate configuration again becomes statically unstable. The statically unstable equilibrium solution continues past point D on path CD, but is not shown here. At the point just past D, a dynamic transient analysis is initiated without a pressure pulse. Appendix F, in Figs. F.21-F.24, details the response of the dynamic transient analysis. During the transient analysis, the plate moves to a statically stable equilibrium configuration labeled E in Fig. 4.7.10. It shows that this shape has two half-waves in the loading direction with one half-wave perpendicular to the loading direction. Figure 4.7.7 shows that the out-of-plane displacement of the center of the plate moves from approximately 3.75 times the laminate thickness to zero. Figure 4.7.6 shows that the load carrying capacity of the plate is discontinuously reduced as the plate moves to its statically stable equilibrium solution at point E from point D. From point E to point F the load

carrying capability of the plate increases monotonically until the analysis is terminated at F. Figures 4.7.8 and 4.7.9 shows that the continued loading from point E to F causes the two half-wave shape to deepen further. The response of this CL-SS case differs significantly from the CL-CL case due to the existence of secondary buckling that was not observed in the CL-CL case.

Comparing the anti-symmetric CL-SS angle-ply discussed here with its symmetric counterpart discussed in Section 4.6.2 shows a significant difference in response. The primary difference between that two is the secondary buckling that is present in the anti-symmetric case but absent in the symmetric case, Figs. 4.6.6-4.6.9 vs. Figs. 4.7.6-4.7.9. Furthermore, the ultimate load carried at the point of analysis termination is approximately half for the anti-symmetric angle-ply compared to its symmetric counterpart, Figs. 4.7.6 vs. 4.6.6. It is also noted that the anti-symmetric angle-ply laminate buckles at a much lower value of endshortening and at a lower load.

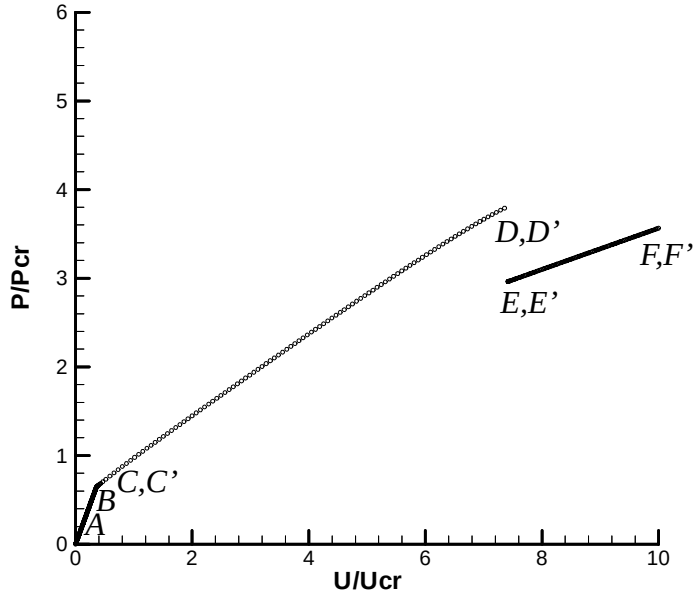

Fig. 4.7.6 Load response of a $[+30_4/-30_4]_T$ laminate (CL-SS)

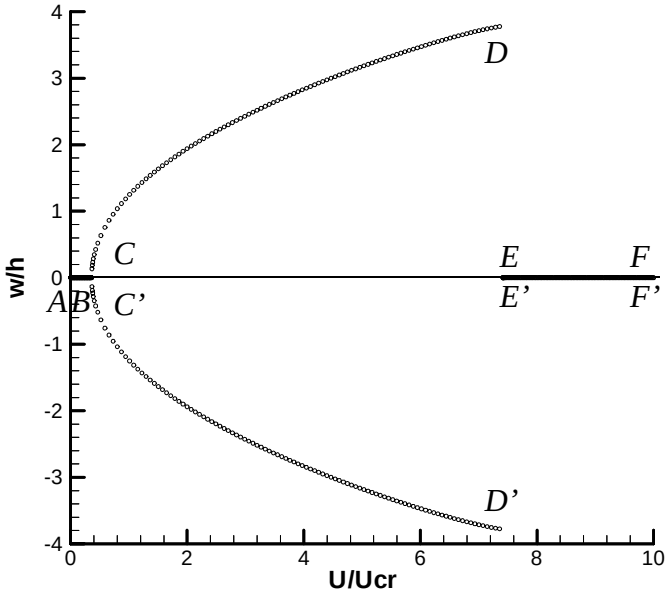

Fig. 4.7.7 Displacement response at II of a $[+30_4/-30_4]_T$ laminate (CL-SS)

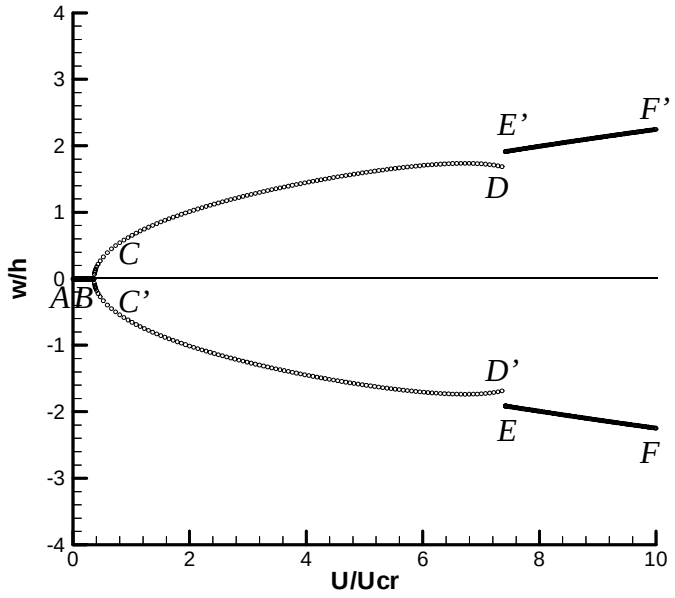

Fig. 4.7.8 Displacement response at III of a $[+30_4/-30_4]_T$ laminate (CL-SS)

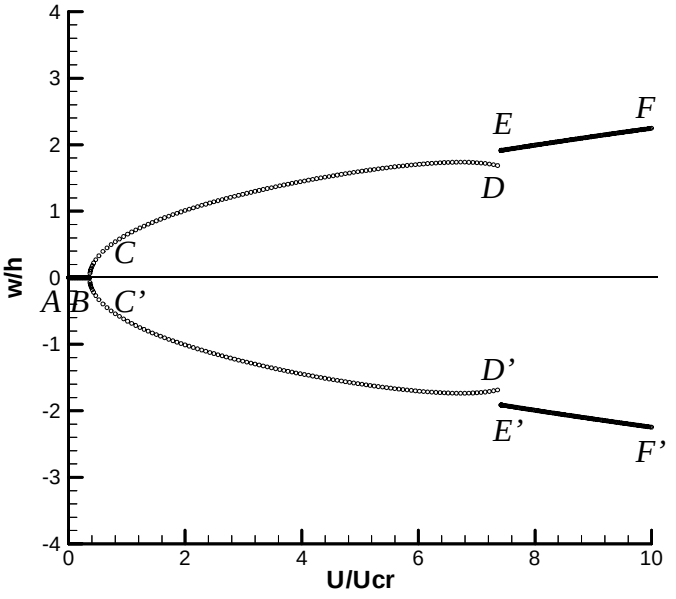

Fig. 4.7.9 Displacement response at I of a $[+30_4/-30_4]_T$ laminate (CL-SS)

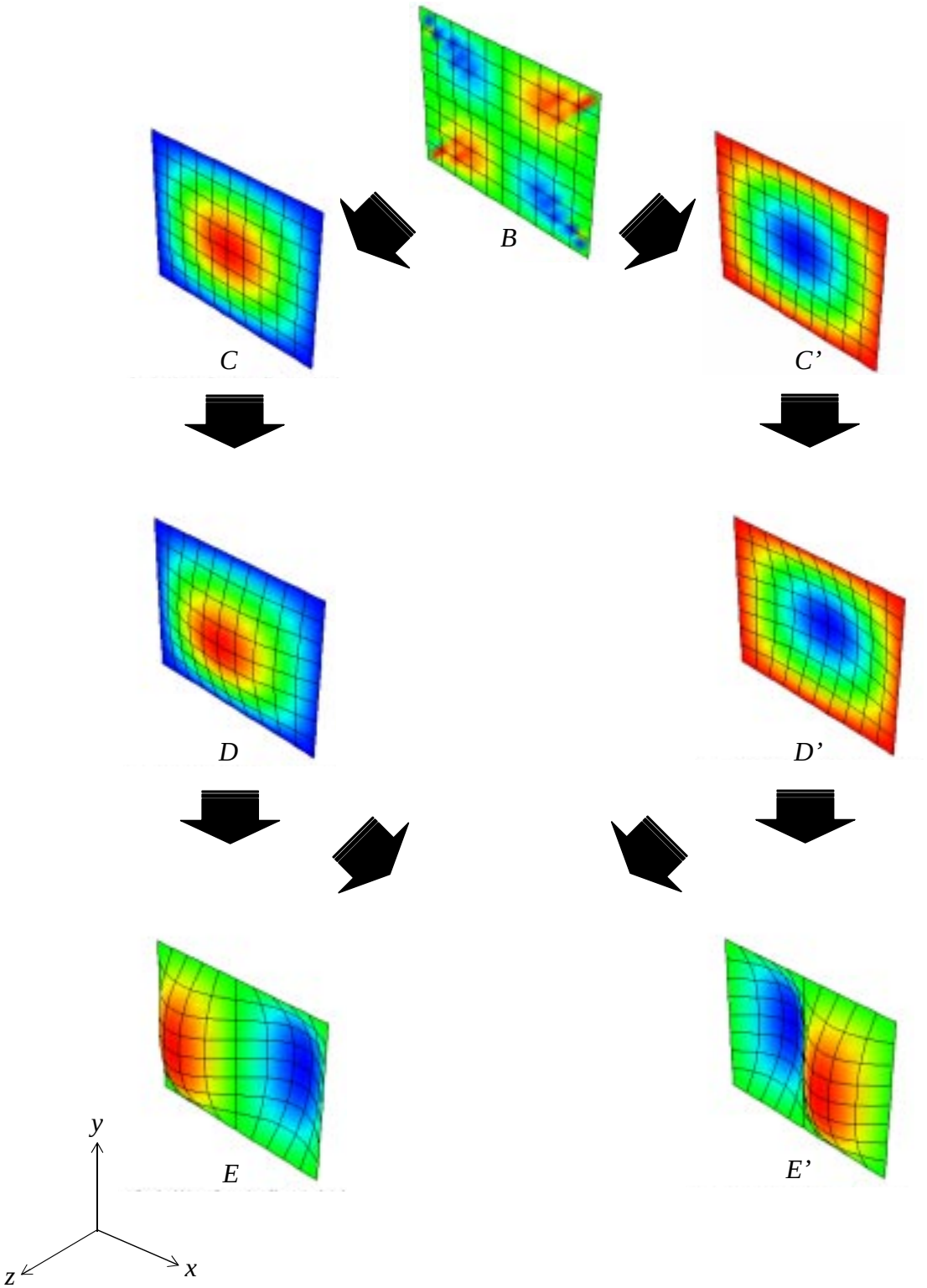

Fig. 4.7.10 Deformed shape flow chart for a $[+30_4/-30_4]_T$ laminate (CL-SS)

4.7.3 $[+30_4/-30_4]_T$ Simply-Supported Ends and Simply-Supported Sides

This section discusses the endshortening response of a $[+30_4/-30_4]_T$ anti-symmetric angle-ply laminate with simply-supported sides and simply-supported ends. This case is the anti-symmetric counterpart to the symmetric angle-ply laminate discussed in Section 4.6.3. Figure 4.7.11 shows the load vs. endshortening response for the $[+30_4/-30_4]_T$ anti-symmetric angle-ply laminate. Corresponding out-of-plane displacements at locations I, II and III are shown in Figs. 4.7.12-4.7.14. Similar to the two previous cases seen in Section 4.7, small deformations are seen from the onset, Fig. 4.7.15. Again, these deformations are felt to be due to numerical anomalies resulting from round-off errors in the finite-element code. The plate remains flat as it is compressed from point A to a point just beyond B, where the configuration becomes statically unstable. Notice that the plate becomes unstable at a lower value of endshortening and at a lower buckling load when compared to the other two case, namely, the CL-CL case shown in Fig. 4.7.1 and the CL-SS case shown in Fig. 4.7.6. This is attributed to the increased degrees of freedom introduced to the SS-SS case relative to the other two cases, effectively reducing the overall stiffness of this laminate. At a point just past B, a dynamic transient analysis is employed using a small pressure pulse, $\pm P_o$, perpendicular to the plate. The detailed response of the dynamic transient analysis is shown in Appendix F, Figs. F.25-F.28. The statically stable equilibrium configuration at point C has one half-wave in the loading direction with one half-wave perpendicular to the loading direction. From this new configuration, the endshortening is continued until it becomes statically unstable again at point D. The load response, Fig. 4.7.11, shows that the load increases nonlinearly up to the point of secondary buckling, point D. Figure 4.7.12 shows that the out-of plane displacement at the geometric center of the plate increases until at approximately U/Ucr equal eight, then the displacement magnitude begins to decrease. At the same time, Figs. 4.7.13 and 4.7.14 show that the magnitude of displacements for the two quarter locations increase monotonically until point D. This leads to a new intermediate shape, shown in Fig. 4.7.15, prior to the loss of stability. This intermediate shape was not observed in the CL-SS case discussed in the previous section. Comparing the secondary buckling response of this laminate with the CL-SS shows that secondary buckling for the SS-SS case occurs at a larger magnitude of endshortening. Furthermore, comparison of the secondary buckling out-of-plane displacement of the geometric center, Figs. 4.7.12 vs. 4.7.7, shows an interesting difference. Namely, the out-of-plane displace-

ment at the center of the plate does not go to zero for the SS-SS case at point E, while it does go to zero for the same points for the CL-SS case. Another difference may be observed when comparing the secondary postbuckling response at the the two quarter locations, Figs. 4.7.13 and 4.7.14 vs. Figs. 4.7.8 and 4.7.9. At point D the magnitudes of out-of-plane displacements of the SS-SS case are larger than those of the CL-SS case. Interestingly, the out-of-plane displacements of the quarter locations for the SS-SS case move to a lesser magnitude at point E relative to point D, while they move to a larger magnitude for the CL-SS case.

Comparing the response of the $[+30_4/-30_4]_T$ anti-symmetric angle-ply laminate with SS-SS boundary conditions with its symmetric counterpart discussed in Section 4.6.3 leads to more differences. The most obvious difference being the existence of a secondary instability in the anti-symmetric laminate, whereas the symmetric laminate remains stable after the primary instability. It can also be observed from Figs. 4.7.11 and 4.6.11 that the anti-symmetric laminate initially buckles at a lower value of endshortening at a lower load. Another difference is that the out-of-plane displacement at the geometric center of the anti-symmetric laminate shows a decrease as it approaches point D, while the out-of-plane displacement at the same point for the symmetric laminate continues to increase monotonically, Figs. 4.7.12 vs. 4.6.12.

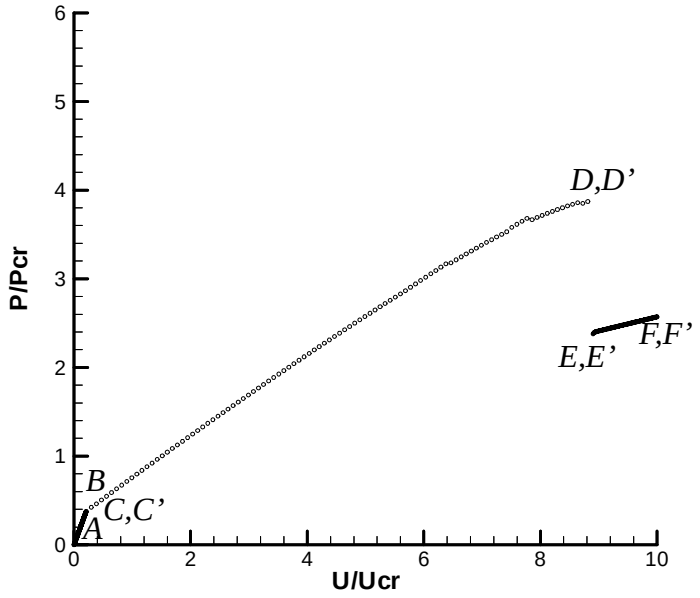

Fig. 4.7.11 Load response of a $[+30_4/-30_4]_T$ laminate (SS-SS)

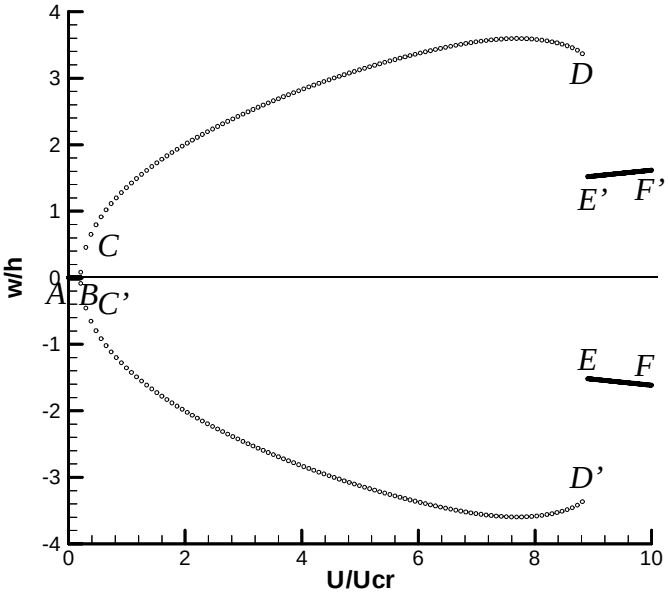

Fig. 4.7.12 Displacement response at II of a $[+30_4/-30_4]_T$ laminate (SS-SS)

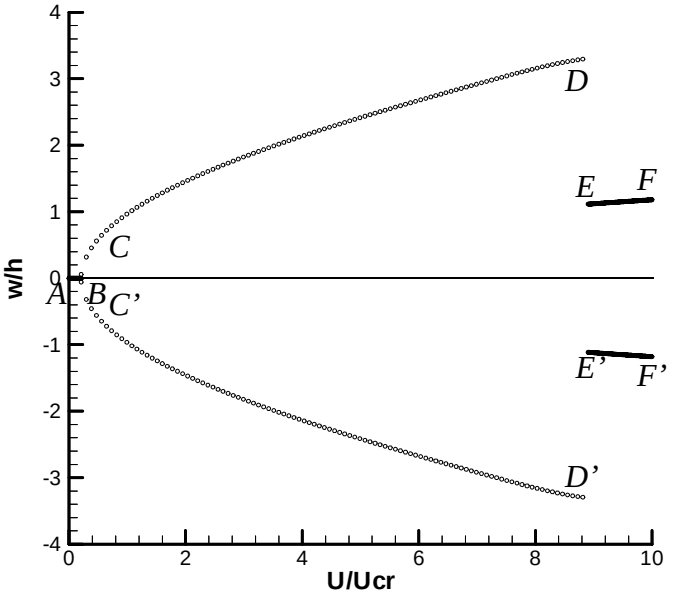

Fig. 4.7.13 Displacement response at III of a $[+30_4/-30_4]_T$ laminate (SS-SS)

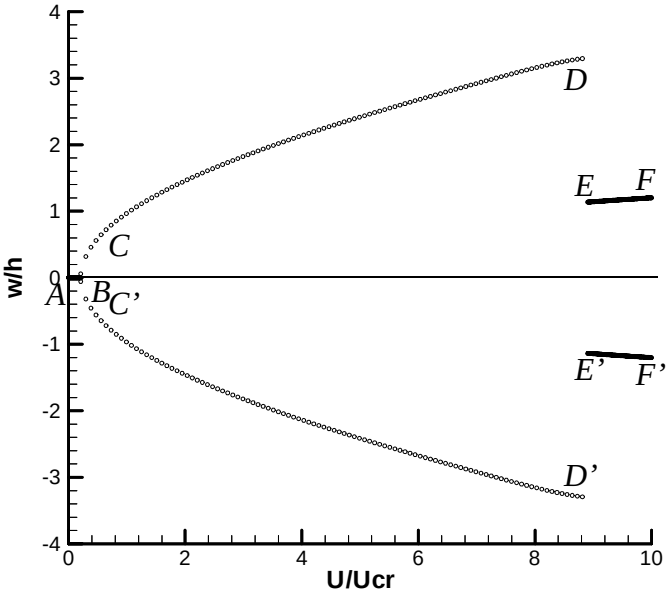

Fig. 4.7.14 Displacement response at I of a $[+30_4/-30_4]_T$ laminate (SS-SS)

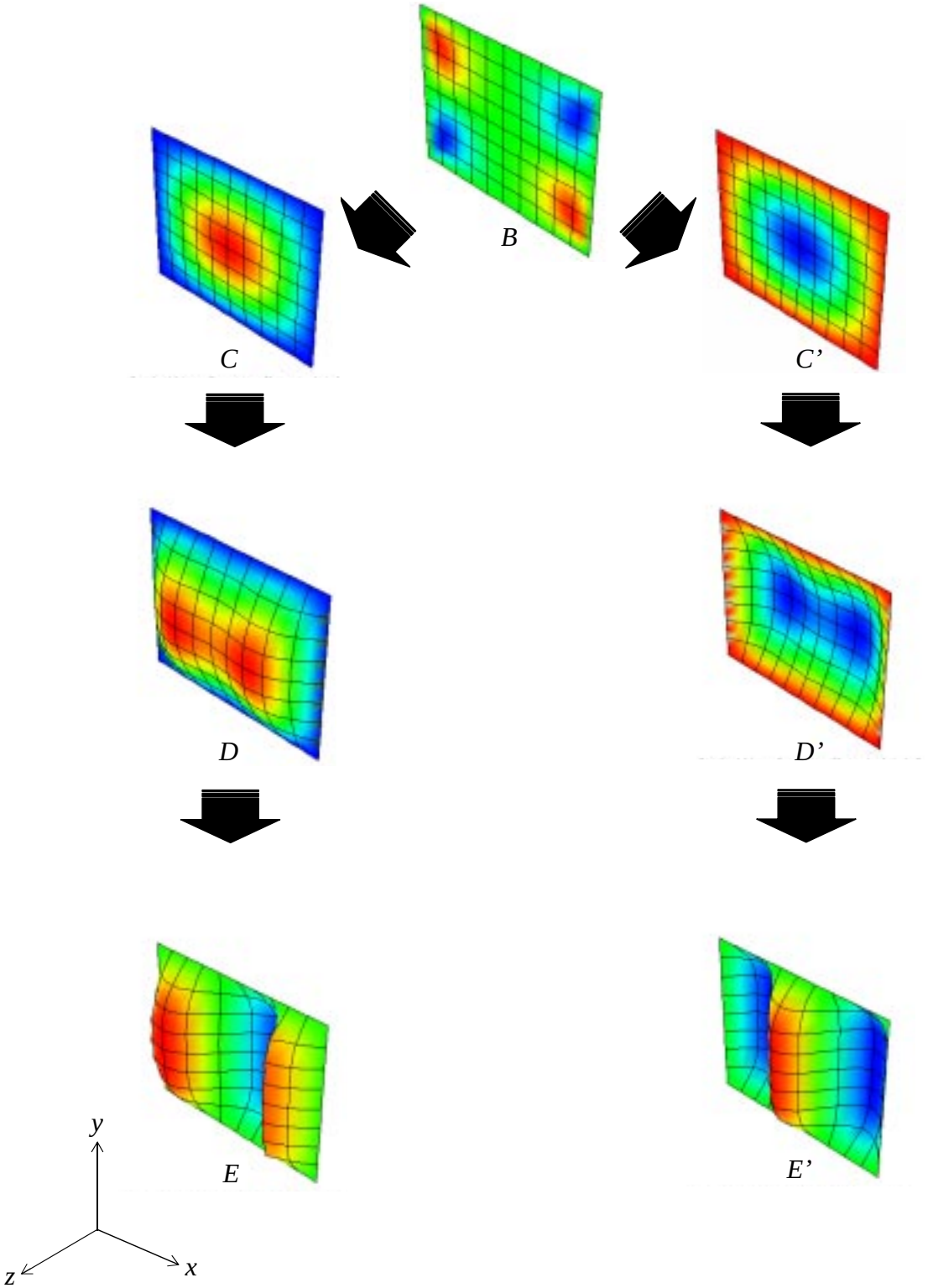

Fig. 4.7.15 Deformed shape flow chart for a $[+30_4/-30_4]_T$ laminate (SS-SS)

4.8 $[\pm 30/90/0]_{2T}$ Unsymmetric Laminate

Section 4.8 discusses the response of a $[\pm 30/90/0]_{2T}$ unsymmetric laminate due to axial endshortening. This laminate is comprised of a combination of the angle-ply and cross-ply layers, +30°, -30°, 0°, and 90° layers, discussed in Sections 4.3-4.7. Because of the lamination sequence, the laminate cannot be classified as cross-ply, angle-ply, symmetric or anti-symmetric, leading to a fully elastically coupled unsymmetric laminate. The laminate, however, is balanced. Due to elastic couplings induced by the highly unsymmetric nature of this laminate, the mechanical response is complex, difficult to analyze and rarely investigated. Therefore, the results in this section and the following section are especially unique contributions to the field of structural mechanics, backed by the progressive development of solutions and techniques discussed in Sections 4.3-4.7. This particular laminate will also serve as a comparative counterpart to the unbalanced unsymmetric $[30_2/90/0]_{2T}$ laminate to be discussed in the next section. Like the previous sections, the response of this laminate will be evaluated by applying the same three boundary condition combinations, CL-CL, CL-SS, and SS-SS.

4.8.1 $[\pm 30/90/0]_{2T}$ Clamped Ends and Clamped Sides

The first boundary conditions applied to the $[\pm 30/90/0]_{2T}$ unsymmetric laminate is that of clamped ends and clamped sides. Figure 4.8.1 shows the load vs. endshortening response. Figures 4.8.2-4.8.4 show the out-of-plane displacement vs. endshortening response at locations I, II, and III. The figures show that the plate remains relatively flat from the onset of endshortening at point A to the primary buckling point at B. Figure 4.8.5 illustrates the deformed shape at selected points along the statically stable equilibrium solution path. It shows that there are small magnitudes of prebuckling deformation prior to point B. However, according to Leissa, they should be zero due to the CL-CL conditions. Hence, the laminate should experience a primary instability. Therefore a dynamic transient analysis is initiated at a point just past B using a small pressure pulse, $\pm P_o$, perpendicular to the plate to induce motion. Both positive and negative pressure pulses cause the plate to move to point C, implying that this is the only statically stable solution at this point. The result of the dynamic transient analysis is shown in Appendix G, Figs. G.1-G.4. Figure 4.8.5 shows that this shape has one half-wave in the loading direction with one half-wave perpendicular to the

loading direction. It is again noted that there are statically unstable solutions past point B on path AB, but they are not shown here. Figure 4.8.1 shows that the transition from point B to C is continuous but the slope of the load vs. endshortening relation is reduced. From point C, the plate is shortened on path CD until the configuration becomes statically unstable again at a point just past D. Similar to the primary instability, it is noted that there are statically unstable equilibrium solutions extending past point D on path CD, not shown. At the point just past D, a dynamic transient analysis is again initiated using a small pressure pulse, $\pm P_o$, perpendicular to the plate. The result of the transient analysis is shown in Appendix G, Figs. G.5-G.8. The results shows that the secondary instability leads to two statically stable equilibrium configurations E and E'. Figure 4.8.5 show that this configuration has two half-waves in the loading direction with one half-wave perpendicular to the loading direction. Figure 4.8.1 shows the transitions from point D to E and E' are accompanied by a discontinuous drop in the load carrying capacity of the laminate, followed by another reduction in slope. As the plate is compressed further from points E or E', Fig. 4.8.1 shows that the load increases monotonically until the analysis is terminated at point F and F'. Figures 4.8.2-4.8.4 show that this is accompanied by a deepening of the two half-wave shape seen at point E.

It should be noted that the behavior of this laminate with these boundary conditions are unlike that seen in the past cases. Specifically, here there is but one stable solution before the secondary instability and two stable solutions after the secondary instability. Past cases have had two stable solutions after the secondary instability, but they resulted from two stable solutions before secondary buckling.

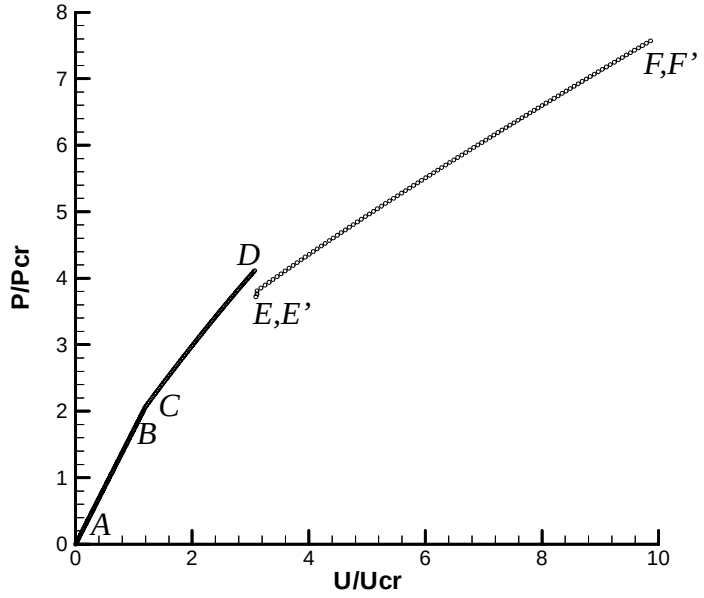

Fig. 4.8.1 Load response of a $[\pm 30/90/0]_{2T}$ laminate (CL-CL)

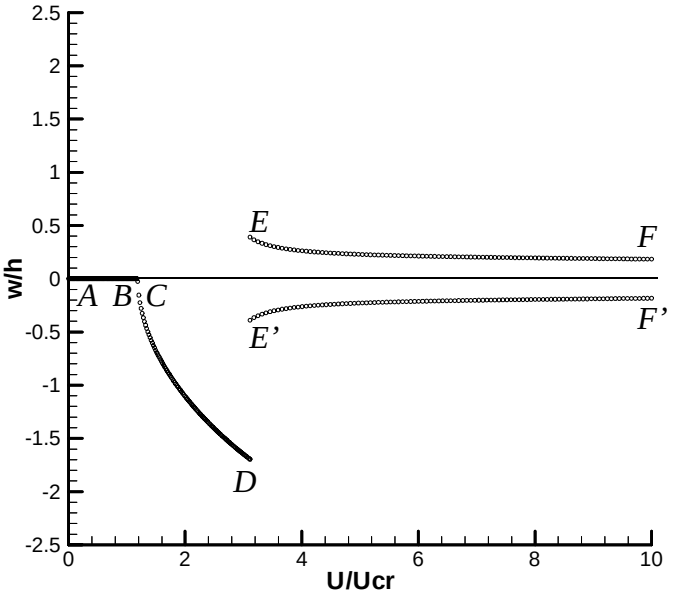

Fig. 4.8.2 Displacement response at II of a $[\pm 30/90/0]_{2T}$ laminate (CL-CL)

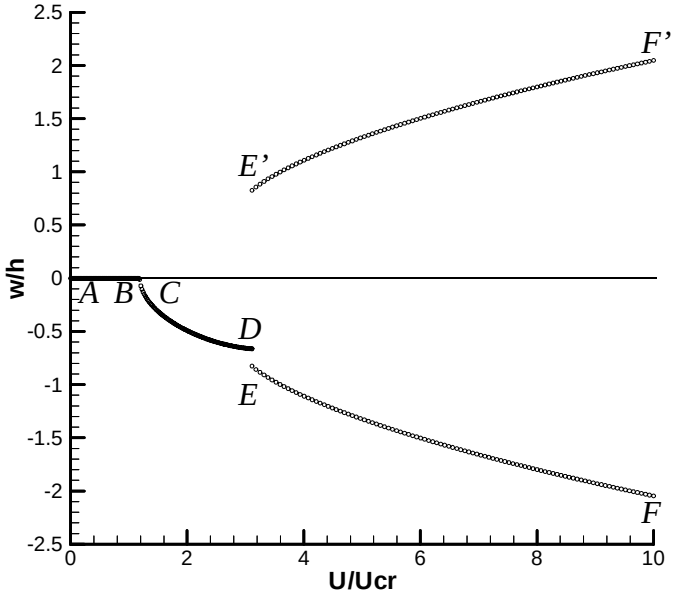

Fig. 4.8.3 Displacement response at III of a $[\pm 30/90/0]_{2T}$ laminate (CL-CL)

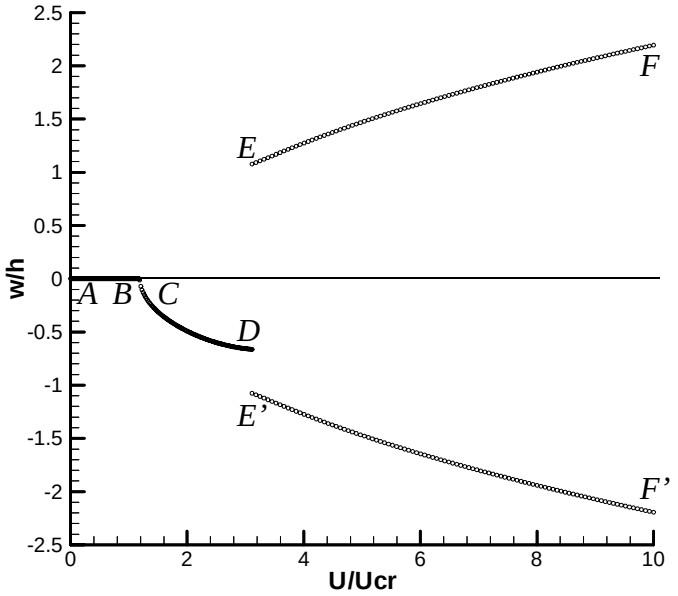

Fig. 4.8.4 Displacement response at I of a $[\pm 30/90/0]_{2T}$ laminate (CL-CL)

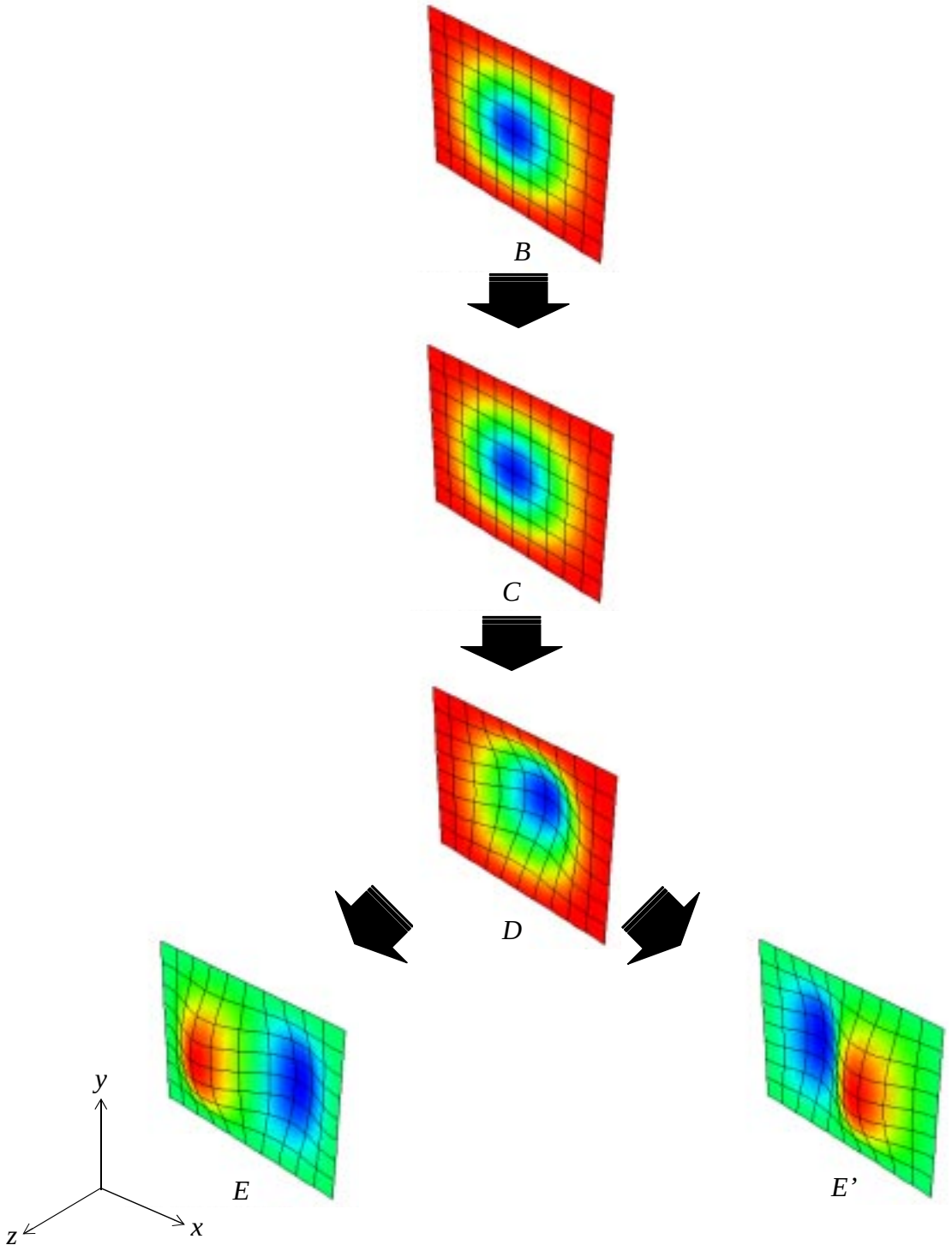

Fig. 4.8.5 Deformed shape flow chart for a $[\pm 30/90/0]_{2T}$ laminate (CL-CL)

4.8.2 $[\pm 30/90/0]_{2T}$ Clamped Ends and Simply-Supported Sides

This section discusses the response of the $[\pm 30/90/0]_{2T}$ unsymmetric laminate due to axial endshortening with clamped ends and simply-supported sides. Figure 4.8.6 shows the load vs. endshortening response, and corresponding out-of-plane displacements at locations I, II, and III are shown in Figs. 4.8.7-4.8.9. The figures show that the plate immediately deforms out-of-plane from the onset of endshortening at point A. Figure 4.8.10 shows that the deformed shape in this initial range has one half-wave in the loading direction and one half-wave perpendicular to the loading direction. Unlike the CL-CL case, as the plate is compressed past point B, the configuration makes a continuous transition to one with a deeper single half-wave in the two perpendicular directions. This behavior shows that the removal of the clamped conditions along the sides has a significant effect on the response of this laminate, allowing it to deform out-of plane to the extent that it makes a smooth transition from a flat shape at point A to the deep one half-wave shape seen at point past C on path ABC. Figure 4.8.6 shows that the continuous transition at point B is reflected in the load vs. endshortening relation, marked by a reduction in slope. This load response, taken by itself, is similar to the one observed in the CL-CL case, Fig. 4.8.1. Further comparison of Fig 4.8.1 to Fig. 4.8.6 shows that the transition for the CL-SS case occurs at a smaller value of endshortening and a lower load. This trend is consistent with those observed earlier in this chapter, caused by the reduced structural stiffness due the added degree of freedom along the sides for the CL-SS case. At a point just past C, the one half-wave configuration becomes statically unstable. There are statically unstable solutions past point C on path BC, however they are not shown. At the point just past point C, a dynamic transient analysis is initiated with and without a pressure pulse perpendicular to the plate. Some results from the transient analysis are shown in Appendix G, Figs. G.9-G.12. They show that the solution makes a transition from just past point C to the statically stable equilibrium solutions D and D’. Figure 4.8.10 shows the plate configuration to have two half-waves in the loading direction with one half-wave perpendicular to the loading direction. Figure 4.8.6 shows that the transition from point C to D is accompanied by a discontinuous drop in the load vs. endshortening relation. Comparing this with the results of the CL-CL case, Fig. 4.8.1, shows that this transition occurs at a larger magnitude of endshortening and a higher load for the CL-SS case. It is further noted that the discontinuous drop in load for the CL-SS case is larger than that of the CL-CL case. Comparing the out-of-plane dis-

placements for the two cases, Figs. 4.8.7-4.8.9 vs. Figs. 4.8.2-4.8.4, shows that response is very similar, except that the geometric center, location II, of the CL-SS case comes closer to zero at point D compared to the CL-CL case at point E. The plate is then further shortened from point D to E, where the analysis is terminated. Comparing the load response for this case, Fig. 4.8.6, with that of the CL-CL case, Fig. 4.8.1, shows the slope for the CL-SS case is less than that of the CL-CL case. Furthermore, it can be seen that the ultimate load carried at the point where the analysis is terminated is less for the CL-SS case, in line with expectations and responses observed in the previous sections. Figures 4.8.7-4.8.9 show that the two half-wave shape at point D deepens further until the analysis is terminated at point E. The out-of-plane deflection at the center of the plate, location II, approaches zero as the endshortening increases.

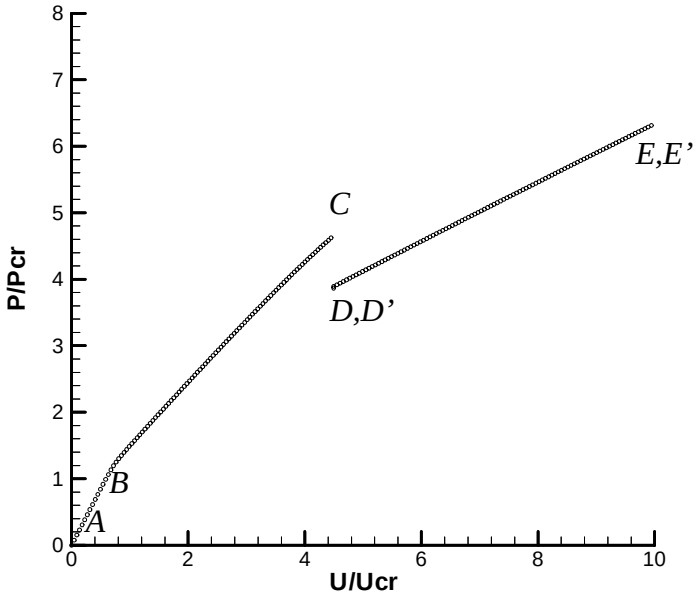

Fig. 4.8.6 Load response of a $[\pm 30/90/0]_{2T}$ laminate (CL-SS)

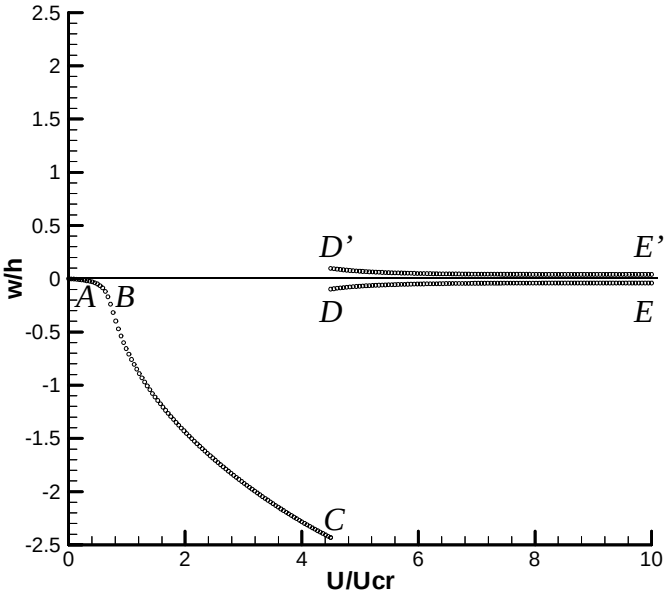

Fig. 4.8.7 Displacement response at II of a $[\pm 30/90/0]_{2T}$ laminate (CL-SS)

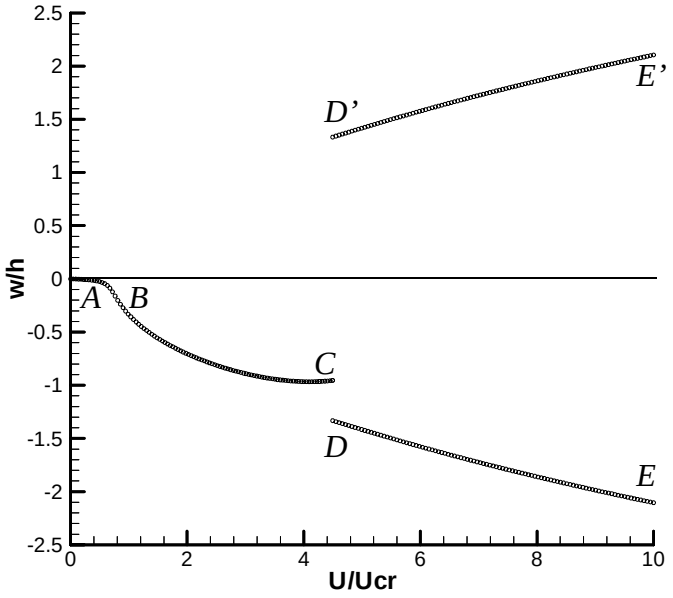

Fig. 4.8.8 Displacement response at III of a $[\pm 30/90/0]_{2T}$ laminate (CL-SS)

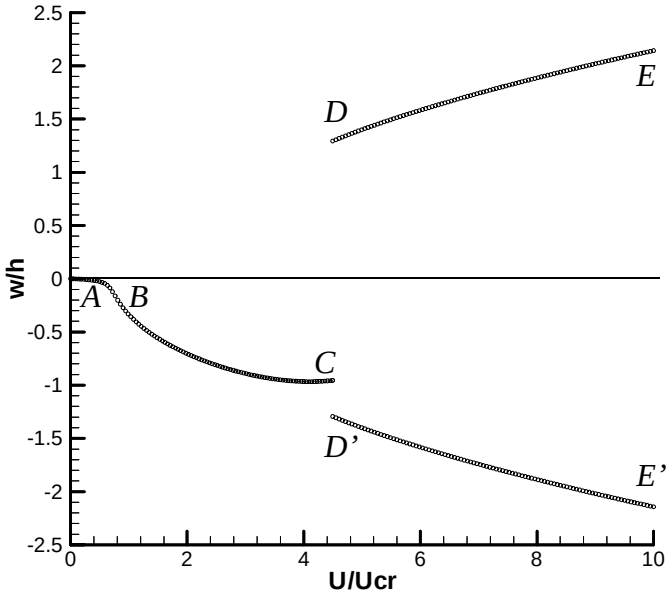

Fig. 4.8.9 Displacement response at I of a $[\pm 30/90/0]_{2T}$ laminate (CL-SS)

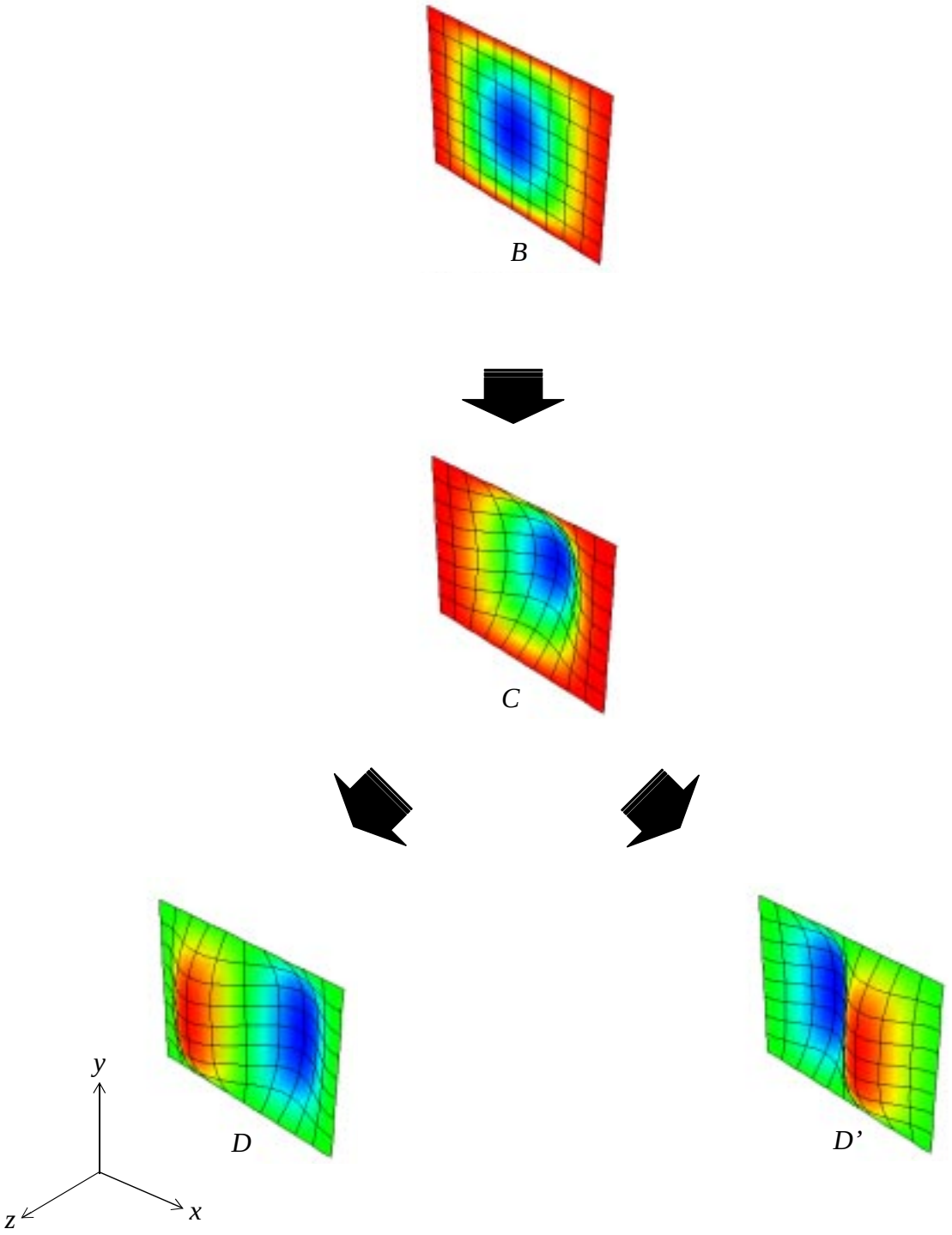

Fig. 4.8.10 Deformed shape flow chart for a $[\pm 30/90/0]_{2T}$ laminate (CL-SS)

4.8.3 $[\pm 30/90/0]_{2T}$ Simply-Supported Ends and Simply-Supported Sides

This section discusses the axial endshortening response of a $[\pm 30/90/0]_{2T}$ unsymmetric laminate with simply-supported sides and simply-supported ends. Figure 4.8.11 shows the load vs. endshortening response. Figures 4.8.12-4.8.14 show the out-of-plane displacements vs. endshortening response at locations I, II, and III. The figures show that the plate deforms out-of-plane immediately following the onset of endshortening at point A. Figure 4.8.15 shows that the shape has one half-wave in the loading direction with one half-wave perpendicular to the loading direction. As seen for the the CL-SS case, the laminate configuration makes smooth transitions from point A to B then to C without becoming statically unstable. Comparing the load response of the present case to the CL-SS case, Figs. 4.8.11 vs. 4.8.6, it can be observed that the initial transition at point B occurs at a lower magnitude of endshortening and load for the SS-SS case. Furthermore, the transition is marked by a less pronounced change in slope at point B for the SS-SS case. Most interestingly, the load response from point B to C becomes noticeably nonlinear for the SS-SS case as point C is approached. This was not the case for CL-SS case nor the CL-CL case, Figs. 4.8.6 and 4.8.1. Comparing the out-of plane displacements at the geometric center of the plate for the three boundary condition combinations, Figs. 4.8.12, 4.8.7, and 4.8.2, shows another difference in response. Namely, the out-of-plane displacement response from point B to C for the SS-SS case begins to decrease at approximately U/Ucr equal four. The CL-SS case and the CL-CL case, on the other hand, showed a monotonic increase in displacement as point C was approached. For the SS-SS case, Fig. 4.8.15 shows that the laminate at point B takes on a new configuration as point C is approached. Namely, the laminate develops three shallow half-waves in the loading direction, with one half-wave perpendicular to the loading direction. This intermediate configuration was not observed in the CL-CL nor the CL-SS cases. At a point just past C, the configuration loses its static stability and a dynamic transient analysis is initiated with and without a pressure pulse. The result of the dynamic transient analysis is shown in Appendix G, Figs. G.13-G.16. It shows that the solution makes a transition from point C to the two statically stable equilibrium solutions D and D'. Figure 4.8.15 shows that deformed shapes at points D and D' have three half-waves in the loading direction and one half-wave perpendicular to the loading direction. Continued shortening of the plate past point D to E monotonically deepens this three half-wave shape until the analysis is terminated. Comparing this response of the SS-SS case with those of the CL-

CL case and the CL-SS case highlights an important difference. Namely, the SS-SS case never deforms into the two half-wave configurations seen in the other two cases, Figs. 4.8.12 vs. 4.8.5 and 4.8.10. It makes a transition directly from the one half-wave configuration to its final shape with three half-waves in the loading direction. Comparing the load response of the SS-SS case to that of the CL-SS case, Figs. 4.8.11 vs. 4.8.6, shows that the transition from point C to D for the SS-SS case occurs at a higher magnitude of endshortening and at a slightly higher load. However, the ultimate load carried at point E of the SS-SS case is less than that carried by the CL-SS case.

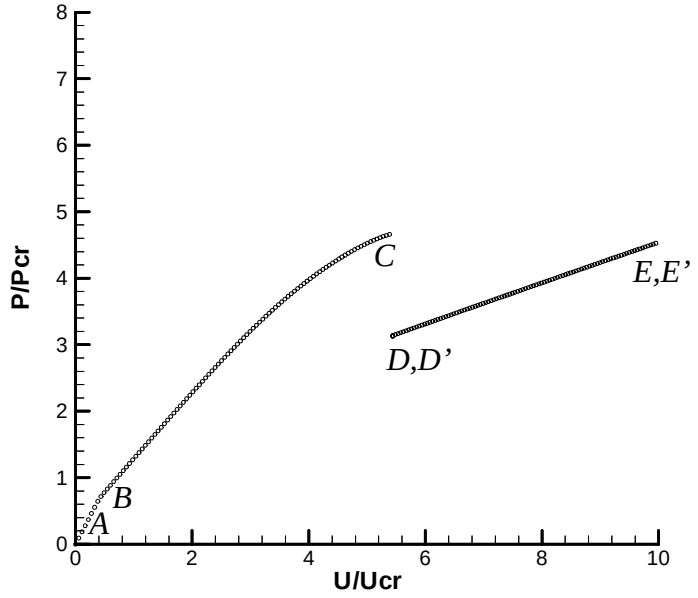

Fig. 4.8.11 Load response of a $[\pm 30/90/0]_{2T}$ laminate (SS-SS)

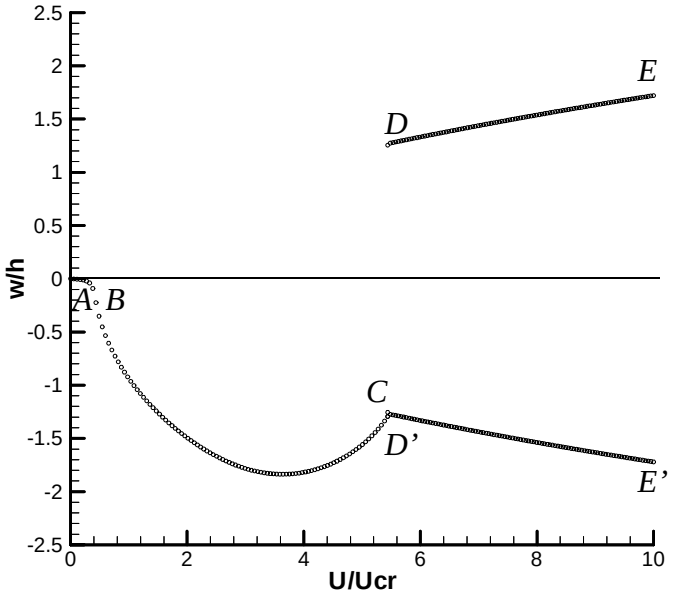

Fig. 4.8.12 Displacement response at II of a $[\pm 30/90/0]_{2T}$ laminate (SS-SS)

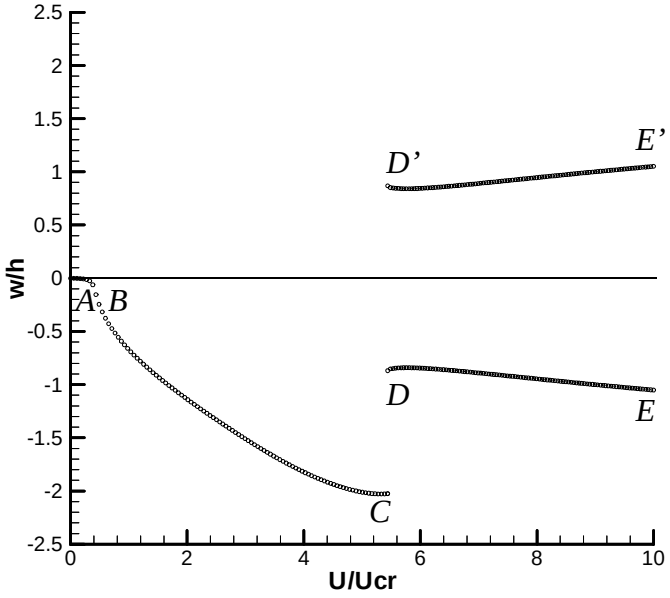

Fig. 4.8.13 Displacement response at III of a $[\pm 30/90/0]_{2T}$ laminate (SS-SS)

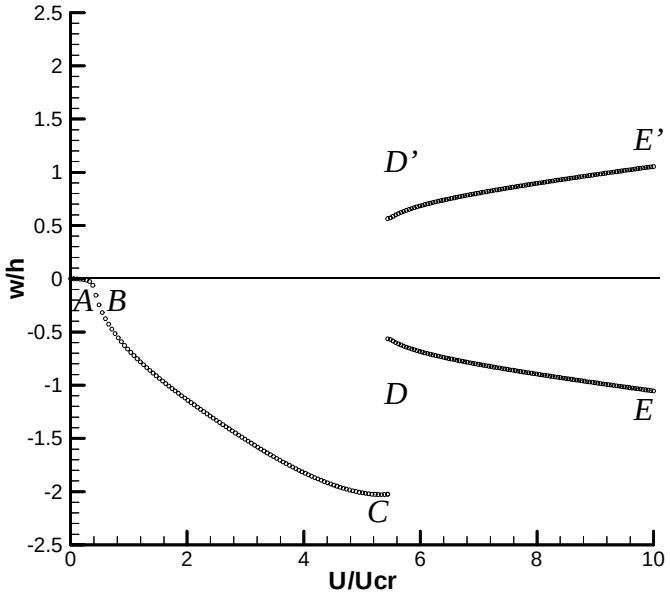

Fig. 4.8.14 Displacement response at I of a $[\pm 30/90/0]_{2T}$ laminate (SS-SS)

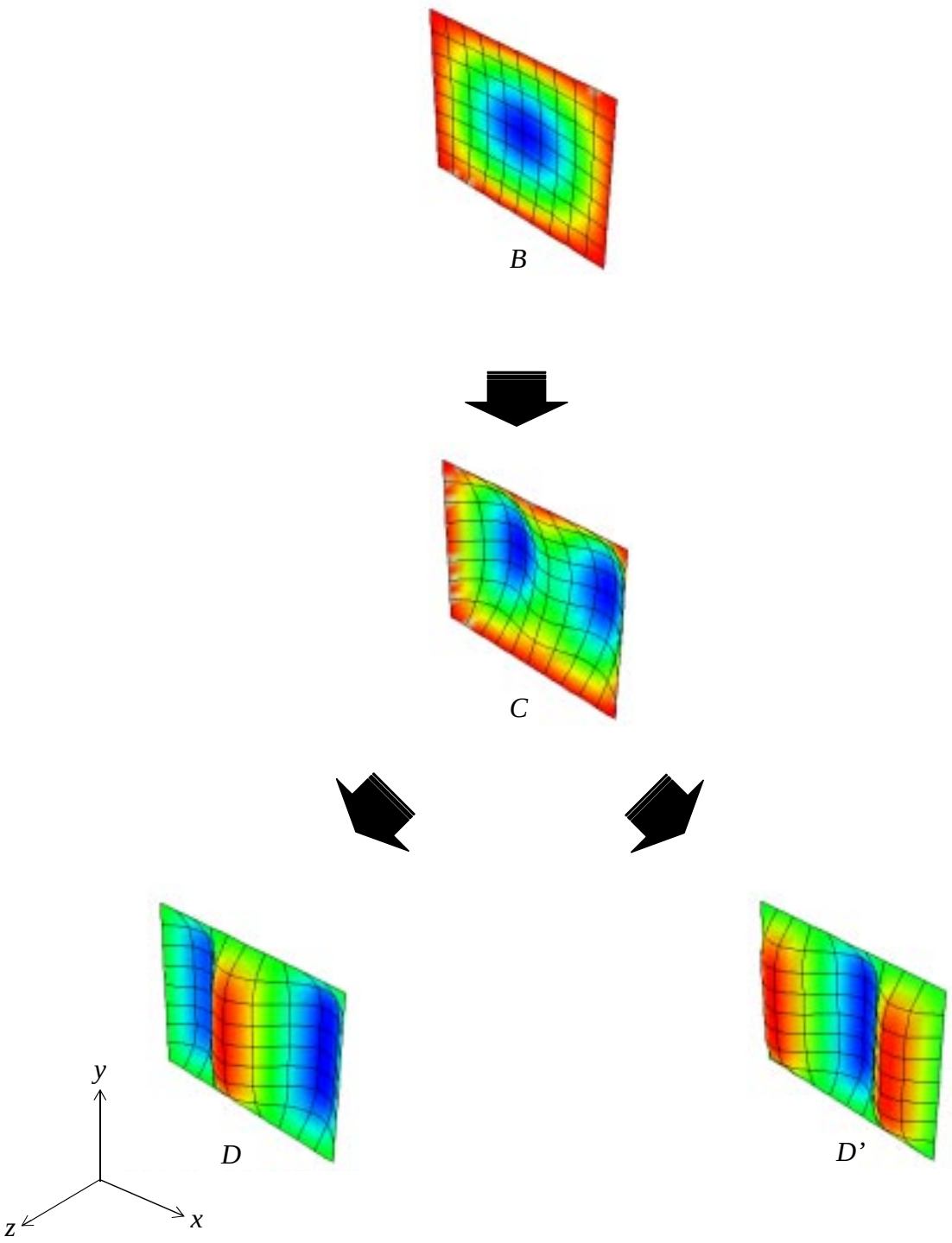

Fig. 4.8.15 Deformed shape flow chart for a $[\pm 30/90/0]_{2T}$ laminate (SS-SS)

4.9 $[30_2/90/0]_{2T}$ Unsymmetric Laminate

Section 4.9 discusses the response of a $[30_2/90/0]_{2T}$ unsymmetric laminate due to axial endshortening with various boundary condition combinations. This laminate is an unbalanced ($A_{16}\neq0$, $A_{26}\neq0$) counterpart to the $[\pm30/90/0]_{2T}$ laminate discussed in Section 4.8 due to the lack of -30° layers that serve to counteract the +30° layers. Therefore this laminate will be the most extremely coupled laminate to be discussed in this present work. The same three boundary condition combinations, CL-CL, CL-SS, and SS-SS will be discussed and compared with their counterparts in Sections 4.8.1-4.8.3.

4.9.1 $[30_2/90/0]_{2T}$ Clamped Ends and Clamped Sides

This section discusses the endshortening response of a $[30_2/90/0]_{2T}$ unbalanced unsymmetric laminate with clamped ends and clamped sides. Figure 4.9.1 shows the load vs. endshortening relationship. Figures 4.9.2-4.9-4 illustrate the corresponding out-of-plane displacements vs. endshortening response at locations, I, II, and III The figures show that the laminate begins to deform out-of-plane from the onset of endshortening at point A. This appears to contradict the findings of Leissa [8]. As the laminate is compressed to point B, the shape deepens to the configuration shown in Fig. 4.9.5, namely, one half-wave in the loading direction and one half-wave perpendicular to the loading direction. In all previous cases involving the CL-CL boundary condition combinations, the clamped conditions along the edges constrained the out-of-plane deformations so that an instability caused a classic buckling behavior at point B. However, the unbalanced nature of the $[30_2/90/0]_{2T}$ laminate caused significant initial deformations, even with the clamped edges, to lead to the smooth continuous transition seen in Figs. 4.9.1-4.9.4 at point B without an instability leading to classic buckling behavior. Note in Fig. 4.9.5 the highly skewed nature of the deformed shape at point B due to the unbalanced nature of the laminate. Figure 4.9.1 shows that the transition at B is accompanied by a reduction in the slope of the load vs. endshortening response similar to that observed in the $[\pm30/90/0]_{2T}$ laminate discussed in Section 4.8, Fig. 4.8.1. However, there is an important difference in the deformed shape of this laminate compared to its counterpart in Section 4.8.1, namely the direction of the out-of-plane deflection. The $[\pm30/90/0]_{2T}$ laminate deformed out-of-plane in the -*z*-direction, whereas the $[30_2/90/0]_{2T}$ laminate deforms in

the +z-direction. As the $[30_2/90/0]_{2T}$ laminate is further compressed beyond point B, the load increases linearly and the deformed shape deepens dramatically to point C, illustrated in Fig. 4.9.5. The skewing present at point B is not evident at point C. At a point just past C, the one half-wave configuration becomes statically unstable. This statically unstable equilibrium solution path extends beyond point C on path BC, but it is not shown here. A dynamic transient analysis is initiated at a point just past C, with and without a pressure pulse perpendicular to the plate. The response of the dynamic transient analysis is shown in Appendix G, Figs. G.17-G.20. In all cases, the laminate settled into a single statically stable equilibrium solution, point D. Figure 4.9.5 illustrates the statically stable equilibrium shape at D to have two half-waves in the loading direction with one half-wave perpendicular to the loading direction. Comparing again the response of the CL-CL $[30_2/90/0]_{2T}$ laminate with its counterpart in Section 4.8.1 at this point shows another important difference. The $[\pm30/90/0]_{2T}$ laminate has two statically stable equilibrium solutions at this point. The $[30_2/90/0]_{2T}$ laminate has just one. As the plate is further compressed from point D to point E, this configuration further deepens until the analysis is terminated. Comparing the load responses, Figs. 4.9.1 vs. 4.8.1, shows a similar discontinuous drop in load followed by a linear increase with a reduced slope. Aside from the fact that the $[30_2/90/0]_{2T}$ laminate has just one statically stable equilibrium path, the out-of-plane displacement response is similar in that the geometric center of the plate approaches zero, while the two quarter locations monotonically move out-of-plane, Figs. 4.9.2-4.9.4 vs. Figs. 4.8.2-4.8.4, as the endshortening increases.

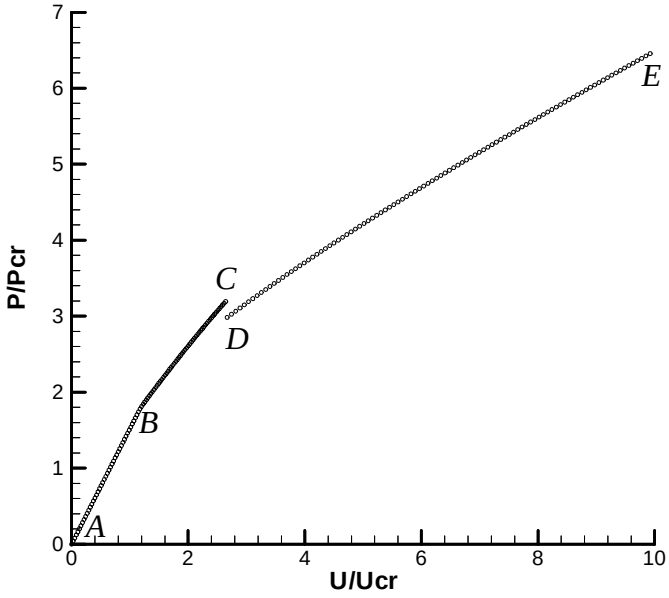

Fig. 4.9.1 Load response of a $[30_2/90/0]_{2T}$ laminate (CL-CL)

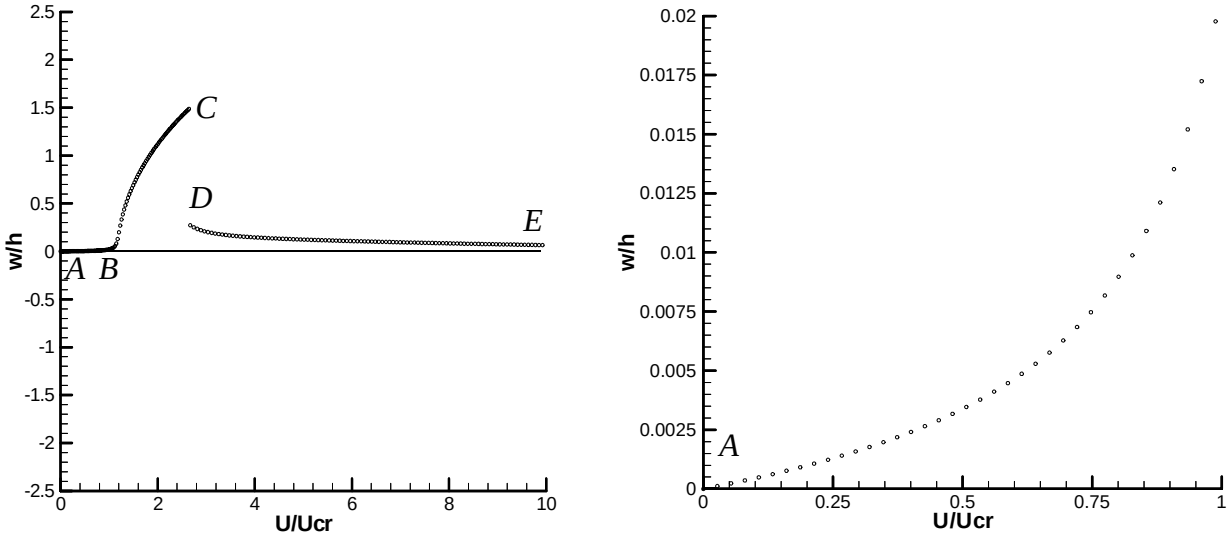

Fig. 4.9.2 Displacement response at II of a $[30_2/90/0]_{2T}$ laminate (CL-CL)

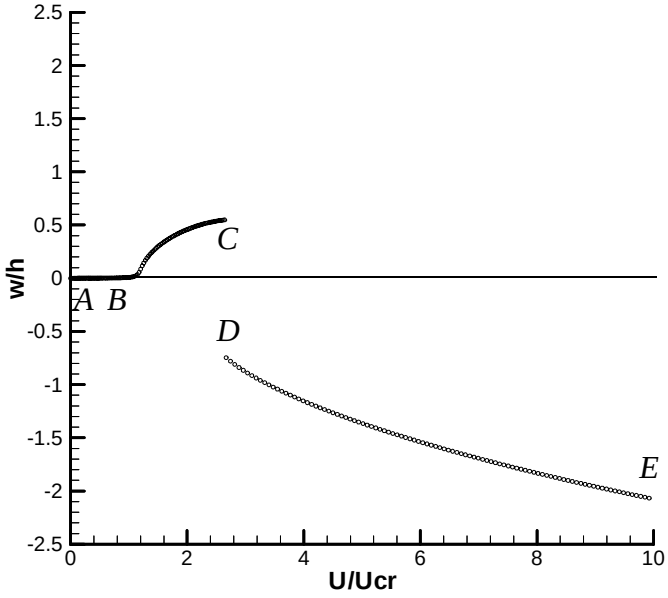

Fig. 4.9.3 Displacement response at III of a $[30_2/90/0]_{2T}$ laminate (CL-CL)

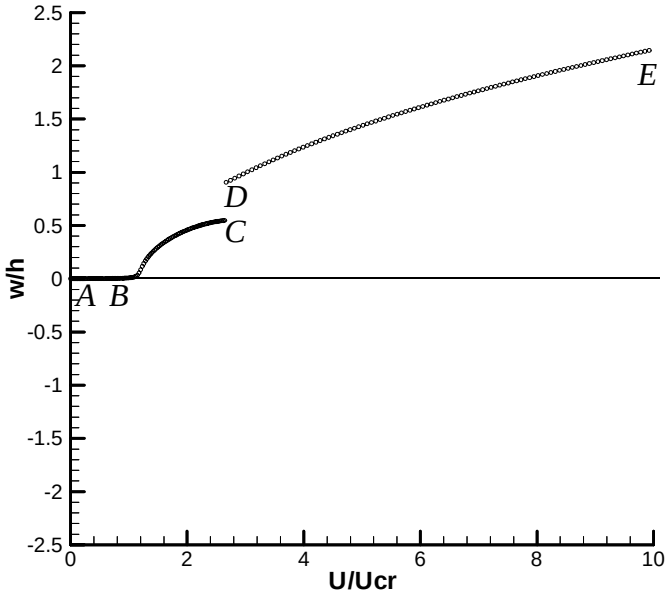

Fig. 4.9.4 Displacement response at III of a $[30_2/90/0]_{2T}$ laminate (CL-CL)

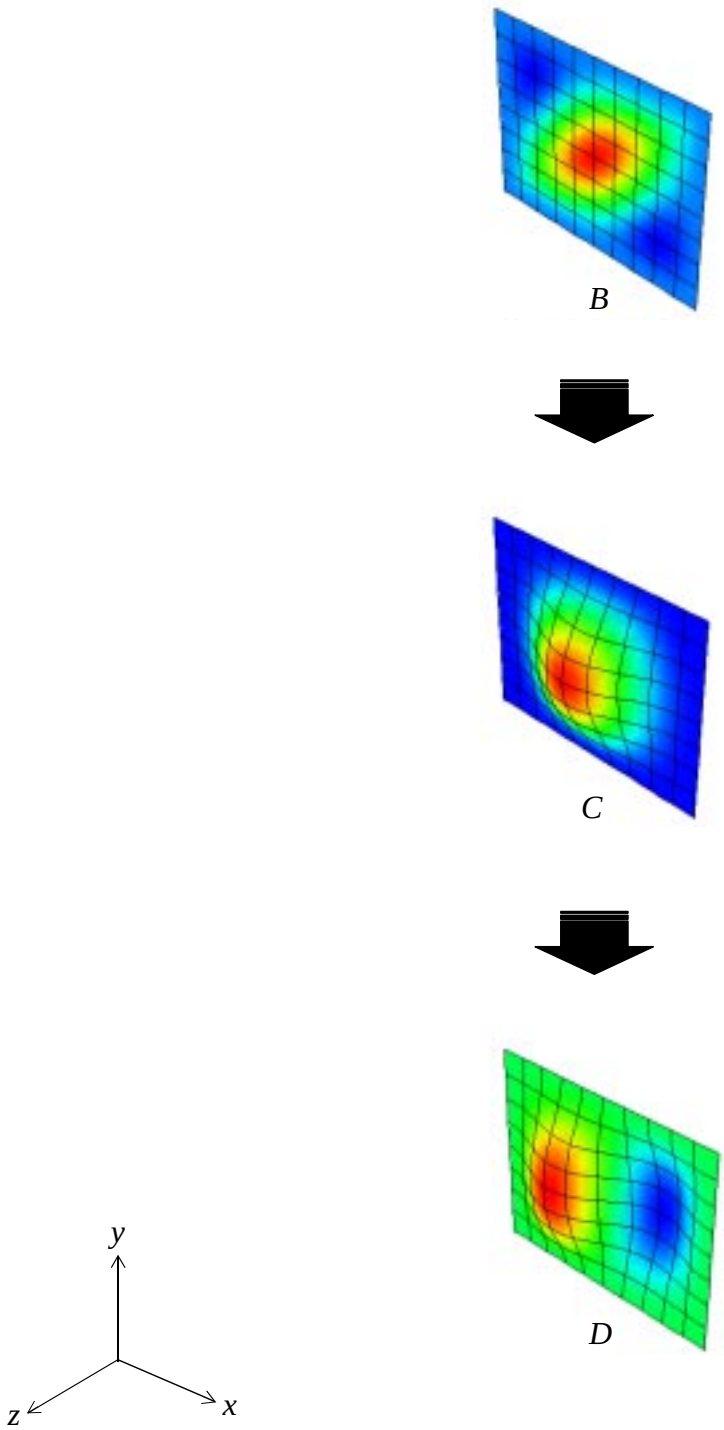

Fig. 4.9.5 Deformed shape flow chart for a $[30_2/90/0]_{2T}$ laminate (CL-CL)

4.9.2 $[30_2/90/0]_{2T}$ Clamped Ends and Simply-Supported Sides

This section discusses the deformation response of a $[30_2/90/0]_{2T}$ laminate in axial endshortening with clamped ends and simply-supported sides. Figure 4.9.6 shows the load vs. endshortening response, while Figs. 4.9.7-4.9.9 illustrate the out-of-plane displacements vs. endshortening at locations I, II, and III. As the laminate is compressed from point A, Figs. 4.9.7-4.9.9 show that the laminate deforms out-of-plane in the -*z*-direction. Figure 4.9.10 shows that the deformed configuration at B has one half-wave in the loading direction with one half-wave perpendicular to the loading direction. It is very interesting to note that the one half-wave deforms in the -*z*-direction, while the same laminate with CL-CL boundary conditions discussed in previous section deformed in the +*z*-direction. The deformation pattern at point B is somewhat unusual, again presumably due to the coupling effects of A_{16} and A_{26}. It should be mentioned that all the *16* and *26* terms are larger for this laminate than for the $[\pm30/90/0]_{2T}$ laminate of the previous section. (see Table 4.4) Like the CL-CL case, however, the CL-SS case deforms out-of-plane at point B to such an extent that a classic buckling instability does not occur. Instead, the response makes a continuous transition past point B to a point just past point C where the configuration becomes unstable. Aside from the direction of the out-of-plane displacement, the response of the CL-SS case is very similar to that of the CL-CL case up to this point. Namely, the load responses, Figs. 4.9.6 vs. 4.9.1, show that the load capacity of the laminate makes a smooth transition at point B without a discontinuous slope, followed by a linear increase, but with a slight decrease in slope. As expected, the transition at B occurs at a lower magnitude of endshortening and at a lower load level for the CL-SS case due to the reduced overall structural stiffness induced by the introduction of an additional degree of freedom along the sides. In contrast, the instability at point C for the CL-SS case occurs at a higher magnitude of endshortening and at a higher load level compared to the CL-CL case. At a point just past C, where the laminate configuration becomes statically unstable, a transient dynamic analysis is initiated. Once again, a pressure pulse, $\pm P_o$, is used to set the laminate in motion. The response of the transient analysis is shown in Appendix G, Figs. G.21-G.24. The result of the dynamic transient analysis shows that this laminate has two statically stable equilibrium solutions at this point, in addition to the statically unstable equilibrium solution that continues past point C on path BC, not shown. Figure 4.9.10 shows that the statically stable equilibrium shapes at points D and D' have two half-waves in the loading direction with one half-

wave perpendicular to the loading direction. This transition is accompanied by a discontinuous drop in the load vs. endshortening relationship, Fig. 4.9.6. As the laminate is further compressed from point D to the point where the analysis is terminated, point E, the load increases linearly with a further reduced slope. Again, the CL-SS case carries slightly less ultimate load at point E compared to the CL-CL case. Figures 4.9.7-4.9.9 show that the two half-wave configuration continues to deepen from point D to point E. Comparing this response with the CL-CL case, Figs. 4.9.1-4.9.4, shows that the trend is very similar except for the fact that the CL-SS case has two statically stable equilibrium paths, DE and D'E', while the CL-CL case has only one statically stable equilibrium path in the same interval.

Comparing the response of the $[30_2/90/0]_{2T}$ laminate with CL-SS boundary conditions discussed in this section with its less coupled counterpart, the $[\pm 30/90/0]_{2T}$ laminate discussed in Section 4.8.2, shows that the two laminates respond almost identically. Small differences may be found by comparing the load vs. endshortening response, Figs. 4.9.6 vs. 4.8.6. Comparison shows that the $[\pm 30/90/0]_{2T}$ laminate undergoes initial transition at point B at a slightly lower magnitude of endshortening but a slightly higher magnitude of endshortening at point C. The ultimate load carried at point E is less for the unbalanced laminate, $[30_2/90/0]_{2T}$, compared to its balanced counterpart, $[\pm 30/90/0]_{2T}$. Otherwise, the two laminates respond in a very similar fashion.

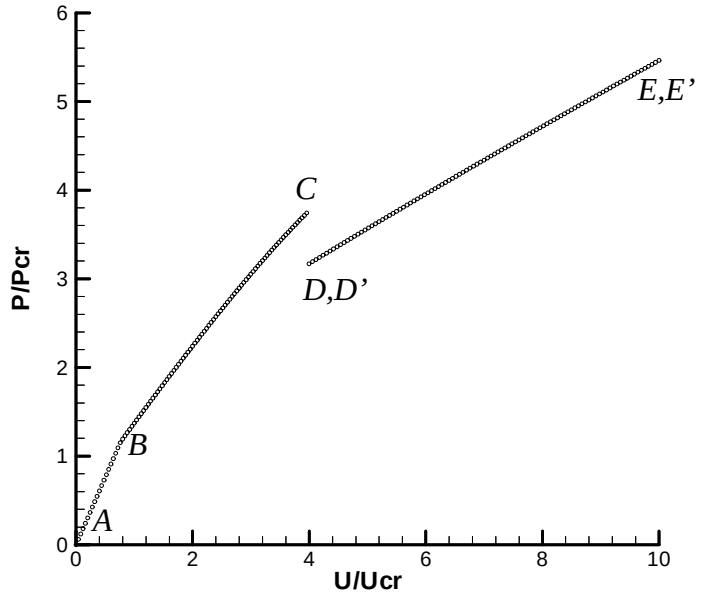

Fig. 4.9.6 Load response of a $[30_2/90/0]_{2T}$ laminate (CL-SS)

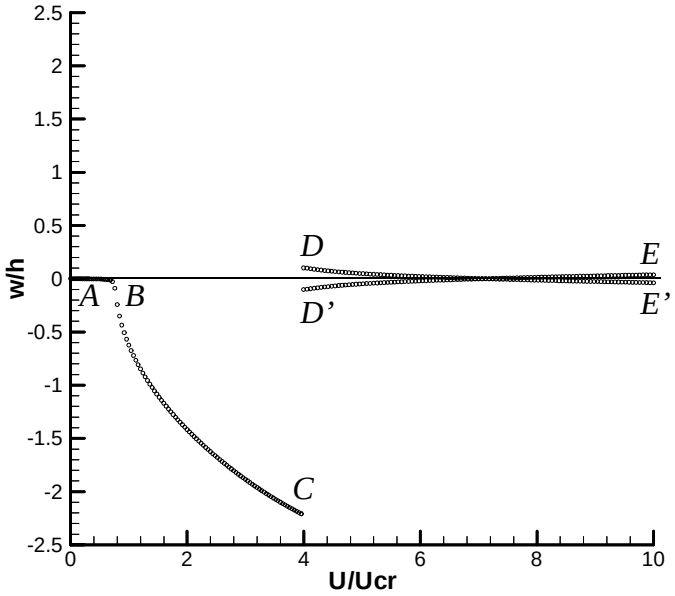

Fig. 4.9.7 Displacement response at II of a $[30_2/90/0]_{2T}$ laminate (CL-SS)

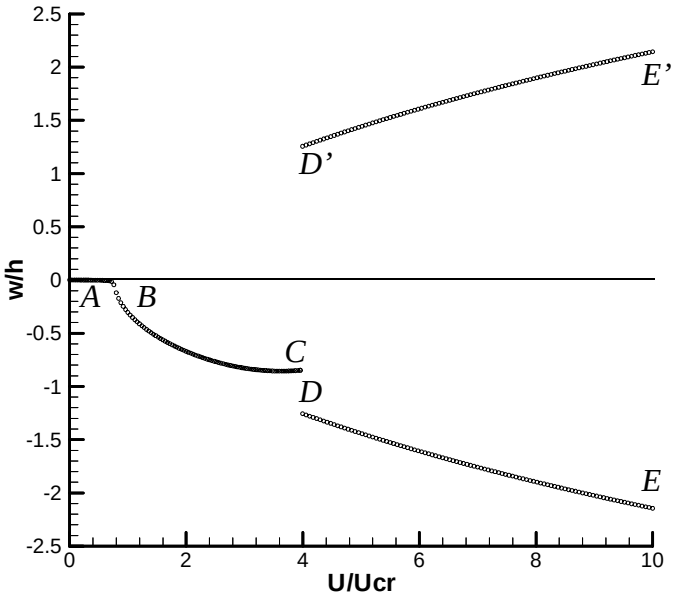

Fig. 4.9.8 Displacement response at III of a $[30_2/90/0]_{2T}$ laminate (CL-SS)

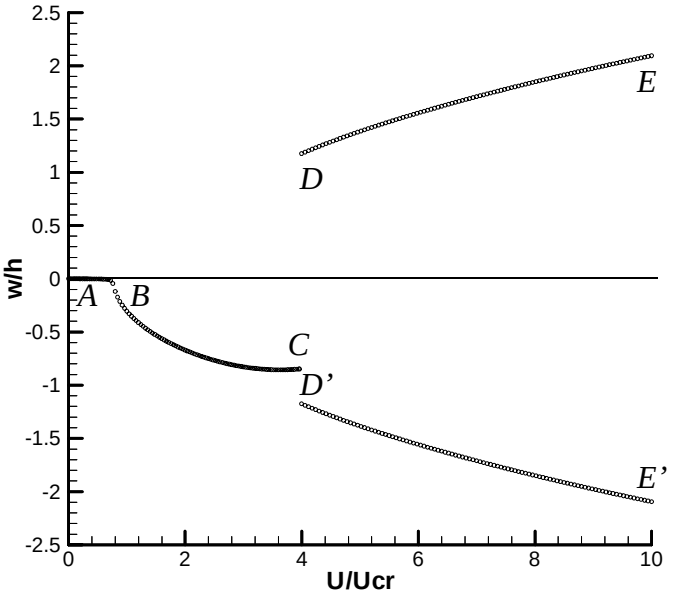

Fig. 4.9.9 Displacement response at I of a $[30_2/90/0]_{2T}$ laminate (CL-SS)

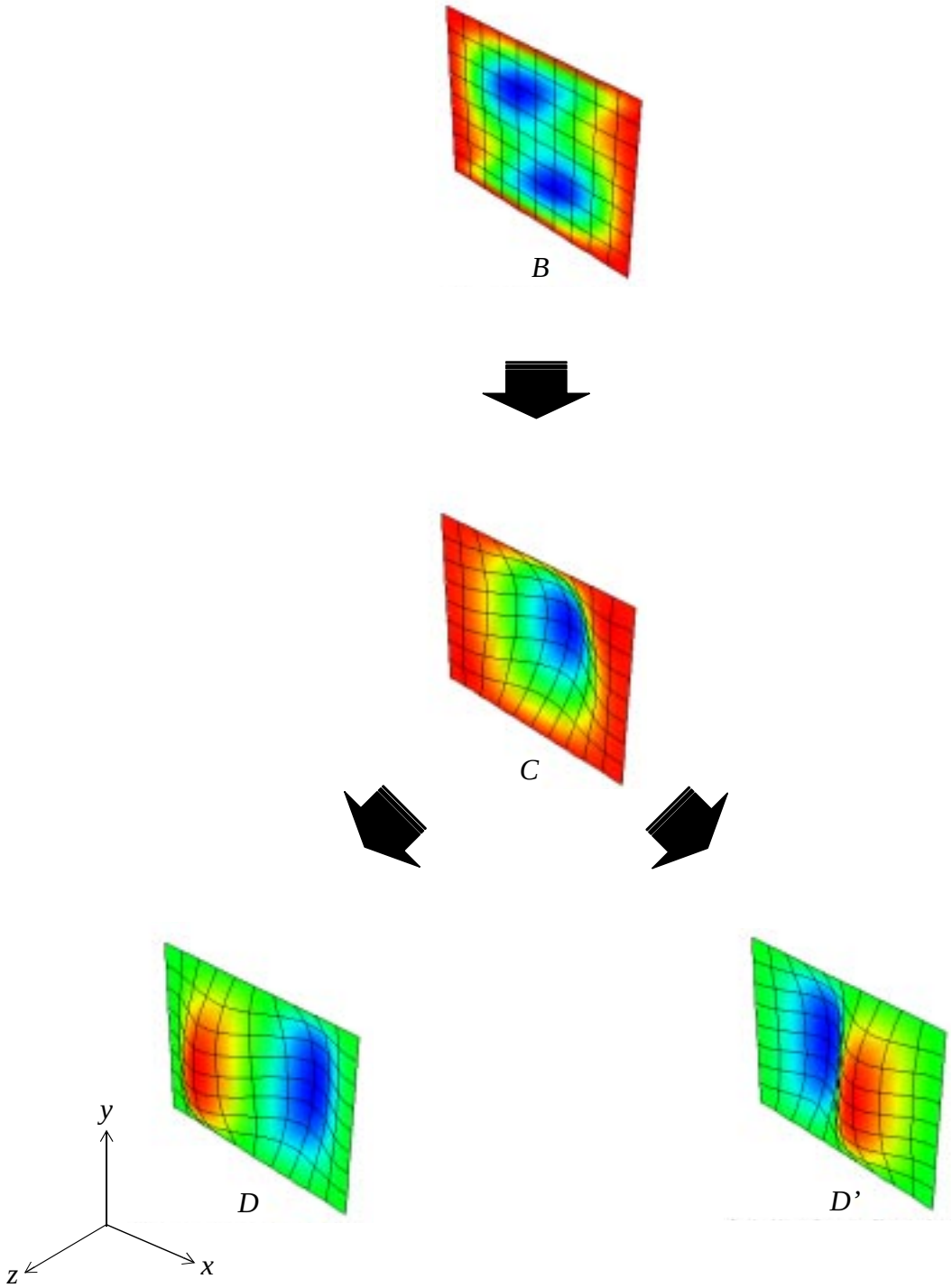

Fig. 4.9.10 Deformed shape flow chart for a $[30_2/90/0]_{2T}$ laminate (CL-SS)

4.9.3 $[30_2/90/0]_{2T}$ Simply-Supported Ends and Simply-Supported Sides

Section 4.9.3 discusses the deformations of an axially compressed $[30_2/90/0]_{2T}$ laminate with simply-supported boundary conditions along all four edges. Once again, this case serves as an unbalanced case to be compared to the $[\pm30/90/0]_{2T}$ laminate discussed in Section 4.8.3. Figure 4.9.11 shows the load vs. endshortening response of the $[30_2/90/0]_{2T}$ laminate. Corresponding out-of-plane displacements at locations I, II, and III are shown in Figs. 4.9.12-4.9.14. These figures show that the plate deforms out-of-plane almost immediately following the onset of endshortening at point A. Figure 4.9.15 illustrates the deformed shapes at selected points along the statically stable equilibrium solution paths shown in Figs. 4.9.11-4.9.14. These figures show that the laminate deforms with one half-wave in the loading direction and one half-wave perpendicular to the loading direction. The out-of-plane displacements are in the +z-direction, like the CL-CL case seen in Section 4.9.1 and opposite to the CL-SS case discussed in Section 4.9.2. As the plate is compressed along path AB, the out-of-plane displacements grow monotonically with a smooth but rapid increase as the endshortening value passes point B. Again, classic buckling instability is not observed at point B due to the highly unsymmetric nature of the laminate and the simply-supported boundary conditions that cannot constrain the initial deformations seen between point A and point B. Figure 4.9.11 shows that the load vs. endshortening relation undergoes a slight decrease in slope at point B. As the laminate is further compressed from point B to C, the load vs. endshortening relationship becomes nonlinear, unlike the other two boundary condition cases considered in Sections 4.9.1 and 4.9.2. More unusual response is also observed in the out-of-plane displacement relations shown in Figs. 4.9.12-4.9.14. Comparing the displacements at the geometric center for the SS-SS case to those of the CL-SS case and the CL-CL case, Fig. 4.9.12 vs. Figs. 4.9.7 and 4.9.2, respectively, shows an intriguing difference. The SS-SS case shows a decrease in displacements as point C is approached. The other two cases show a monotonic increase in displacements in the same region. Most importantly, Fig. 4.9.15 shows that the SS-SS case has smoothly made a transition into an intermediate configuration with what might be interpreted as three shallow half-waves in the loading direction with one half-wave perpendicular to the loading direction. This is significant because the CL-CL case and the CL-SS case never achieved this particular configuration. At a point just past C, this configuration becomes statically unstable. However, this statically unstable equilibrium solution extends beyond point C on path

BC, but it is not shown here. A dynamic transient analysis, the results of which are shown in Appendix G, Figs. G.25-G.28, is initiated with and without a small pressure pulse perpendicular to the plate. Each transient analysis terminates at the same statically stable equilibrium solution, point D. Figure 4.9.15 shows that the laminate configuration at point D has three half-waves in the loading direction with one half-wave perpendicular to the loading direction. Figure 4.9.11 shows that the transition from point C to D is accompanied by a discontinuous drop in load. As the plate is further shortened from point D to E, Fig. 4.9.11 shows a linear increase in load. Figures 4.9.12-4.9.14 shows that the three half-wave configuration monotonically deepens until the point of analysis termination at E. Comparing these responses with those of the CL-CL and CL-SS cases, Section 4.9.1 and 4.9.2 respectively, highlights yet more differences and similarities. The similarity can be observed by comparing the load vs. endshortening relations, Figs. 4.9.1, 4.9.6, and 4.9.11. These figures show that all three cases do not show a classic buckling response at point B, but rather they show there is a smooth transition from solution path AB to BC. Furthermore, the instability at point C causes a discontinuous drop in load, followed by a linear increase in load from point D to point E. The ultimate load carried by each case at point E is consistent with expectations, namely the CL-CL case carries the most load, while the SS-SS case the least. Again, this is consistent with the reasoning that the overall structural stiffness is reduced with the introduction of additional degrees of freedom along the laminate boundaries. Pronounced differences in the response of the three cases may be observed by comparing the out-of-plane displacements and the corresponding laminate configurations, Figs. 4.9.2-4.9.5, Figs. 4.9.7-4.9.10, and Figs. 4.9.12-4.9.15. This comparison shows that the SS-SS case is unique because it deforms from the one half-wave configuration directly to a three half-wave configuration without ever deforming into the two half-wave shape of the CL-CL and CL-SS cases. Furthermore, the CL-CL and CL-SS cases never deform into the three half-wave configuration seen in the SS-SS case.

Finally, comparing the response of the SS-SS $[30_2/90/0]_{2T}$ laminate with its balanced counterpart, the $[\pm 30/90/0]_{2T}$ laminate discussed in Section 4.8.3, shows more similarities and differences. Similarities may be observed by comparing the load vs. endshortening relationship, Fig. 4.9.11 vs. Fig. 4.8.11. The profile of these two figures are very similar. Namely, the laminate undergoes a smooth transition, without classic buckling instability, from path AB to path BC. Furthermore, path BC shows the same type of nonlinear response that was absent in most other boundary condition combinations. This is followed, for both laminates, by a large drop in load past point C, with

a subsequent monotonic increase in load on path DE. The $[\pm 30/90/0]_{2T}$ laminate discussed in Section 4.8.3 consistently carries more load, at the instability point C and at the point of analysis termination, point E. The deformed configuration shows a similarity as well, Fig. 4.9.15 vs. Fig. 4.8.15. Namely, these laminates deform from a one half-wave configuration into a three half-wave configuration without going through a two half-wave configuration. However, comparing the out-of-plane displacements, Figs. 4.9.12-4.9.14 vs. Figs. 4.8.12-4.8.14, shows important differences. The first difference can be seen in the direction of the one half-wave displacements. The $[\pm 30/90/0]_{2T}$ laminate deforms in the -*z*-direction while the $[30_2/90/0]_{2T}$ laminate deforms in the +*z*-direction. More importantly, the $[\pm 30/90/0]_{2T}$ laminate has two statically stable equilibrium solutions paths past point C, path DE and path D'E', while its unbalanced counterpart, the $[30_2/90/0]_{2T}$ laminate has only one statically stable solution path, path DE.

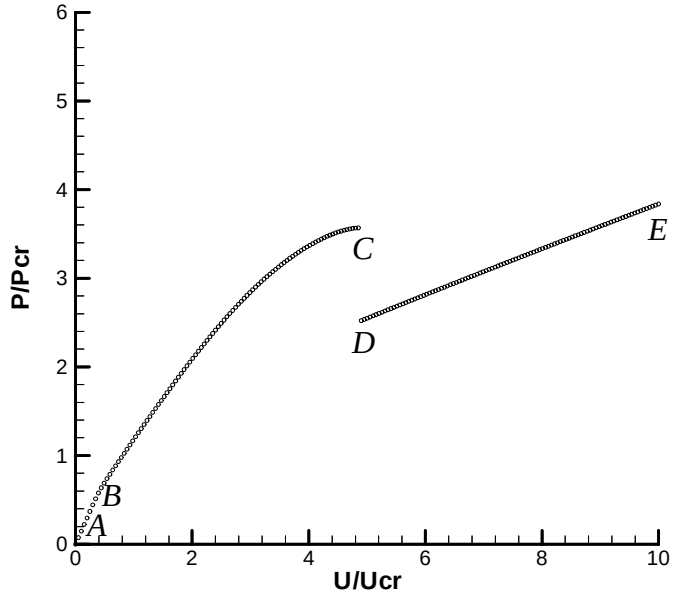

Fig. 4.9.11 Load response of a $[30_2/90/0]_{2T}$ laminate (SS-SS)

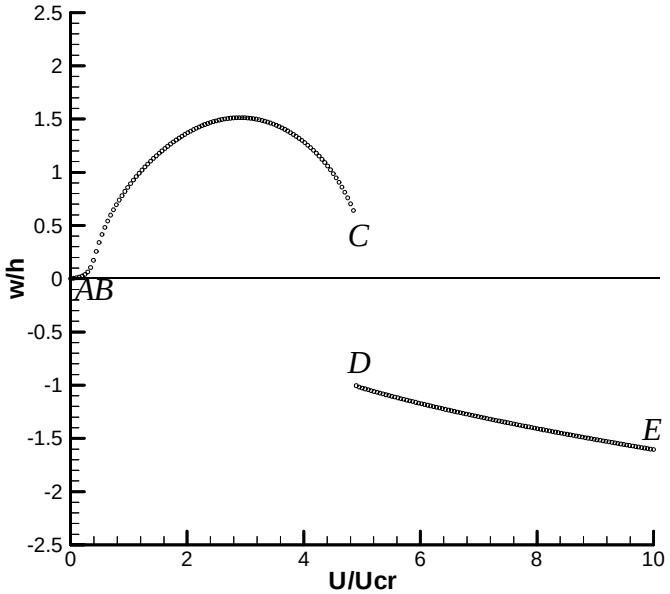

Fig. 4.9.12 Displacement response at II of a $[30_2/90/0]_{2T}$ laminate (SS-SS)

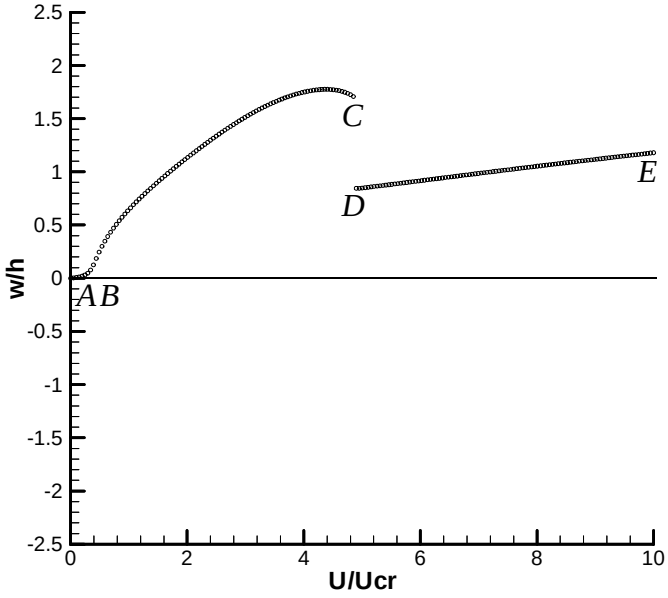

Fig. 4.9.13 Displacement response at III of a $[30_2/90/0]_{2T}$ laminate (SS-SS)

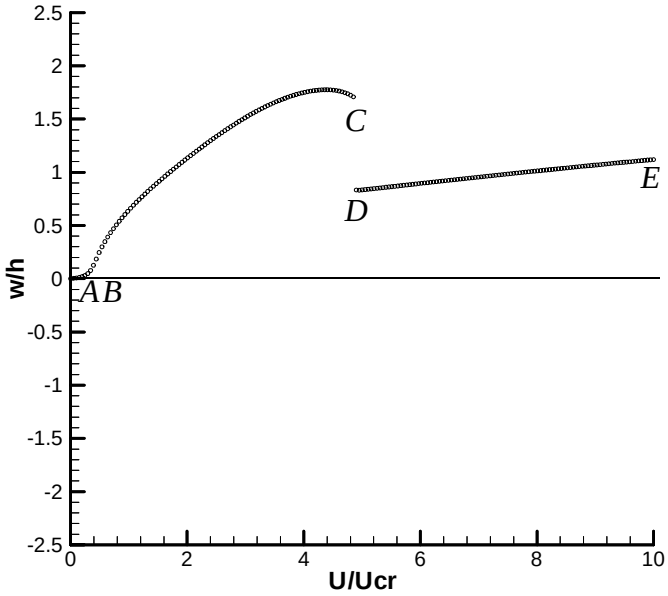

Fig. 4.9.14 Displacement response at I of a $[30_2/90/0]_{2T}$ laminate (SS-SS)

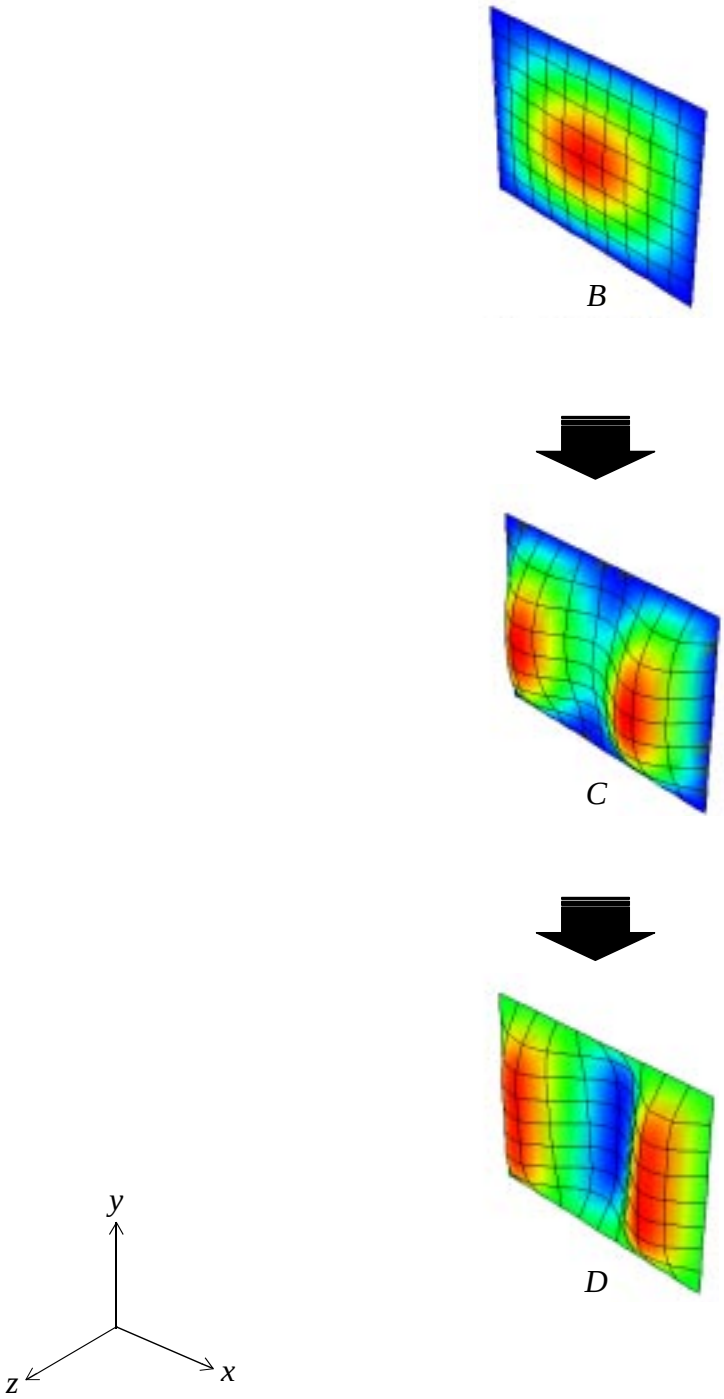

Fig. 4.9.15 Deformed shape flow chart for a $[30_2/90/0]_{2T}$ laminate (SS-SS)

4.10 Chapter Conclusions

Chapter 4 has discussed the deformations of plates with various boundary conditions due to axial endshortening. It was seen that the response generally depended on the laminate construction and boundary conditions applied along the ends and sides of the plate. Table 4.5 summarizes some of the key characteristics of each case considered. The second and fourth columns indicate if the case being considered exhibits a primary and/or secondary instability. The third and fourth columns shows the number of stable solutions that follow these instabilities. Though not really the topic of this research, isotropic aluminum plates and symmetric cross-ply plates were discussed. Each of these six cases had no out-of plane deformations until the classic buckling, or primary instability, and then each has two stable solutions. Each also exhibited a secondary instability that results in two stable solutions. For both the aluminum and symmetric cross-ply plates, the boundary conditions really had no influence on the overall behavior of the plates. It can also be said that the boundary conditions had no influence on the symmetric angle-ply $[\pm 30]_{2S}$ plate. Unlike the aluminum and cross-ply plates, however, the angle-ply plate did not exhibit a secondary instability. Referring to Table 4.3, it is felt that either the disparity in the two Poisson ratios for this laminate, or the rather large value of ν_{xy}, is responsible for the lack of a secondary instability with the symmetric angle-ply plate.

The behaviors of the unsymmetric laminates showed a mixture of characteristics. Some cases exhibited a primary instability, other cases did not exhibit a primary instability. Some cases exhibited a secondary instability, other cases did not. Of the cases that exhibited a secondary instability, some had two stable solutions after the secondary instability, some had only one. Specifically, the CL-CL boundary condition for the $[0_4/90_4]_T$ laminate is the only one that resulted in classic bifurcation. The CL-SS and SS-SS cases for this laminate showed that these boundary conditions led to secondary buckling, while the CL-CL case did not, though the rectangular geometry and the CL-CL boundary conditions did lead to somewhat anomalous behavior. Also, the unsymmetric cross-ply CL-SS and SS-SS laminates had only one stable solution after secondary buckling, while most other laminates and boundary condition combinations had two stable solutions. The characteristics of the unsymmetric $[+30_4/-30_4]_T$ laminate showed that the CL-CL case is the only one that did not exhibit secondary buckling, whereas the CL-SS and SS-SS cases did. The characteristics of the $[\pm 30/90/0]_{2T}$ laminate showed that the CL-CL boundary conditions caused the

plate to exhibit classical bifurcation, while the other two boundary condition cases did not. Interestingly, all boundary conditions for this laminate resulted in two stable solutions as U/Ucr approached 10. Perhaps the unique response of the CL-CL boundary condition cases may be attributed to the effects described by Leissa [8]. His work discussed the suppression of prebuckling deformations by constraining the plate boundaries by using the clamped conditions. The clamped conditions provided the necessary bending and twisting moments to keep the plate flat, thus leading to classic bifurcation behavior. However, consideration of the unbalanced unsymmetric laminate, the $[30_2/90/0]_{2T}$ laminate, shows that the aforementioned trend in the characteristics may not be observed. Namely, all three boundary condition combinations for this laminate exhibited no bifurcation. The laminates simply began deforming out-of-plane from the no-load condition. This contradicts the findings of Leissa, since the clamped conditions applied for the CL-CL case failed to suppress the initial out-of-plane deformations, allowing the laminate to make a transition from the flat state to the state with one half-wave in the two perpendicular plate directions without undergoing bifurcation behavior.

It is also interesting to note that for the unbalanced unsymmetric $[30_2/90/0]_{2T}$ laminate, the boundary conditions controlled the sign of the out-of-plane deflection from the onset of endshortening. The CL-CL and SS-SS boundary conditions resulted in positive out-of-plane displacements, while the CL-SS boundary conditions resulted in negative out-of-plane displacements. Generally speaking, the CL-CL case for each laminate carried the most load, followed by the CL-SS and then the SS-SS cases. This finding is in line with expectations stemming from the reduction of overall structural stiffness associated with the introduction of additional degrees of freedom. In every case considered in this work, the plate configuration became statically unstable at some point during the endshortening. Therefore, a transient dynamic analysis was always required to find the statically stable equilibrium solutions. Finally, the very nature of the problems considered requires geometrically nonlinear kinematic relationships.

Table 4.5 Summary of key characteristics

plate	primary instability	number of stable primary solutions	secondary instability	number of stable secondary solutions
Aluminum (CL-CL)	yes	2	yes	2
Aluminum (CL-SS)	yes	2	yes	2
Aluminum (SS-SS)	yes	2	yes	2
$[0_2/90_2]_S$ (CL-CL)	yes	2	yes	2
$[0_2/90_2]_S$ (CL-SS)	yes	2	yes	2
$[0_2/90_2]_S$ (SS-SS)	yes	2	yes	2
$[0_4/90_4]_T$ (CL-CL)	yes	1	square, yes; rectangle, no	1; -
$[0_4/90_4]_T$ (CL-SS)	no	1	yes	1
$[0_4/90_4]_T$ (SS-SS)	no	1	yes	1
$[\pm 30]_{2S}$ (CL-CL)	yes	2	no	-
$[\pm 30]_{2S}$ (CL-SS)	yes	2	no	-
$[\pm 30]_{2S}$ (SS-SS)	yes	2	no	-
$[+30_4/-30_4]_T$ (CL-CL)	yes	2	no	-
$[+30_4/-30_4]_T$ (CL-SS)	yes	2	yes	2
$[+30_4/-30_4]_T$ (SS-SS)	yes	2	yes	2
$[\pm 30/90/0]_{2T}$ (CL-CL)	yes	1	yes	2
$[\pm 30/90/0]_{2T}$ (CL-SS)	no	1	yes	2
$[\pm 30/90/0]_{2T}$ (SS-SS)	no	1	yes	2
$[30_2/90/0]_{2T}$ (CL-CL)	no	1	yes	1
$[30_2/90/0]_{2T}$ (CL-SS)	no	1	yes	2
$[30_2/90/0]_{2T}$ (SS-SS)	no	1	yes	1